CHARACTERIZATION AND EVALUATION OF SURFACE MODIFIED SUPERPARAMAGNETIC IRON OXIDE NANOPARTICLES FOR UPTAKE INTO HUMAN PROSTATE CARCINOMA CELLS

by

Nefertiti Patrick Jackson

A dissertation submitted in partial fulfillment
of the requirements for the degree of
Doctor of Philosophy
(Applied Physics)
In the University of Michigan
2011

Doctoral Committee:

Professor Bradford G. Orr, Chair
Professor Roy Clarke
Associate Professor Cagliyan Kurdak
Professor Gary L. Harris, Howard University

DEDICATION

This monumental achievement is dedicated to the most important people in my life. My mother has always been my faithful cheerleader, my grandmother keeps me rooted and my remaining family members have been pillars, supporting me at every angle. The greatest surprise in my life was the greatest gift and my greatest inspiration in the final stretch toward completion of this work which was the birth of my daughter, Nailah Anaya Jackson. The most supportive, encouraging, self-sacrificing man in my life is my husband; Tracy K. Jackson III, the love of my life, who never let me give up. God provided me the initial desire and motivation to take on the challenge of a Ph.D., the strength, intelligence and determination to persist through the adversity and the unwitted gall to take nothing less.

ACKNOWLEDGEMENTS

I would like to thank Bradford Orr, the former Chairman of the Applied Physics Program and my dissertation committee Chairman for providing a fair environment and opportunity to complete my degree by accepting me into the Applied Physics Ph.D. Program. Throughout my unique journey, his support and encouragement was unwavering. The main operators of the Applied Physics office, Charles Sutton and Cynthia McNabb were always available and willing to assist in whatever the need. I greatly appreciate the friendship I developed among the staff and fellow students of the program.

I would also like to thank Dr. Gary L. Harris, Professor of Electrical Engineering and Director of the Howard Nanoscale Science and Engineering Facility (HNF) at Howard University. He generously welcomed me into his laboratory. There were many members of HNF that made the working day pleasurable, but most notable was the Lab Manager, Mr. James Griffin, who became a wonderful friend. He was always upbeat, continuously encouraging and willing to help move things forward by assisting in any way possible. His lunch time menu will never be forgotten, raw vegetables, tuna or sardines and a sweet potato was very nutritious and even satisfying at times. Dr. James Mitchell, Professor of Chemical Engineering and Director of the Center of Research Excellence in Science and Technology (CREST) at Howard, was also very supportive.

He shared his expertise and guidance in his own unique way, stern and straight forward. Dr. Winston Anderson and Dr. Clarence Lee, Professors of Biology at Howard University greatly aided me in the biological aspect of my research. As a new graduate student, I acquired a new surrounding of endeared friends within Howard University and the Washington DC community. I was so well received and warmly welcomed into the University, into the church (Shiloh Baptist), and into the Howard Plaza Towers, where I worked and lived. While at Howard University, I also had the opportunity to link in with Catholic University and Princeton University. Dr. Otto Wilson, Professor of Biomedical Engineering of Catholic University introduced me to a technique for synthesizing nanoparticles. Dr. Winston Soboyejo, Professor of Mechanical and Aerospace Engineering at Princeton University provided his resources to further my research. There were also others, too numerous to mention by name, who also helped and supported me in different ways. I thank all of you.

TABLE OF CONTENTS

LIST OF FIGURES

LIST OF TABLES

ABSTRACT

Magnetic nanoparticles (MNPs) were synthesized from Fe^{2+} and Fe^{3+} by the co-precipitation method. Two nanoparticle surface coatings (gum arabic and sodium citrate) provided additional functionalization and cell selectivity. The incorporation of surface modifiers to the synthesized nanoparticles generated three nanoparticle systems from which the research was based. The physical and chemical properties were determined with a variety of standard characterization techniques. Upon characterization of the nanoparticles, in vitro cell culture experiments were conducted. Nanoparticles were allowed to co-exist with prostate cells for 48 hours under sterile conditions. A range of iron oxide nanoparticle concentrations ($0.5 \times 10^{16} – 50 \times 10^{16}$ particles/mL) were studied and compared for their effects on cell viability, intercellular uptake and quantitative analysis of prostate cell selectivity.

Nanoparticles have a natural tendency to agglomerate; therefore, the addition of gum arabic as a stabilizing agent provided increased electrostatic repulsion which freely dispersed the particles and greatly contributed to more stabilized particles in both water and cell nutrient media. Sodium citrate was an excellent capping agent for nanoparticles in water but not in serum rich nutrient media. The contents of the media contributed to the destabilization of the

nanoparticle solution; hence, particle size measurements decreased over time for sodium citrate coated particles in media as well as non-coated nanoparticles in media, which

formed larger particles (350 – 375 nm), then gradually fell out of solution. Initial measurements for sodium citrate MNPs were more than four times greater in media as compared to stabilized sodium citrate particles in water (160 nm). Non-coated nanoparticles demonstrated agglomeration in water and size measurements increased to 700nm over the 48 hour period. Despite the degree of particle stability, prostate cells intracellularly received nanoparticles from each of the three nanoparticle systems. Cellular encapsulation of iron nanoparticles by prostate cells was demonstrated with TEM. Iron filing and cell mobility in response to a magnet was captured with video. The gum arabic nanoparticle system exhibited the highest differential uptake (ratio 6.8) at a lower nanoparticle concentration (2.5×10^{16}). There is possibility of greater specificity when the size of prostate cancer and normal cells are compared.

CHAPTER 1

INTRODUCTION

1.1 Problem Statement

Second to heart disease, cancer is the leading cause of death in the United States. The combined totals for heart disease and cancer account for almost 50% of total reported U.S. deaths. Among the various types of cancers, prostate cancer is the number one killer specific to men, with an occurrence just behind lung and tobacco cancer, the primary killer for both men and women. The current therapies are not adequate treatment for prostate cancer. They are invasive and occur with high incidence of life changing side effects, which negatively impact the quality of life. An alternative treatment is required and the current tools of technology may provide the means for effective treatment.

1.2 Background

1.2.1 Prostate Cancer

The prostate is a gland that is present only in the male anatomy (Figure 1.1) **(1)**. A normal, healthy prostate is about the size of a walnut. It is located just below the bladder and in front of the rectum. The primary function of the gland is to control urination and the

The need to urinate, as it presses directly against the part of the urethra it surrounds. It participates in production of the fluid composition of semen and physically supports the urethra (urine tube). In the case of prostate cancer, the gland enlarges (Figure 1.1). The earlier stages of prostate cancer may not demonstrate any symptoms and is therefore, best diagnosed with a prostate specific antigen (PSA) test and/or a digital rectal exam (DRE). Symptoms that may be experienced and denote abnormality include either slowed/weakened urine flow or increased frequency to urinate. These are symptoms that are also present in non-cancerous diseases of the prostate such as benign prostatic hyperplasia (BPH). When prostate cancer is advanced, blood in the urine and erectile dysfunction may be present. Advanced prostate cancer often spreads to the bones and causes pain in the hips, back, and ribs. Infected bones of the spine can press on the spinal cord or its nerves which can result in weakness or numbness in the legs or feet, or even loss of bladder or bowel control.

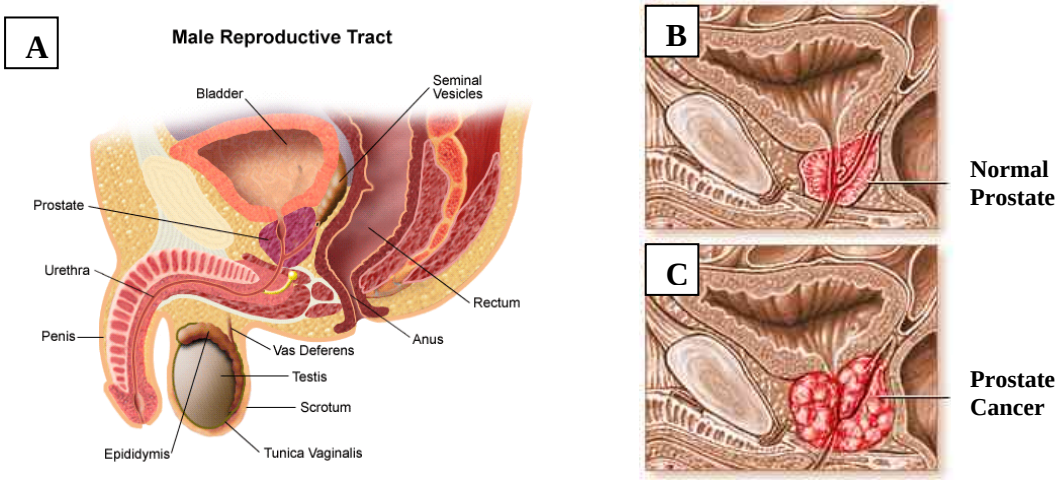

Figure 1.1: Images of prostate anatomy (A) male reproductive tract, (B) normal prostate, (C) prostate cancer

1.2.1.1 Prevalence

Prostate cancer strikes one in six American men. Cancer statistics compiled by the American Cancer Society, estimates that more than 217,000 men in the United Sates will be diagnosed with prostate cancer and more than 32,000 men will die from this disease **(2) (3) (4) (5)**. Unfortunately, non-smoking men are more likely to develop prostate cancer than colon, bladder, melanoma, lymphoma and kidney cancer. More alarming is the fact that African American men are affected by prostate cancer at an even higher rate than other ethnic groups **(4) (5) (6) (2) (3)**. The disease is more prevalent in North America and northwestern Europe than in Asia and South America. Genetic studies have shown that 5-10% of prostate cancers are due to familial predispositions, while data from the Cancer Prevention Study suggests a correlation between development of the disease to dietary practices **(6) (7) (8)**. Ultimately, the cause of prostate cancer is unknown, and the prevalence of the disease alone warrants a concentrated effort toward revealing a solution which will reduce one of the leading causes of death among men

1.2.1.2 Current Therapies

According to the Prostate Cancer Institute, therapy is a "one shot deal" which means that therapy can be administered once to stop or slow the cancer and will either work or not work; leading to further attempts of treatment by more aggressive means **(6) (7) (8)**. To date, prostatectomy (surgical removal of the prostate) and radiation therapy are the most commonly utilized treatments. Unfortunately, every available therapy is followed by side effects, some more severe than others. Brachytherapy (radiation) and cryotherapy (freezing) are minimally invasive treatments that can be applied more than once. Cryotherapy utilizes ultra thin needles to deliver ice balls at sub zero temperatures.

Ultra sound is used to precisely place the needles and control the size and shape of the ice balls. This method destroys the entire prostate gland and cancer cells within it. Cryotherapy can be administered even after failed radiation attempts **(6) (7) (8)**. A few alternative therapies, such as hormone regulation and anti-angiogenic drugs are in clinical trials. For example, the ITL Cancer Clinic utilizes immune therapies with the goal of training the patient's own immune system to recognize and destroy tumor tissue which is said to aggressively treat cancer with no side effects **(7)**. Another approach toward providing an alternative therapy is with anti-angiogenic drugs which are designed to starve proliferating cancer cells and in fact have demonstrated improved outcomes for women with breast cancer and colorectal cancer according to the Prostate Cancer Foundation **(5)**.

1.2.2 Nanobiotechnology

Nanobiotechnology refers to materials in the nano-scale range that are manufactured for use as tools in biologically related environments or situations to address health based concerns, utilizing technical processes. Although dimensional measurements in the nano-scale range are 10^{-9} meters, nanoparticles for cellular applications are usually utilized in the 1-100 nm range. In addition to size, the intrinsic properties of particular materials that can be created and utilized in the nano-size range make nanoparticles attractive tools for solving biological challenges.

1.2.2.1 Biomedical Applications of Magnetic Nanoparticles

Areas of biological interest which require technological intervention exist in the administration of drugs, separation of materials, diagnosis, and treatment. In the scope of treatment, communication with biological cells is inevitable. Nanosized particles are

ideally appropriate in size for entrance into most micron-sized cells. The cell membrane however is a very good guard for protection of the intra-cellular matter. The size, shape, charge/electrophoretic mobility and surface functional groups are parameters that determine the biocompatibility and acceptance of foreign materials by biological systems. The targeting approach for evoking the desired biological response must be designed based upon the intended reaction between the cell and nanoparticle at contact or thereafter. The result may be a measureable structural or chemical conformational change within the cell, a fluorescent indicator for visual or quantitative analysis, the ability to quantify cellular uptake of magnetic material, or the ability the affect the fate of the cell by controlling the overall temperature of the cell. Surface modification of nanoparticles result in a "call and response" phenomena, for example magnetic interaction can result in mobile particles (delivery systems) or temperature sensitive particles (for activation or destruction). In many cases fluorescent molecules have direct interaction with the surface of nanoparticles for the purpose of visual analysis or imaging of static and dynamic molecules of interest.

Wei and coworkers synthesized PEI coated magnetic iron oxide particles for use as gene vectors. It was shown that these 100 nm coated nanoparticles could bind and condense DNA, in addition to expressing green fluorescent proteins **(10)**. Utilization of nanoparticles as delivery systems for therapeutic agents or for delivery of stem cells is currently under investigation. The Baker group has synthesized PAMAM dendrimer-based nanoparticles for drug delivery. Binding avidity was measured and found to be greatly enhanced. Although rates of cellular internalization remained unchanged, the binding avidity was increased by 5 orders of magnitude. The authors stated the

importance of residence time as compared to binding followed by enhanced rate of endocytosis. From their experimental analysis, the principles of multivalency can be effectively applied to synthesize targeted chemotherapies for *in vivo* studies **(10)**. Another interest for nanoparticle use is cell activation or cell destruction which requires precise targeting techniques. Surface alteration of nanoparticles must be attractive to the cells of interest for homing and ultimate association *in vivo*. Kettering and co workers selectively accumulated nanoparticles onto human adenocarcinoma cells and applied an alternating magnetic field in order to destroy them **(11)**. The current research will consider a similar approach to abolish human prostate cancer cells. The application of nanoparticles to biomedical systems offers a marriage of technology, termed nanobiotechnology, and a potential therapy which has shown promise toward impacting lives which may have otherwise been lost.

1.2.2.2 Properties of Magnetite Nanoparticles

Magnetite is a well known ferrimagnetic material, but was considered ferromagnetic until the1940's when Néel provided the theoretical framework for understanding ferrimagnetism In either case, when of the particle size of these materials are reduced below a certain size, the surface energy provides a sufficient energy for domains to spontaneously flip or change polarization directions because they exist as single domain. The critical size where monodomain structures generally occur exist between 10 – 100 nm, but is actually specific to the material. For magnetite, the critical size is about 70 nm. In the presence of an applied magnetic field, the particle moment changes, and is described by either Néel relaxation or Brownian relaxation.

The magnetization behavior of a collection of monodisperse superparamagnetic particles in an applied field can be described using the Langevin function:

$$M(H) = M_s \left(\coth\left(\frac{\mu H}{kT} \right) - \frac{kT}{\mu H} \right) \qquad \text{[eqn 1.1]}$$

where M_s is the saturation magnetization, μ is the particle moment, H is the applied field, k is Boltzmann's constant, and T is the absolute temperature **(2)**. Collections, clusters or agglomerated nannoparticles of superparamagnetic particles exhibit saturation magnetizations that are comparable to yet smaller than those of the corresponding bulk material.

1.2.2.3 Hypothesis and Specific Aims

Aim I: Generate surface modified magnetic magnetite nanoparticles

Hypothesis: The wet chemistry approach, specifically co-precipitation with ammonium hydroxide will result in superparamagnetic magnitite nanoparticles with consistent chemical and physical characteristics.

Aim II: Characterize the physical, chemical and magnetic properties of synthesized magnetite nanoparticles

Hypothesis: The addition of surface modifiers, such as sodium citrate and gum arabic will decrease agglomeration, increase colloid stability, and have a negligible effect on the magnetic properties of the nanoparticles in aqueous solution.

Aim III: Demonstrate the uptake of surface modified iron nanoparticles within prostate cells in different cell nutrient media concentrations and evaluate their effects on cell viability

Hypothesis: The rate of magnetite nanoparticle encapsulation by prostate cells is increased when the surface of nanoparticles is made more attractive with sodium citrate or gum Arabic, therefore enhanced uptake will be observed as compared to non coated nanoparticles and cell viability will not be negatively impacted.

Aim IV: Quantify the uptake of surface modified magnetite nanoparticles within prostate cells which have been exposed to various concentrations of nanoparticles

Hypothesis: Prostate cells exposed to magnetite nanoparticles at higher concentrations will enable greater cellular uptake, while lower concentrations will not allow sufficient uptake for therapeutic effectiveness.

CHAPTER 2

SYNTHESIS AND CHARACTERIZATION OF MAGNETITE NANOPARTICLES

2.1 Abstract

Magnetite nanoparticles were chemically synthesized by the co-precipitation method. From the stock material of the nanoparticles, three experimental types of magnetite nanoparticles were investigated; non-coated (NC), sodium citrate coated (SC), and gum arabic coated (GA). Upon characterization of the magnetic nanoparticles (MNP's), positive identification of the material and its quantitative amount was achieved with spectrophotofluorimetry Inductively Coupled Plasma-Atomic Emission (ICP-AE) via an external source, which confirmed the material as iron. Further elemental analysis was conducted with Energy Dispersive X-ray Spectroscopy (EDS). The hydrodynamic diameters were obtained with a Malvern Zetasizer, while the particle size (dry mass) was determined by Transmission Electron Microscopy (TEM), Atomic Force Microscopy (AFM), and Vibrating Sample Magnetometry (VSM). From the size determination, the concentration of mnp's in the stock solution was calculated and the working concentrations were extrapolated. The colloid stability was evaluated with the combination of analytical methods. Temporal measurements of nanoparticle light scattering were accessed with a Fluorescence Spectrophotometer, while temporal size measurements were collected with the Malvern Zetasizer. In addition, particles size distribution information obtained at the same time

with the Malvern Zetasizer contributed to the analysis of colloid stability. The degree of magnetization also contributed to the characterization of MNP's, which was accessed with VSM. The three experimental types of nanoparticles responded differently in water versus cell nutrient media (RPMI 1640). The hydrodynamic diameters, degree of colloid stability and level of magnetization are discussed in this chapter.

2.2 Introduction

Synthesis and characterization of a material for experimentation is required for analysis and comprehension of the results. The material composition, physical, chemical, and magnetic properties of iron oxide nanoparticle must be determined in order to move forward and incorporate non-biological material with human biological materials. The size, surface morphology, and chemical composition are important concerns when micron sized human cells are expected to receive an unfamiliar material through its cell membrane into the cytosol. The surface morphology and the chemical composition of the nanoparticle surface are huge determinants for acceptance into human cells. The addition of functional agents on the surface of nanoparticles, such as sodium citrate and gum arabic requires further analysis, since the surface modification alters the size, surface morphology, colloidal stability, and magnetic properties. Quantification of the adherent surface material to the nanoparticle should also be determined. The effect of the functionalizing agents on the health of the cell must be known before continuing to the next step of the work. For this reason, material characterization is mandatory. An additional parameter to consider is the unique characteristic of magnetite, which is the fact that it is a magnetic material. The expected result of this work relies upon the density of magnetic material that each prostate cell will allow into its environment. The

killing mechanism by hyperthermia is dependent upon this density, along with the parameters for adjustment of the magnetic field. Characterization of the nanoparticles before interaction with the nanoparticles

2.2.1 Co-Precipitation Technique

There are many techniques for synthesis of nanoparticles **(13) (14) (15) (16) (17)**. The method of synthesis employed for the production of superparamagnetic magnetite nanoparticles is a well known bottom up approach termed co-precipitation. The 2:1 molar ratio of ferric to ferrous chloride, in the presence of aqueous ammonium hydroxide formed magnetite. The aqueous ammonium hydroxide in water served as the reducing agent (electron rich) which donated electrons to reduce the oxidation state of the metal ions (electron poor). In the process, ionic bonding between the iron and chloride molecules of the iron salts ($FeCl_2$ and $FeCl_3$) was dissociated and the precipitation reaction caused the chloride ions to bind with the ammonium of the original ammonium hydroxide while the oxygen contributed to the development of FeO and Fe_2O_3. The two oxidation states of iron (Fe^{2+} and Fe^{3+}) provide the appropriate number of binding sites for the formation of the two part magnetite complex composed of wusitite and hematite. A typical reaction scheme is shown in Equation 2.1.

$$2\ FeCl_3 + 1\ FeCl_2 + 8\ NH3 + 4\ H_2O \quad \square\ Fe_3O_4 + 8\ NH_4Cl \quad \text{[Eqn 2.1]}$$

Magnetite has a cubic inverse spinel crystal structure and a schematic representation is shown in Figure 2.1 **(18) (19) (20)**.

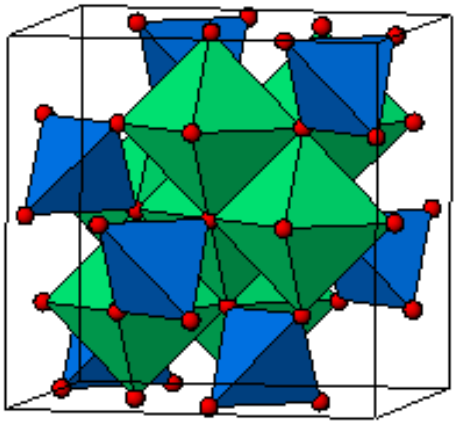

Figure 2.1: Base structure of magnetite; cubic inverse spinel.

2.2.2 Characterization Techniques

Several techniques have been utilized for nanoparticle characterization. Size, morphology (i.e. shape and structure), and colloidal stability have been determined with dynamic light scattering, various spectrophotometric techniques, such as energy dispersive x-ray spectroscopy, x-ray diffraction (XRD), and x-ray photo electron spectroscopy (XPS). Magnetic property information on nanoparticles alone typically utilize techniques such as Mossbauer, vibrating sample or squid magnetometry. Characterization of nanoparticles with or within human biological cells have made use of scanning electron microscopy, transmission electron microscopy, Fourier transform infrared spectroscopy (FTIR), XPS, XRD, magnetophoresis, and magnetic force microscopy.

2.3 Materials and Methods

2.3.1 Method of Synthesis for Magnetite Nanoparticles

Magnetite was utilized as the base material for the superparamagnetic iron oxide nanoparticles (SPION) in the form of non-coated MNPs. A stock solution of magnetite MNPs was synthesized in aqueous solution and aliquots were measured for preparation of surface modified magnetite nanoparticles. The methods given below describe the nanoparticles synthesis utilized in the experiments of this entire work.

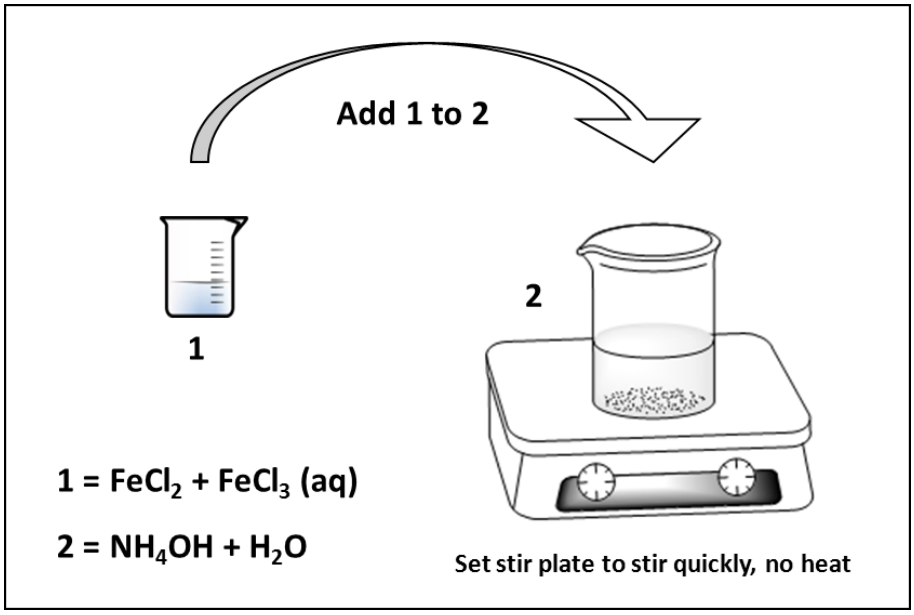

Figure 2.2: Schematic Set Up of Magnetite Nanoparticle Synthesis

2.3.1.1 Non-Coated Magnetite Nanoparticles

SPION were synthesized by co-precipitation of $FeCl_3$ and $FeCl_2$ (Fischer Scientific Fairlawn, NJ) in a 2:1 molar ratio. Iron salts and de-ionized water (20 mL) were stirred in Nalgene polycarbonate containers with a Teflon coated stir bar until completely dissolved (approximately 20 minutes). At the same time a dilute ammonium hydroxide solution, which contained 15 mL of NH_4OH and 65 mL of de-ionized water was prepared in a similar container and allowed to stir about 5 minutes. The 20 mL

mixture of iron salts were then quickly poured into 80 mL of ammonium hydroxide solution. The container was covered as the 100mL alkaline solution stirred at high speed for 1 hour to create naked magnetite nanoparticles. The resulting mixture was a deep brown almost black solution with a slightly acidic pH of 5.94, this iron oxide nanoparticle solution was poured into plastic 50 mL centrifuge tubes, then ultra centrifuged for 10 minutes at 10,000 rpm. The supernatant was decanted and discarded. Fresh de-ionized water was used as a medium to re-suspend the pelleted nanoparticles as they were sonicated, (Fisher Scientific, New Jersey, USA). Centrifigation and sonication were serially repeated until the nanoparticles were washed free of chloride ions. The length of time required for each step increased as the nanoparticles became free of extraneous material. Centrifugation cycles reached 1 hour and speeds up to 20,000 rpm, 10˚C. Sonication was aided with vortexing to help disrupt the pellet. One molar silver nitrate was prepared in water and dropped into the supernatant received from ultra-centrifugation of the nanoparticles. A cloudy precipitate formed in the presence of chloride ions. This step for material purification was repeated until no precipitate was formed. The particles were re-dispersed in ultra pure water and placed in a 4˚C refrigerator for storage. Surface modification of naked magnetite nanoparticles occured post synthesis. Gum arabic and sodium citrate were materials applied post synthesis as agents for colloid stability.

2.3.1.2 Gum Arabic Coated Magnetite Nanoparticles

Gum arabic (GA) was utilized as a 10% weight to volume solution; and was prepared upon dissolving 1 gram of gum arabic in 9 mL of de-ionized water. This solution was stirred for about 30 minutes, until the gum arabic was completely dissolved,

then sonicated for 10 minutes. To avoid contamination, the gum arabic solution was sterile filtered with a 0.22 micron filter. One milliliter of the nanoparticle stock solution was dried and weighed. The weight of 1 mL of nanoparticles was equivalent to 0.035 gram. Utilizing a previously determined relationship for calculation of the amount of gum arabic required for 1 g of nanoparticles, (0.2 g gum arabic : 1g SPION) and the weight of the nanoparticle stock solution per mL, it was found that 70 μL of the 10 wt% gum arabic solution was required for every 1 mL of SPION. From the nanoparticle stock solution 5 mL was obtained, and 350 μL of the gum arabic solution was added. This formulation was sonicated for 30 minutes and referred to as the working solution. Dilutions from the working solution created the various concentrations utilized for the experiments of this research.

2.3.1.3 Sodium Citrate Coated Magnetite Nanoparticles

The nanoparticles utilized for the production of sodium citrate coated nanoparticles were obtained from the synthesized stock solution of SPION. A 1.5 molar solution of sodium citrate was prepared (5g in 10 mL water). The ratio of sodium citrate (stabilizing agent) to SPION was 62.5 μL in 5 mL of SPION (1.25 wt%) to form a more colloid stable solution. This combination was sonicated for 10 minutes at room temperature (25˚C). The resulting nanoparticles were referred to as the working solution of sodium citrate coated magnetic nanoparticles; while dilutions of the working solution were used for experiments. The dilutions were made with Millipore water. The concentrations of interest were created as follows:

mnp stock		RPMI media		Final Concentration
5 mL	+	5 mL	→	50×10^{16}
1 mL		9 mL		10×10^{16}
750 μL		9.250 mL		7.5×10^{16}
500 μL		9.500 mL		5×10^{16}
250 μL		9.750 mL		2.5×10^{16}
100 μL		9.900 mL		0.1×10^{16}
50 μL		9.950 mL		0.5×10^{16}

Figure 2. 3: Formulation for a 10 mL volume of magnetite nanoparticles in media

2.3.2 Analytical Methods for Characterization of Magnetic Magnetite Nanoparticles

2.3.2.1 Spectrophotofluorimetry Inductively Coupled Plasma-Atomic Emission (ICP-AE)

The ICP method was utilized to determine compound composition of the material contained in a water based solution which contained non-coated magnetite nanoparticles. Four individual preparations of 100 mL were prepared. One milliliter of nanoparticles was added to 100 mL of ultra pure water. Four 100 mL volume replicates of nanoparticles in water were sent out for external analysis by Microbac Laboratories in Baltimore, MD. The iron in solution was first digested, and then measured by ICP. The resultant iron concentration provided by Microbac was expressed in gram per liter.

2.3.2.2 Energy Dispersive X-Ray Spectroscopy (EDS)

Positive identification of the synthesized SPION material was achieved by EDS. This chemical microanalysis technique was performed in conjunction with the scanning electron microscope (SEM). X-rays are emitted from the surface of the unknown material as electrons from the electron beam bombard the surface. The emitted x-rays

versus the resultant energy were measured by the EDS detector to evaluate and determine the qualitative and relative quantitative elemental composition of the unknown specimen.

2.3.2.3 Size Measurements of Magnetite Nanoparticles in Liquid Phase by Light Scattering

The Malvern Zetasizer Nanoseries nano-zs was used to obtain size measurements of magnetite nanoparticles in aqueous medium. This instrument, obtains size information by eliciting the intrinsic properties of particles dispersed in a liquid to exhibit Brownian motion. The extent to which particles move in a liquid is also dependent on the size of the particles, where, larger particles will move slower than smaller particles. Henceforth, utilizing this information coupled with its relationship to a time-dependent diffusion speed, particle size information can be accurately determined within reasonable error (+/- 3 nm). Utilizing this analytical technique, surface modified nanoparticles dispersed in two different liquid mediums were investigated, specifically; nanoparticles in de-ionized water and in Roswell Park Memorial Institute (RPMI 1640) media. These investigations allowed for the determination of the physical and chemical changes that the magnetic nanoparticles undergo when its surface is modified, and also when it is placed in a cellular environment. It is hypothesized that the surface coating on the nanoparticles dispersed in aqueous solutions will affect the size of the particles, which will have a direct correlation to the colloid stability of the nanoparticles.

2.3.2.4 Colloid Stability of Magnetite Nanoparticles by Resonance Light Scattering

The Hitachi F-7000 Fluorescence Spectrophotometer was utilized to measure the intensity and the wavelength distribution of the light emitted as it interacted with the aqueously dispersed magnetic nanoparticles. The particular fluorescence

spectrophotometer utilized for experimental analysis was equipped with an emission detector positioned at an angle 90^0 to the excitation pathway. For this type of analysis, an excitation emission matrix (EEM) was obtained in order to determine the region of enhanced Rayleigh scattering (Resonance Scattering). This wavelength was then used to analyze the physical and chemical stability of the nanoparticles over a period of 12 hours, for particles dispersed in water and 48 hours for particles dispersed in media.

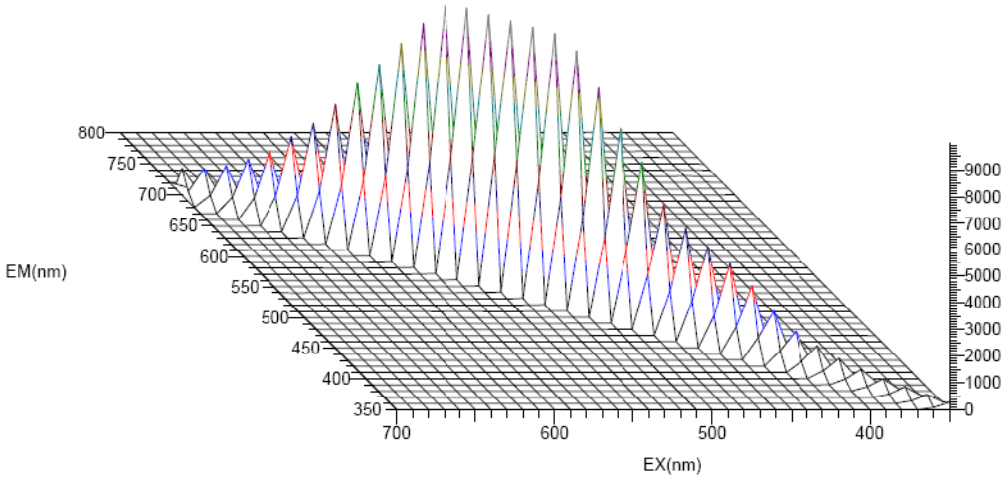

Figure 2.4: Excitation Emission Matrix (EEM) of non-coated magnetite nanoparticles, excitation at 550nm

The Hitachi F7000 fluorescence spectrophotometer utilized for the light scattering experiments offers a unique feature which contributes to the sensitivity and precision in measurements. The emission monochromator is placed 90^0 with respect to the incident light. This arrangement ensures that the energy detected is that from the fluorescing particle and not of the light source or any other variable. The explanation above describes the nephelometer capability and approach utilized for the light scattering experimentation

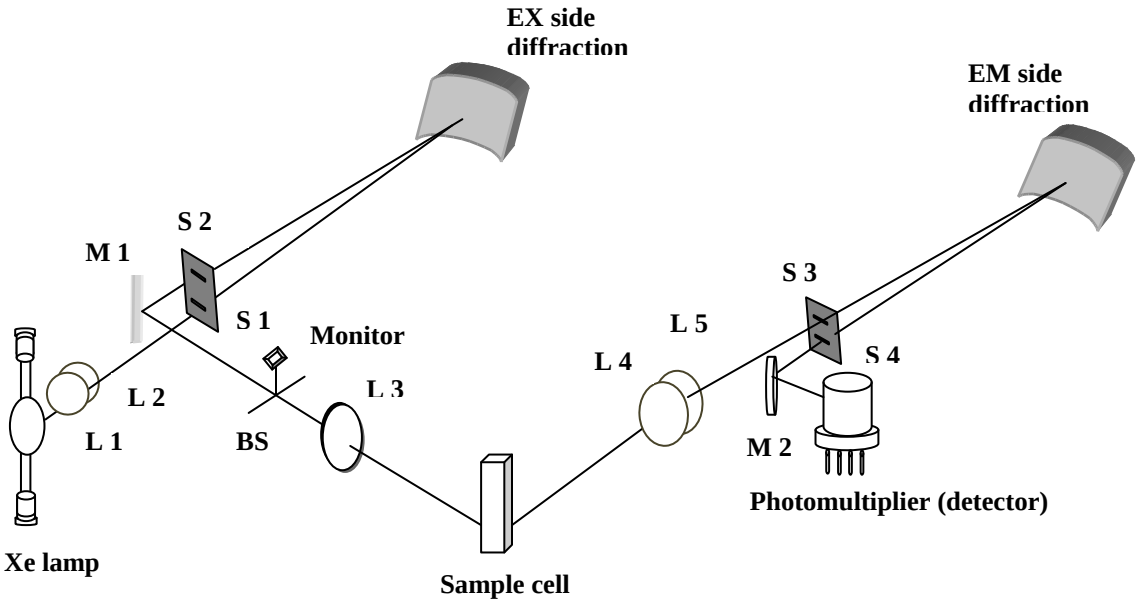

Figure 2.5: Schematic Design of the Hitachi F7000 spectrophotometer optical system.

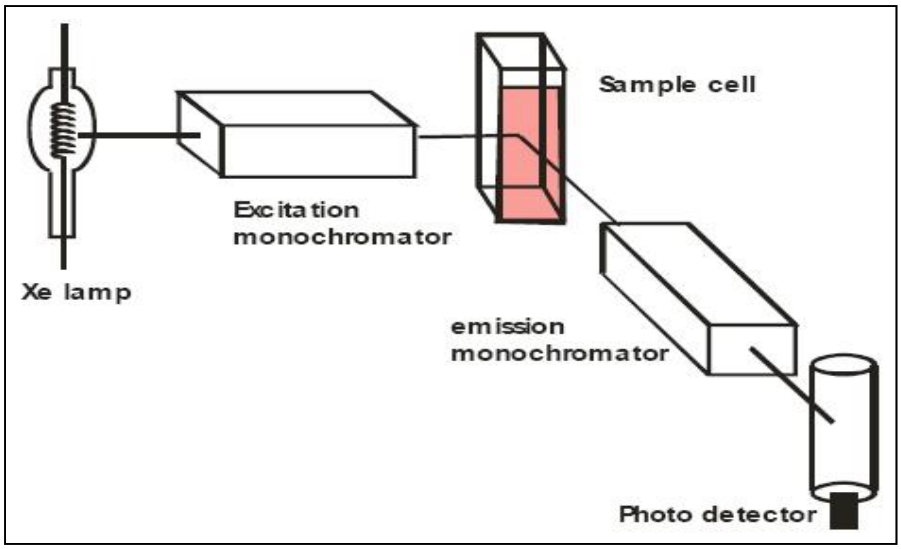

Figure 2.6: Configuration of a Simplified Fluorometer

2.3.2.5 Visual Inspection of Size and Shape of Magnetite Nanoparticles

2.3.2.5.1 Transmission Electron Microscopy (TEM)

TEM is a widely used technique for visual analysis of nano- to micro- scaled materials. Thin copper grids are required for the best clarity. A dilute solution of nanoparticles was dropped on the grid. After the sample was dried at room temperature, it was placed in the vacuum chamber of the TEM. Electrons pass through the material of interest which are then magnified and focused by an objective lens. The image is displayed on a monitor, which can then be photographed and printed for review.

2.3.2.5.2 Scanning Electron Microscopy (SEM)

Scanning electron microscopy is a spectrophotometric technique which provides high resolution three dimensional images of an objects surface morphology. A high intensity electron beam moves across the sample surface which causes it to emit secondary electrons. A resulting pattern produces a three-dimensional image on the screen of a cathode-ray tube. Dilute concentrations of nanoparticle solutions were allowed to dry on clean, smooth silicon wafer chips. A pure titanium sample was used to standardize and calibrate the SEM before making measurements on the nanoparticles of interest.

2.3.2.5.3 Atomic Force Microscopy (AFM)

The Agilent 5500 with AC mode III module and 10 micron scanner was utilized. Topography of the nanoparticle surfaces was imaged with a SiNi tip in contrast mode. Scan sizes ranged from .2 to 1.5 microns. Three dimensional size and shape information

can normally be obtained. Dilute concentrations of nanoparticles were allowed to dry on smooth glass cover slips in an effort to reveal individual dispersions of nanoparticles

2.3.2.6 Magnetic Properties of Synthesized Magnetite Nanoparticles

A vibrating sample magnetometer was utilized to evaluate the magnetic susceptibility and to determine the size of synthesized magnetite nanoparticles (dry weight). Nanoparticle samples from the stock solutoin were dried at room temperature for at least 48 hours. Two milliliters of nanoparticle solution was placed onto a glass slide. Each sample was scraped from the glass slide with the edge of a clean glass slide. The sample was placed into a sample holder and weighed before it was positioned in the sample chamber of the VSM. The magnetic field was set at 5000Oe. Data collection and computation was conducted with a computer interface.

2.4 Results and Discussion

2.4.1 Spectrophotofluorimetry Inductively Coupled Plasma-Atomic Emission (ICP-AE)

Spectrophotofluorimetry inductively coupled plasma-atomic emission provided the material content of the synthesized iron magnetic nanoparticles (non-coated). Five samples from the stock solution was analyzed and averaged. Two separate batches of nanoparticles were prepared on two different occasions. The material content and concentrations were consistent. The actual values of the batches are present in Table 1.2. The concentration of iron in 1 mL of magnetic nanoparticles was approximately 160 mg as determined among the four samples.

Iron Concentrations mg/mL		
	Batch 1	Batch 2
Sample 1	160	160
Sample 2	160	150
Sample 3	150	160
Sample 4	160	160
Avg	**157.5**	**157.5**

Table 2.1: Iron concentrations of synthesized magnetic nanoparticles

The actual iron concentration was determined as 157.5 mg/L. The iron concentration value was rounded up to 160 mg/mL and utilized to calculate the magnetite nanoparticle concentration of the stock solution. The computations can be found in the appendix. The co-precipitation method yielded 209.69 mg of magnetite in 1 mL of nanoparticle stock solution, and 7.77×10^{16} particles/mL.

2.4.2 Energy Dispersive X-Ray Spectroscopy Analysis (EDS)

Energy Dispersive X-Ray Spectroscopy is a semi-quantitative analysis which identifies the elemental components of a sample by atomic and weight percent. The non-coated MNPs were considered the base material. The characteristic peaks which identify the elements, iron and oxygen, were results of the EDS analysis and this information in the appropriate ratio confirmed the core material of the nanoparticles as magnetite. The atomic percents should agree with the ratios for magnetite, Fe_3O_4. If the nanoparticles were pure magnetite the atomic percents would be 3/7 = 43% for iron and 4/7 = 57% for oxygen.

Based on the atomic percents for the non coated nanoparticles,as seen in Figure 2.7, it was revealed that more oxygen was present, therefore,the nanoparticles became oxidized when they were exposed to the air. The ratios however for iron (31.61%) and for oxygen (68.39%) are relatively close to that for magnetite. The EDS analysis qualitatively identified the elements present in the nanoparticles and quantitatively confirmed them as magnetite.

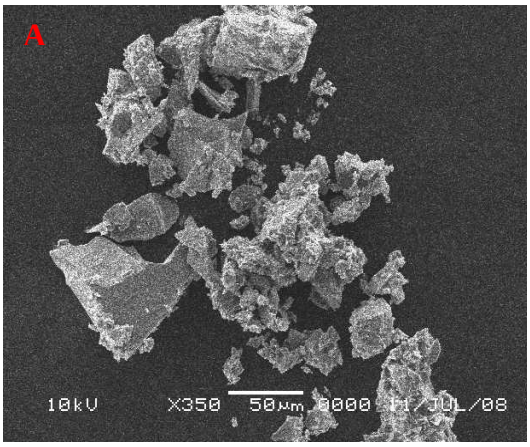

B Element	Weight%	Atomic%
O K	38.26	68.39
Fe K	61.74	31.61
Totals	100.00	100.00

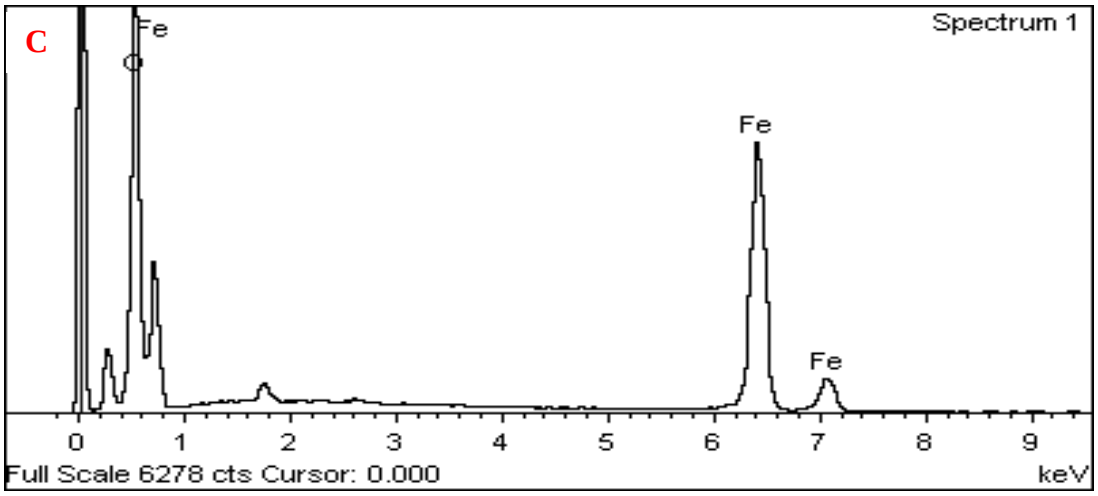

Figure 2.7: EDS analysis of non-coated magnetic nanoparticles (A) showing, (B) the elemental analysis and (C), the compositional distribution

The other two nanoparticle systems demonstrated the material as magnetite, but also revealed the presence of the additional surface material, as seen in Figures 2.8 and 2.9. Sodium contributed to the elemental composition (8.21%) of the sodium citrate nanoparticle system, while iron and oxygen were also present in the appropriate relationship for magnetite characterization

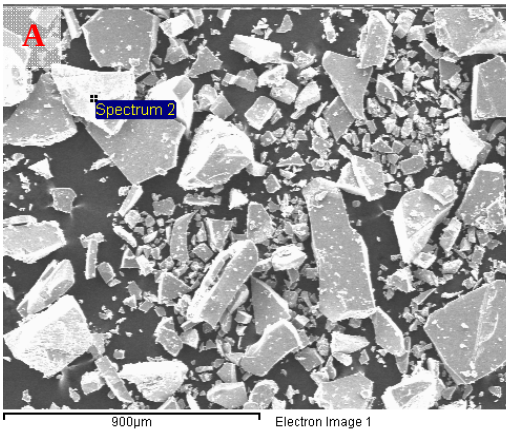

B

Element	Weight%	Atomic%
O K	36.30	63.33
Na K	6.76	8.21
Fe K	56.93	28.45
Totals	100.00	100.00

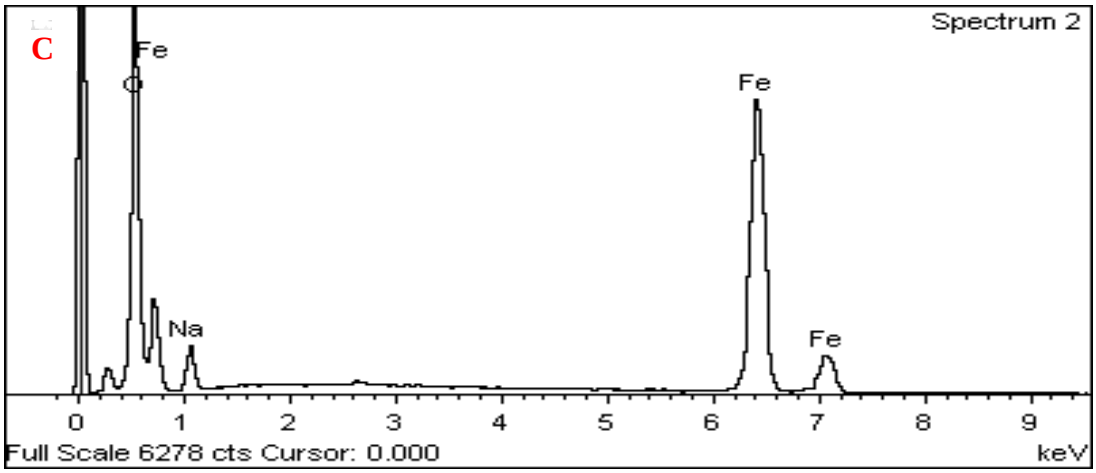

Figure 2.8: EDS analysis of sodium citrate coated magnetic nanoparticles (A), showing, (B) the elemental analysis and (C) the compositional distribution

The gum arabic nanoparticle system is composed of organic material which would be detected as carbon in the EDS system; however, it was not identified as carbon most likely because our system was not able to detect it. The iron and oxygen composition was well represented as elements in proportion for the description of magnetite. Figure 2.10 revealed the atomic percentages for gum arabic, iron at48.28% and oxygen at 51.72%. These values correlate well with the atomic percentages for magnetite, iron (43%) and oxygen (57%).

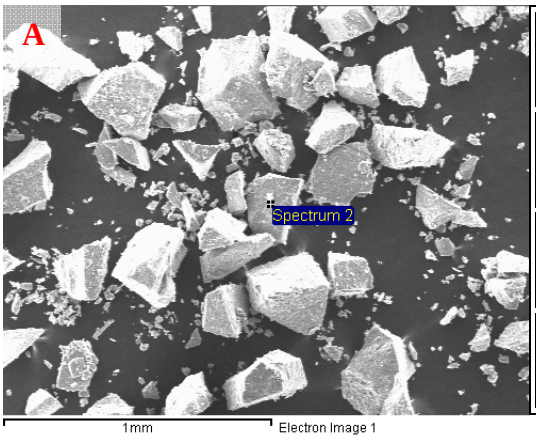

B Element	Weight%	Atomic%
O K	23.48	51.72
Fe K	76.52	48.28
Totals	100.00	100.00

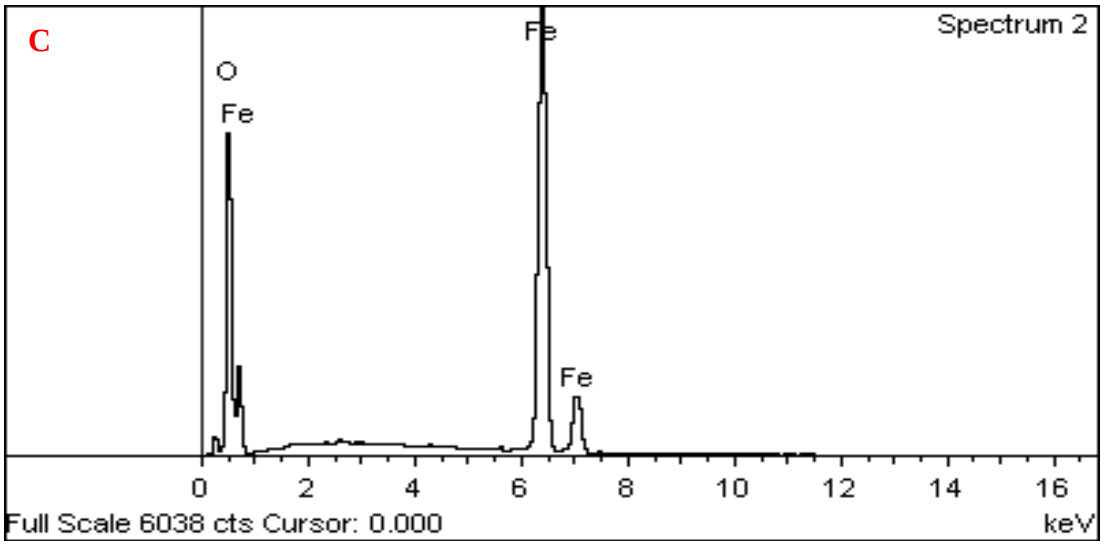

Figure 2.9: EDS analysis of gum arabic coated magnetic nanoparticles (A), showing (B) the elemental analysis and (C), the compositional distribution

2.4.3 Size Determination of Synthesized Magnetite Nanoparticles

2.4.3.1 Size Measurements by TEM

The transmission electron micrograph revealed clusters of fine round shaped particles. The prepared particles were non-coated, which may be the cause of the clustering. Smaller to individually sized particles were also visible in the micrograph, however there seemed to be a

range of nano-sized particles. Preparation of the sample for TEM did not involve sonication before application to the grid.

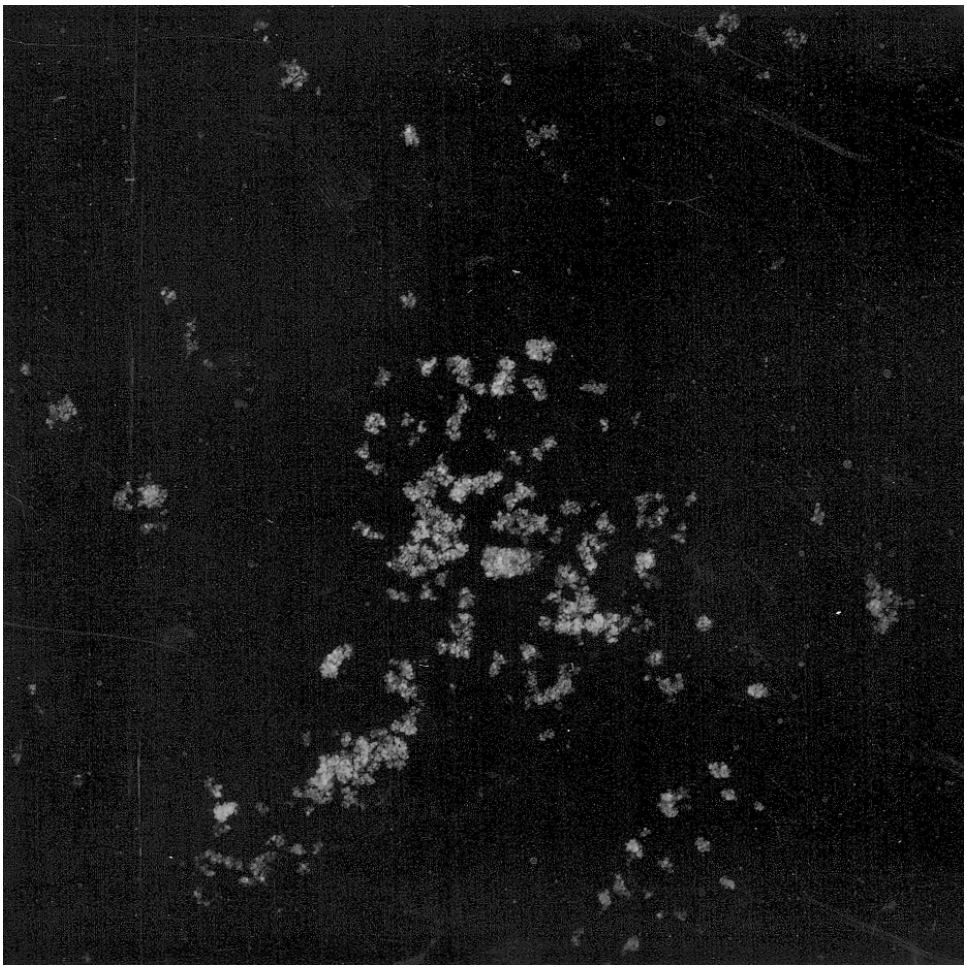

Figure 2.10: TEM of non-coated MNP's at 20,000X

2.4.3.2 Size Measurements by Scanning Electron Microscopy (SEM)

SEM was achieved with the Hitachi S-4700 and a GBC CCTV camera. The MNP surfaces were scanned and viewed at high magnification (10,000 – 500,000X). Particle size and shape was observed. Rounded nanoparticles approximately 20 – 30 nm were

captured. Larger particles were present, however particles smaller than 20 nm were difficult to resolve.

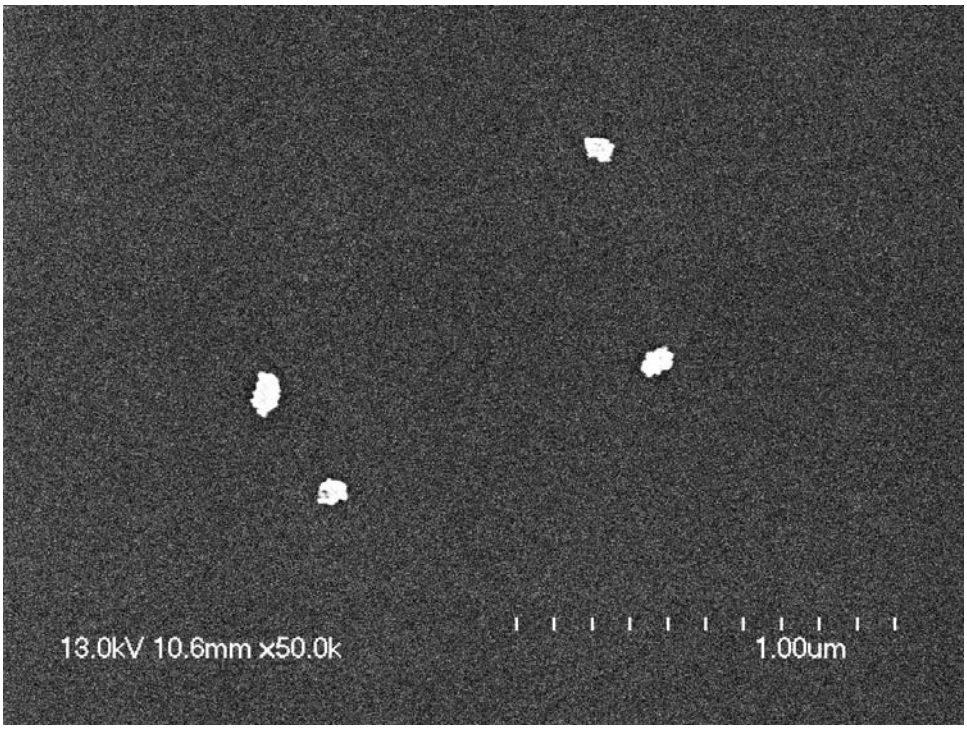

Figure 2.11: SEM of non-coated MNPs at 50,000X

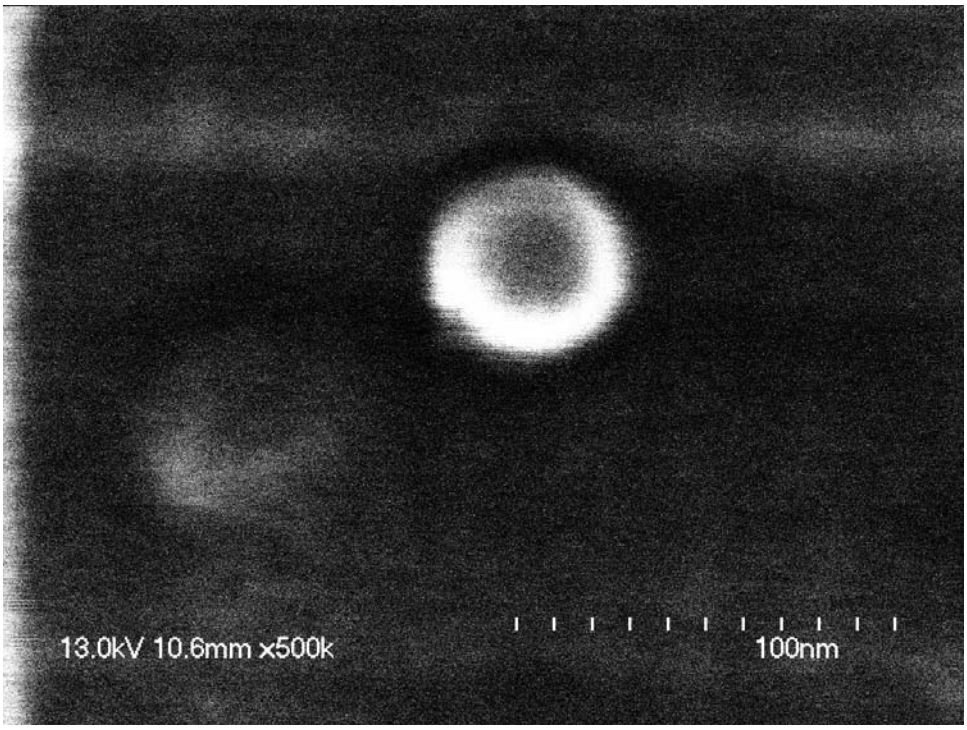

Figure 2.12: SEM of non-coated MNPs at 500,000X

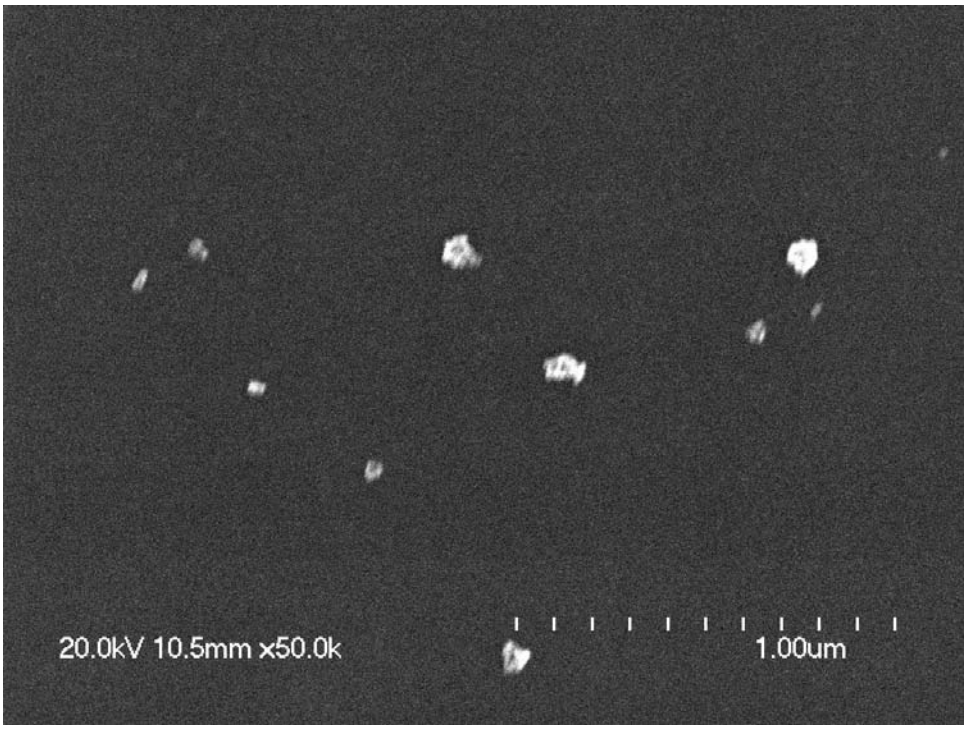

Figure 2.13: SEM of gum arabic coated MNPs at 50,000X

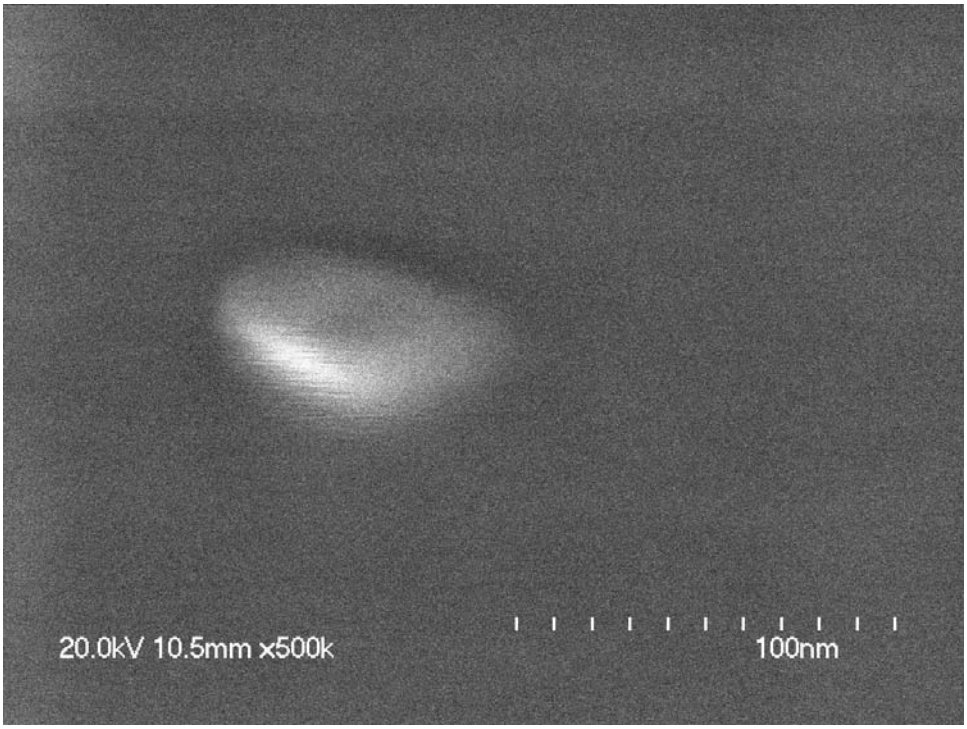

Figure 2.14: SEM of gum arabic coated MNP at 500,000X

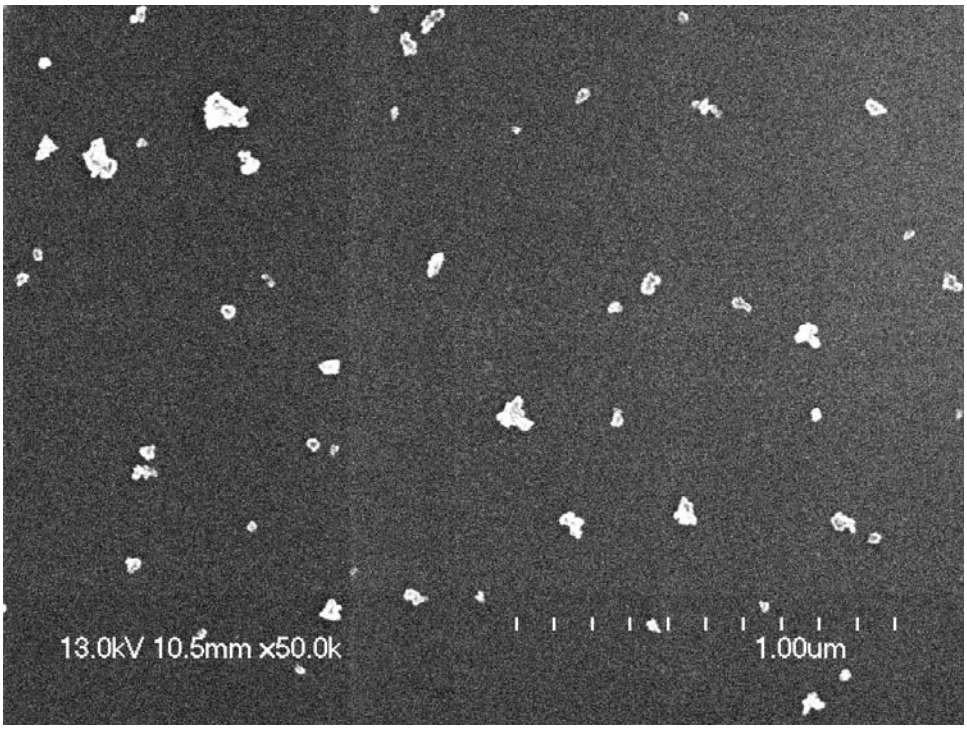

Figure 2.15: SEM of sodium citrate coated MNPs at 50,000X

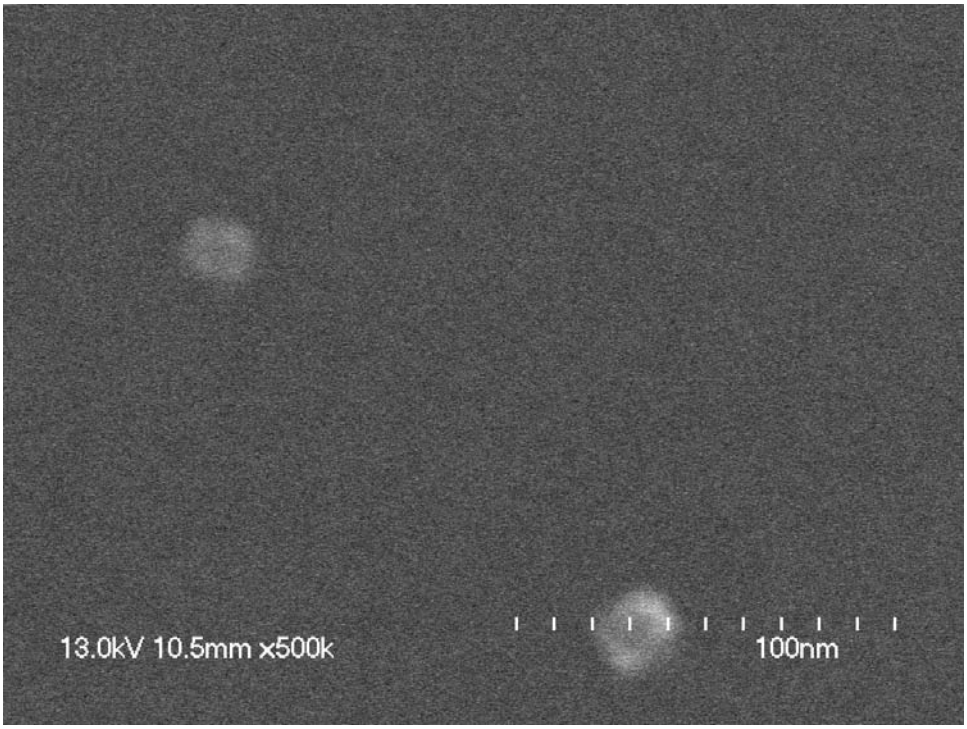

Figure 2.16: SEM of sodium citrate coated MNPs at 500,000X

2.4.3.2.1 Nanoparticle Size Distribution

A scanning electron micrograph from each nanoparticle system was analyzed by Scandium image analysis software, manufactured by Olympus. The various sizes of particles present were obtained and plotted. The average particle size for each system was calculated.

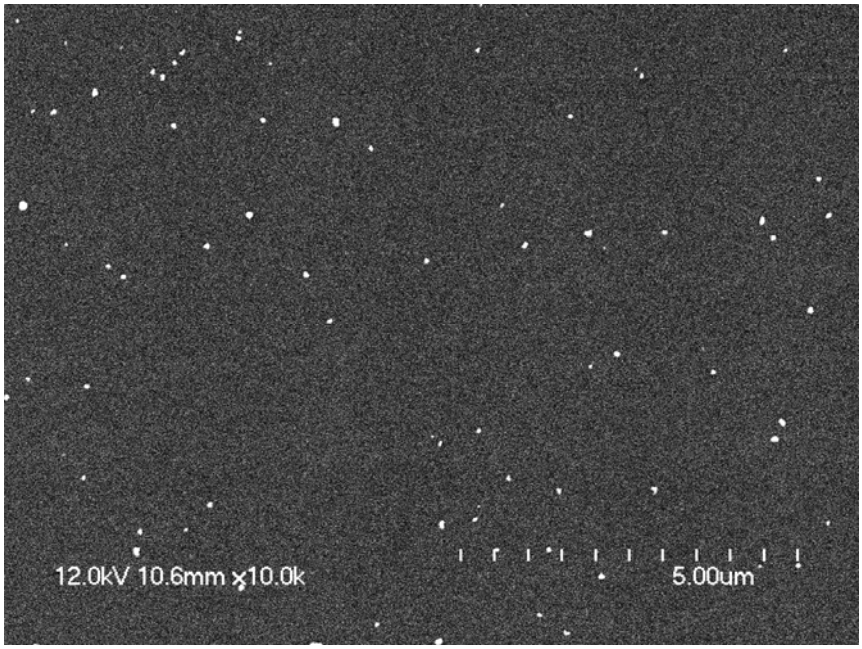

Figure 2.17: SEM of non-coated mnp at 10,000X

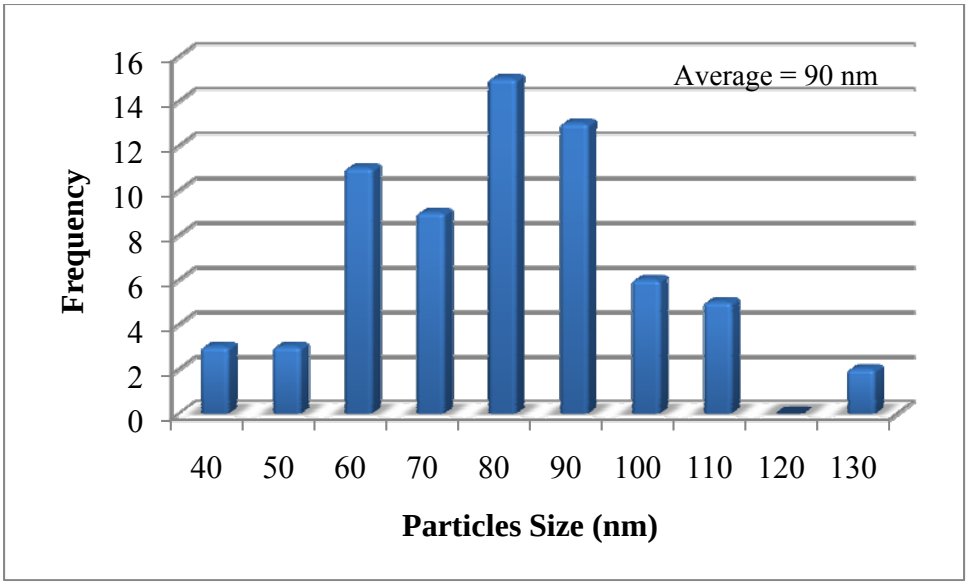

Figure 2.18: Particle cluster size distribution of non coated nanoparticles

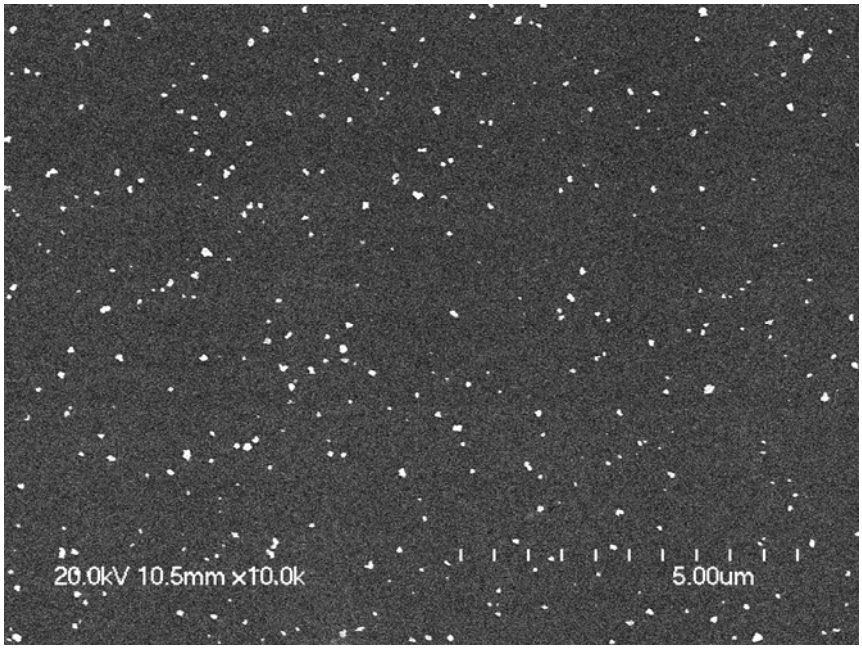

Figure 2.19: SEM of GA coated MNPs at 10,000X

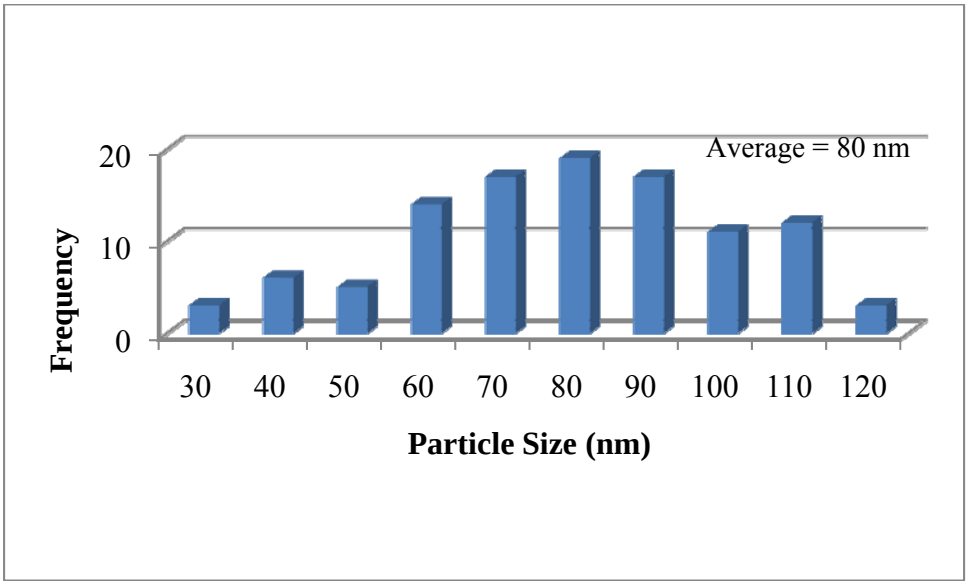

Figure 2.20: Particle cluster size distribution of gum arabic coated nanoparticles

Diluted nanoparticle aliquots were obtained from water solutions and allowed to dry. The average particle cluster sizes resembled the trend observed for the

hydrodynamic diameter of nanoparticles. The non coated nanoparticles had an average particle size of

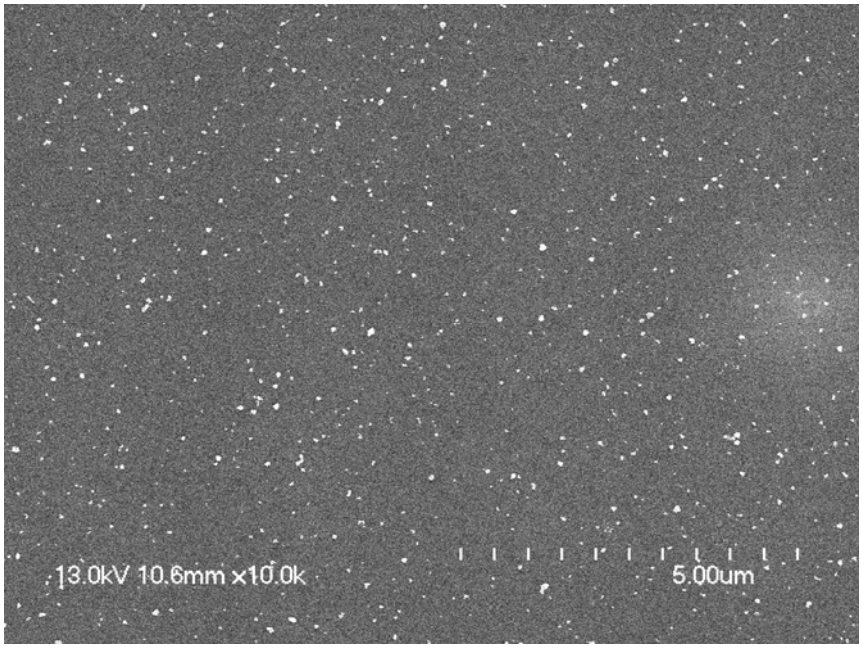

Figure 2.21: SEM of sodium citrate coated mnp at 10,000X

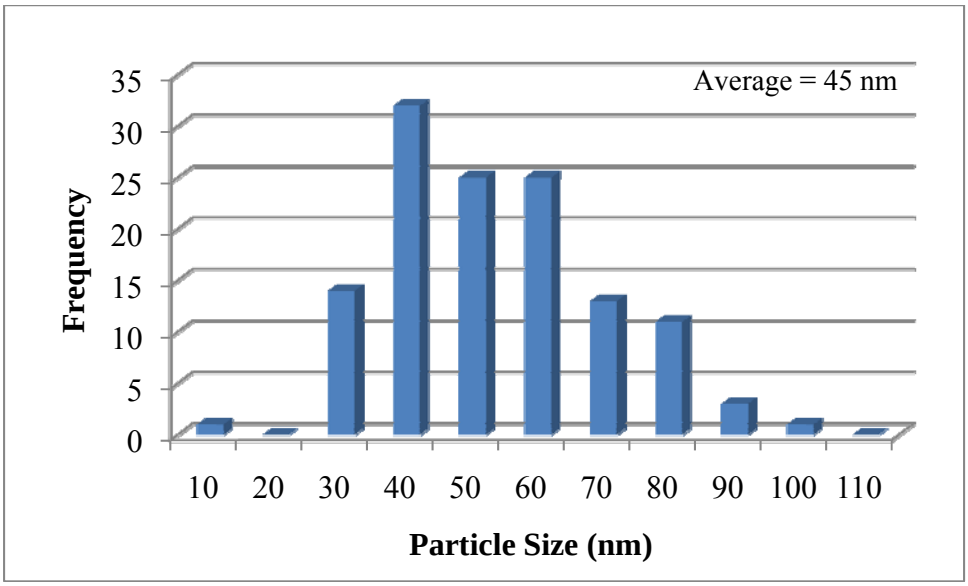

Figure 2.22: Particle cluster size distribution of sodium citrate coated nanoparticles

90 nm, while the gum arabic coated nanoparticles were 80 nm and sodium citrate coated nanoparticles averaged 45 nm. The effect of sodium citrate on the size and stability of nanoparticles in water was clearly demonstrated.

2.4.3.3 Size Measurements by AFM

Nanoparticle size measurements with the Agilent 5500 PicoPlus AFM revealed particle sizes as small as 20nm. Non-coated MNP's exhibited a high degree of agglomeration, and in Figure 2.23 clustering of many smaller sized particles can be seen; however, individual particle sizes could not be deciphered from this tight interaction.

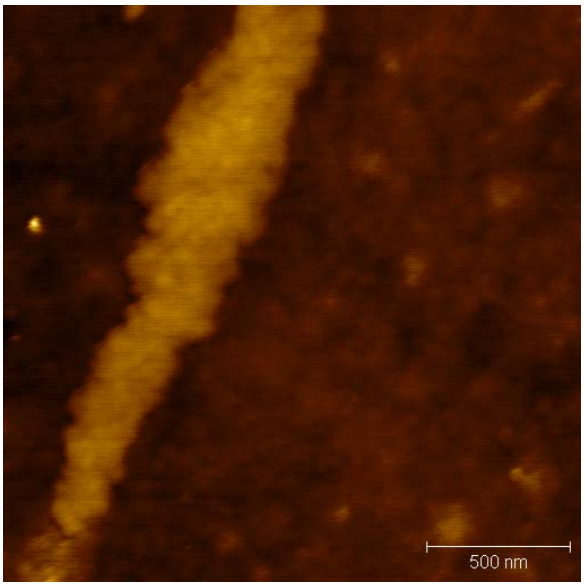

Figure 2.23: AFM of non-coated MNP's

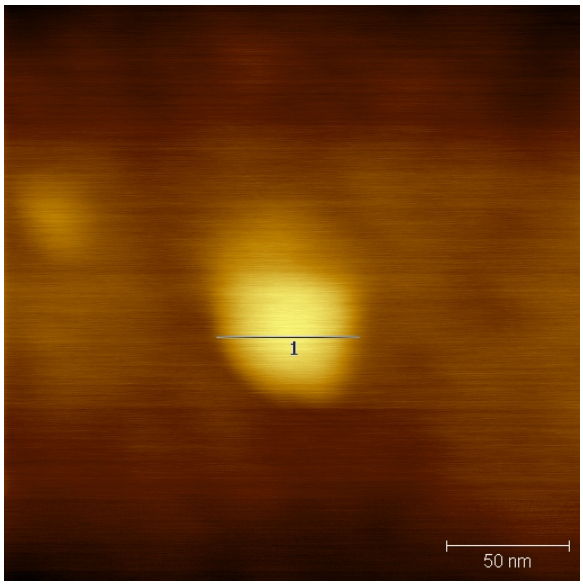

Figure 2.24: AFM of a 50 nm gum arabic coated MNP

A 50 nm gum arabic coated nanoparticle was clearly shown by AFM in Figure 2.24, while sodium citrate coated nanoparticles of the same size were captured by AFM in Figure 2.25. As a secondary source for size measurements of nanoparticles, AFM confirmed the size measurements obtained by SEM.

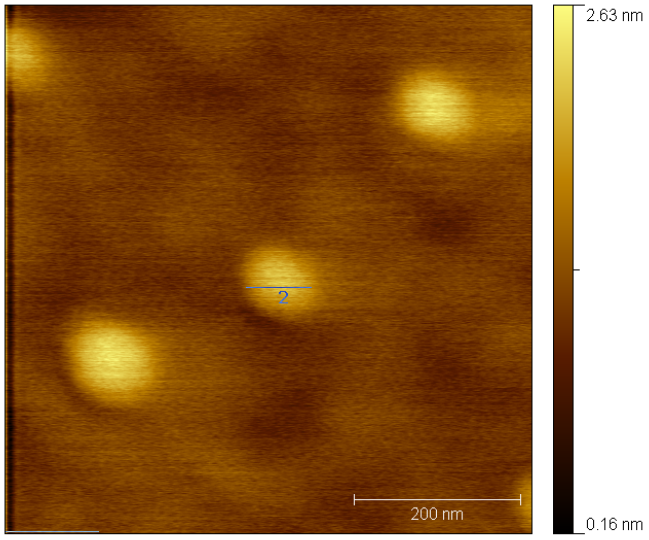

Figure 2.25: AFM of sodium citrate coated MNP's

2.4.3.4 Hydrodynamic Diameter Measurements in water and media by Malvern Zetasizer

The hydrodynamic diameters of surface modified magnetite nanoparticles dispersed in water were compared to the hydrodynamic diameters of particles under the same treatment conditions dispersed in cell nutrient media. Three sample groups were analyzed based on the surface characteristics of the nanoparticles with the following capping agents, non-coated (NC), sodium citrate (SC), and gum arabic (GA). The numerical values of the hydrodynamic diameters are provided in tables below, while the change in diameter over time is displayed in graphs below.

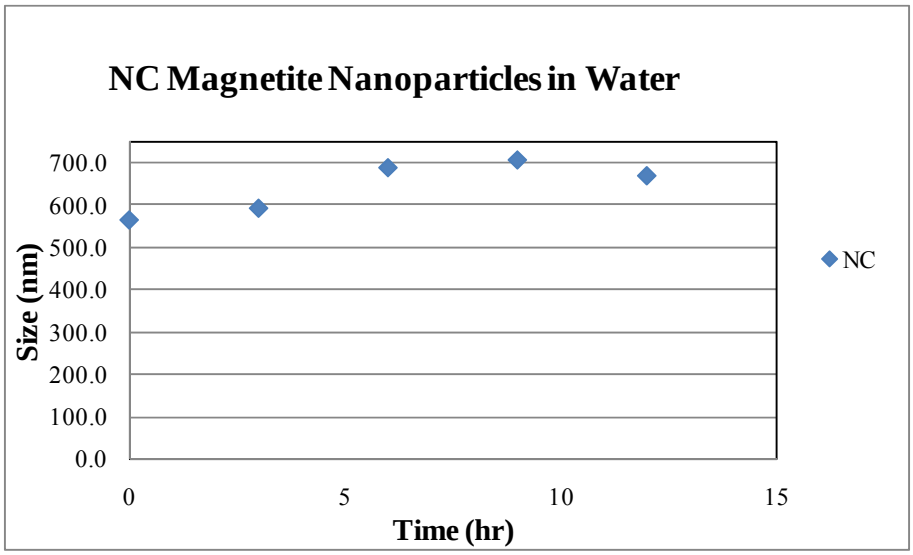

Figure 2.26: Size measurements over time of non-coated magnetite nanoparticles in water

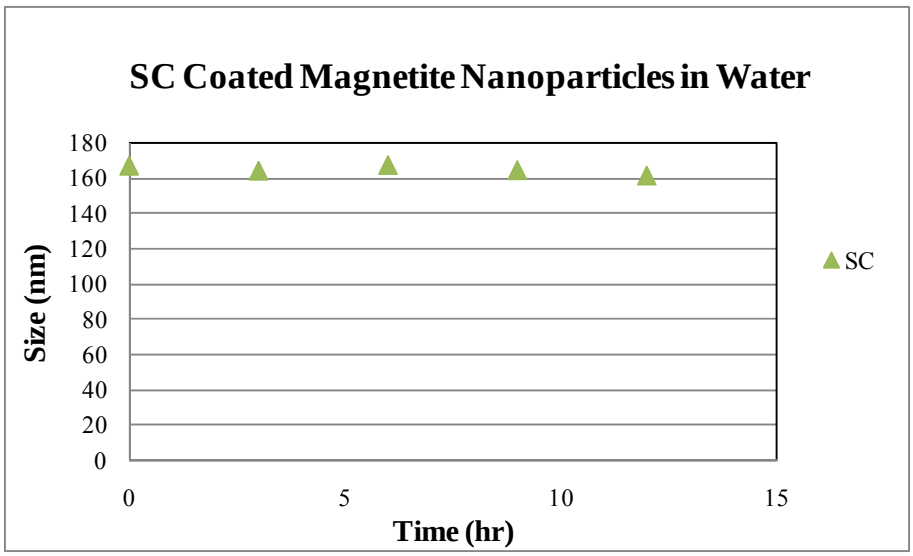

Figure 2.27: Size measurements of sodium citrate coated magnetite nanoparticles in water

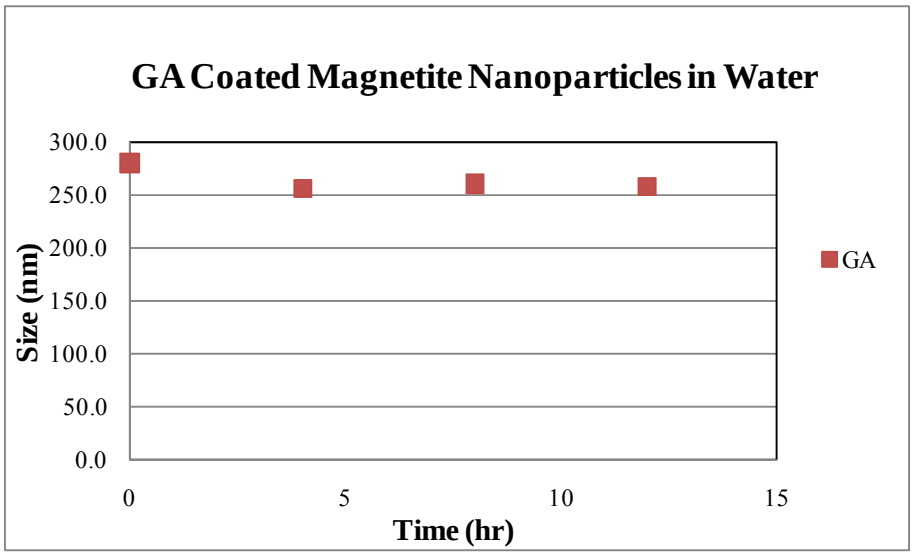

Figure 2.28: Size measurements over time of gum arabic coated magnetite nanoparticles in water

The impact of stabilizing agents, gum arabic and sodium citrate on MNP size in water versus cell nutrient media was investigated. The average hydrodynamic diameters for non-coated MNP over a 12 hour time period ranged from 564 to 708 nm. The size

range of gum arabic coated MNP was minimal, 280 to 258 nm. The largest particles were evident at the start of the analysis and the particle size quickly began to stabilize to approximately 258 nm after 12 hours. The SC-coated MNP remained stable during the same time period. Deviation between 167 nm and 161 nm supports sodium citrate as the better stabilizer in water as compared to gum arabic and non-coated MNPs.

The same particles dispersed in cell nutrient media exhibited a different phenomenon. The smaller more stable SC-coated MNPs became the larger and more unstable system, which ranged in size from 730 nm to 360 nm. The non-coated MNPs in RPMI decreased in size, and ranged from 379 nm to 288 nm. The sodium citrate and non-coated MNP cell nutrient media systems demonstrated a flipped behavior as compared to the same particles solvated in water. The hydrodynamic diameter of gum arabic coated MNPs in RPMI did not deviate much from the gum arabic coated MNPs in water, but actually showed a slight decrease in size. The hydrodynamic diameter ranged from 264 nm to 229 nm.

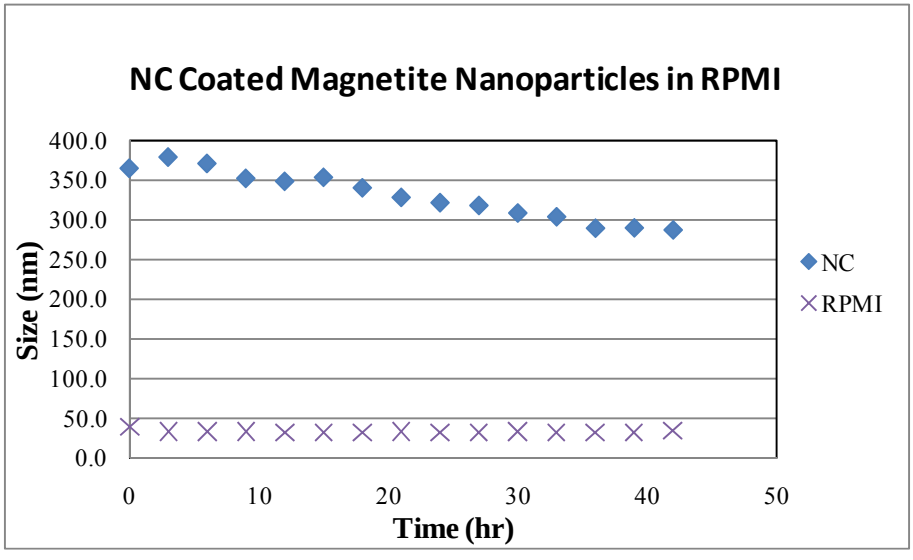

Figure 2.29: Size measurements over time of non-coated magnetite nanoparticles in media

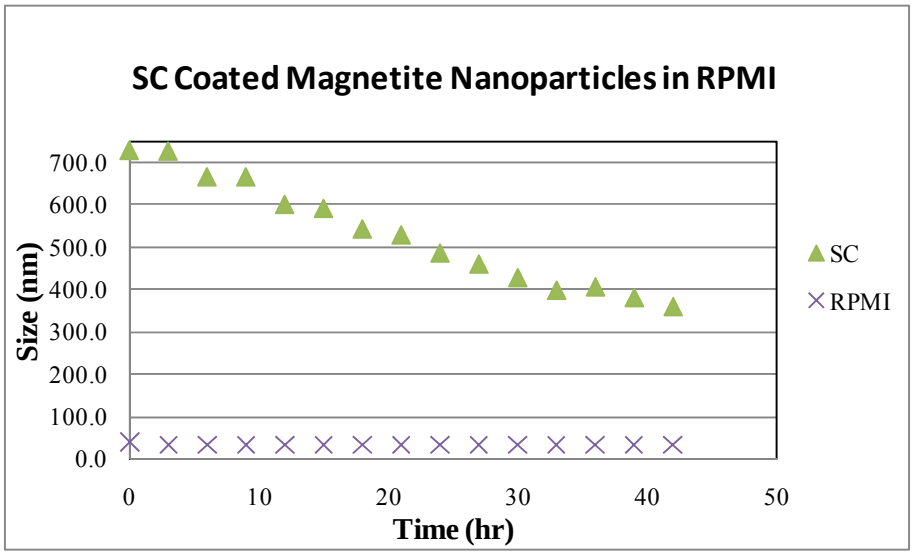

Figure 2.30: Size measurements over time of sodium citrate coated magnetite nanoparticles in media

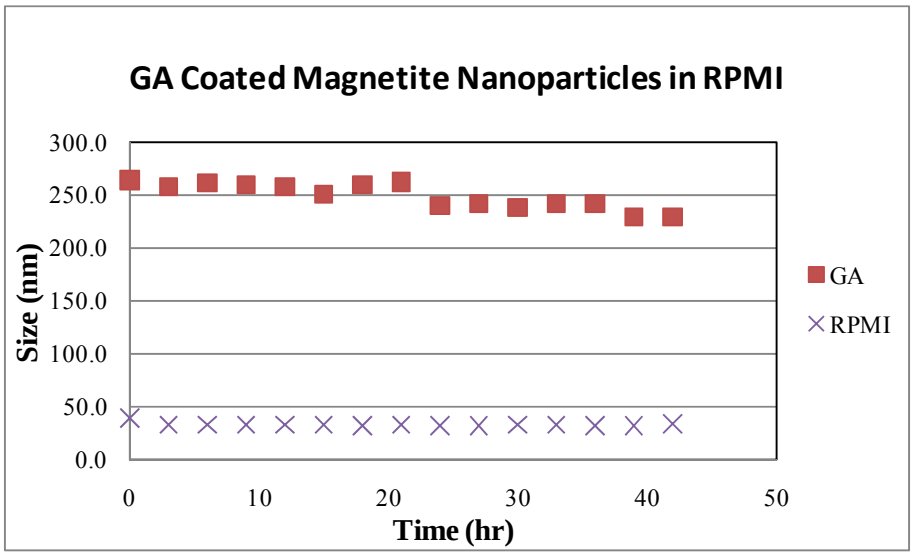

Figure 2.31: Size measurements over time of gum arabic coated magnetite nanoparticles in media

2.4.4 Colloid Stability of Magnetite Nanoparticles in Water vs. Media

In order to accurately report the physical and chemical changes that magnetite nanoparticles undergo in solution over time, stability investigations were conducted in concert with size measurements. Two analytical techniques, specifically by spectrophotometric analysis were simultaneously conducted, (1) temporal change in the resonance light scattering is capable of capturing minuscule changes in the physical and chemical nature of the nanoparticles and (2) size distribution of particles over time. Additionally, the volumetric distribution of the average particle size was chosen as the phenomenon of interest because this type of analysis provided a more detailed and accurate depiction of the polydispersity of the colloidal system than an intensity distribution of the average particles size.

The positioning of the emission detector 90^0 from the excitation pathway avoids the detection of incidence light and allows the analysis of the scattered light via the defined Rayleigh phenomenon. Using this approach, when a particular wavelength of light is exposed to the colloidal solution, Rayleigh scattering occurs depending on the concentration of the analyte. However, within a specific wavelength range, enhanced scattering occurs. This enhancement in scattering behaves linearly with the concentration of particles/analyte in solution. Based upon the size of the nanoparticles of interest, Rayleigh scattering best describes the scatter behavior of the nanoparticle systems of this work

2.4.4.1 In water

The non coated magnetite nanoparticles showed evidence of self assembly in the absence of stabilizing agents. This phenomenon has been well documented among

magnetic nanoparticles. The difference in stable and non-stable dispersions can be seen in Figure 2.32 where sodium citrate coated MNPs provide a dark colored solution (A), while the other two MNP systems had deviated (B) and (C). The lighter colored (GA MNPs) to almost clear (NC MNPs) aqueous mediums depict particles which were falling out of solution.

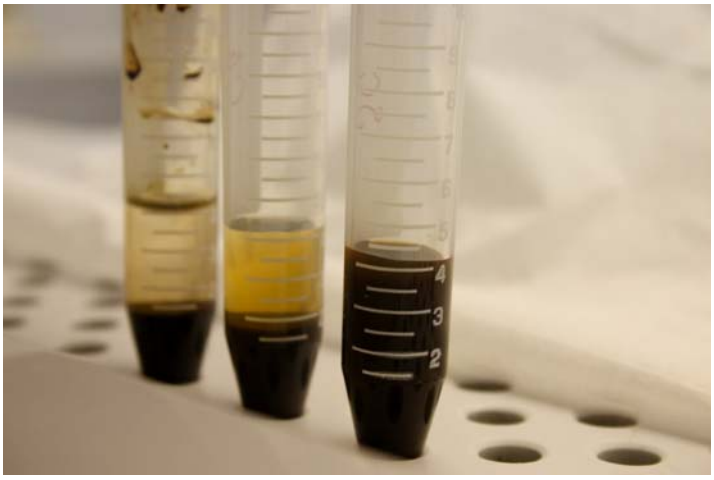

Figure 2.32: Colloidal stability of magnetite nanoparticles in water after 18 hours. (A) sodium citrate coated MNP, (B) gum arabic coated MNP, and (C) non-coated MNP

2.4.4.1.1 Non-Coated MNP's in Water

Upon investigation of the colloidal stability of the non-coated nanoparticles in water, a general increase in the particle size distribution was noted over a period of 12 hours. Analysis of the data obtained from the resonance light scattering of these particles, depicted an initial increase in scattering intensity for the initial 20 hrs. This phenomenon, when observed for a further 24 hrs showed a subsequent decrease in scattering intensity. This scattering trend is typical for multi-dispersed colloidal systems. In these systems, particles of multiple sizes exist. Therefore, as the particles interact with

incident light, a large degree of backscattering occurs because of inter-mingling among larger particles and smaller particles, thus decreasing the amount of detected scattered light. However, as time progresses, the generally less stable larger particles precipitate from the colloidal matrix leaving the smaller, more stable particles in suspension. The smaller particles were then able to exhibit the well documented linear dependence of scatter intensity with particle size. These observations were further corroborated via analysis of the volumetric distribution of aqueous dispersed non-coated magnetite particles. These data depicted an overall tri-modal distribution pattern with three distinct particle size ranges; 580 nm, 5400 nm, and 94 nm over a 12 hour time period. However, during this time period a general decrease in the percentage of larger particles was observed. Extrapolation of the particle size data would lead to the conclusion that as time progresses, the percentage of larger particles in the colloidal matrix would tend to zero, as they would eventually precipitate from solution (as seen in Figure 2.34). This hypothesis is corroborated by the extended light scattering analysis which indicated an initial increase and a subsequent decrease in light scattering. These two phenomenon represent the initial precipitation of larger particles followed by the general destabilization of the entire system respectively.

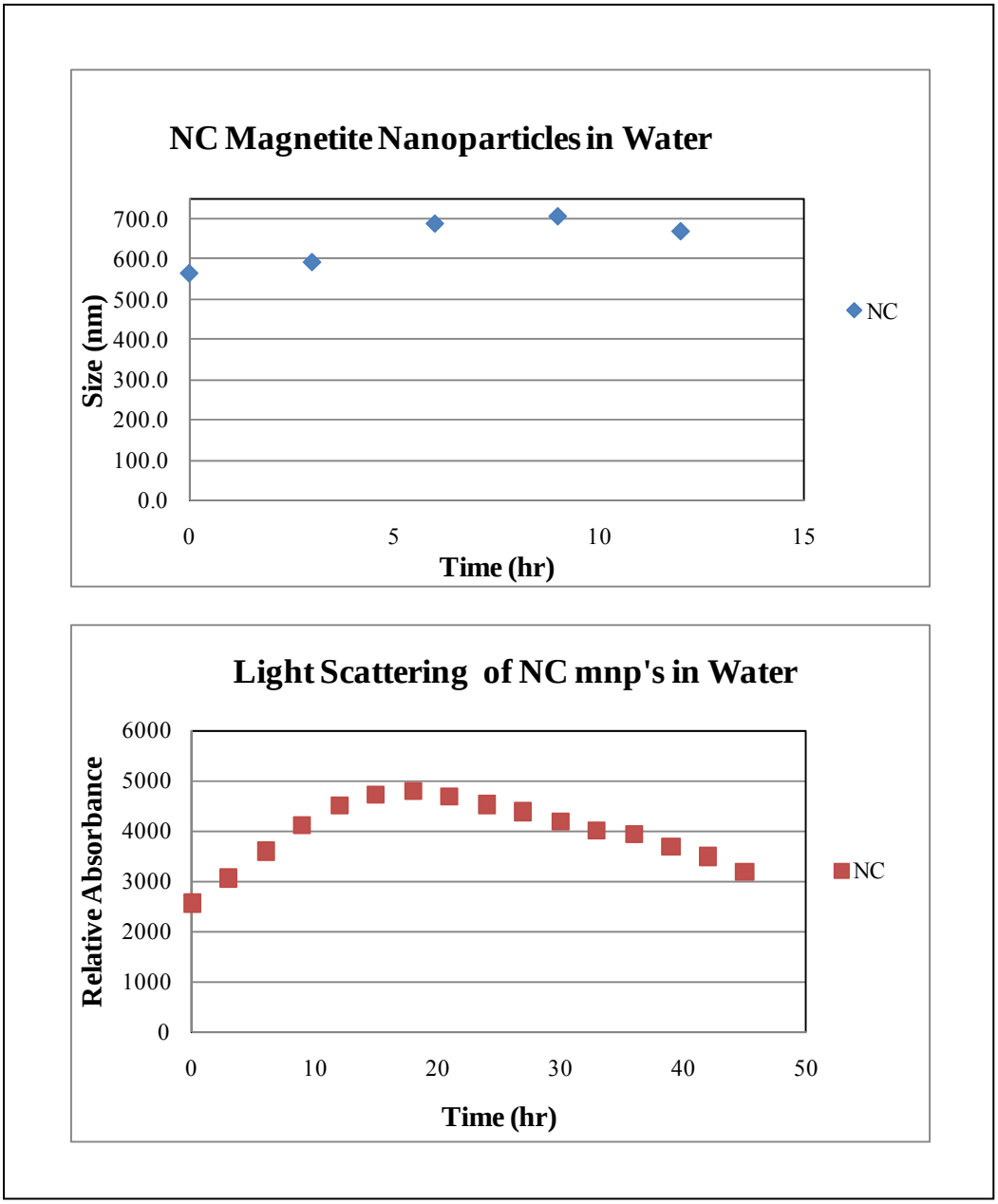

Figure 2.33: Stability analysis, temporal size measurements (top), and light scattering (bottom) of non-coated magnetite nanoparticles in water.

Particle Size Distribution (PSD)			
	NC, water		
	diameter	vol%	time
peak1	580.7	70	0
peak2	5680	23.2	
peak3	94.89	6.8	
peak1	600.2	80.3	3
peak2	5005	19.7	
peak3	0	0	
peak1	615	68.6	6
peak2	5024	27	
peak3	129.8	4.4	
peak1	601.4	68	9
peak2	4923	32	
peak3	0	0	
peak1	564.4	72.4	12
peak2	5040	27.6	
peak3	0	0	

Table 2.2: Particle size distribution by volume of non-coated magnetic nanoparticles in water.

2.4.4.1.2 Gum Arabic Coated MNP's in Water

The hydrodynamic diameters of gum arabic coated MNPs did not fluctuate much, and the particle size distribution can be described as bi-modal. Two different size categories were present, however the volume percent for the larger size particles gradually decreased to 2.5% over the 24 hour period. The smaller particles became the majority. The light scattering curve depicts the dynamic change in particle size which

was observed by the detector. The greater quantities of larger particles were present at the start of the analysis and their impact was manifested in the descending light scattering curve as seen in Figure 2.34. The negative sloping trend represented the increase in population of smaller particles in solution, since larger particles scatter more light than smaller particles.

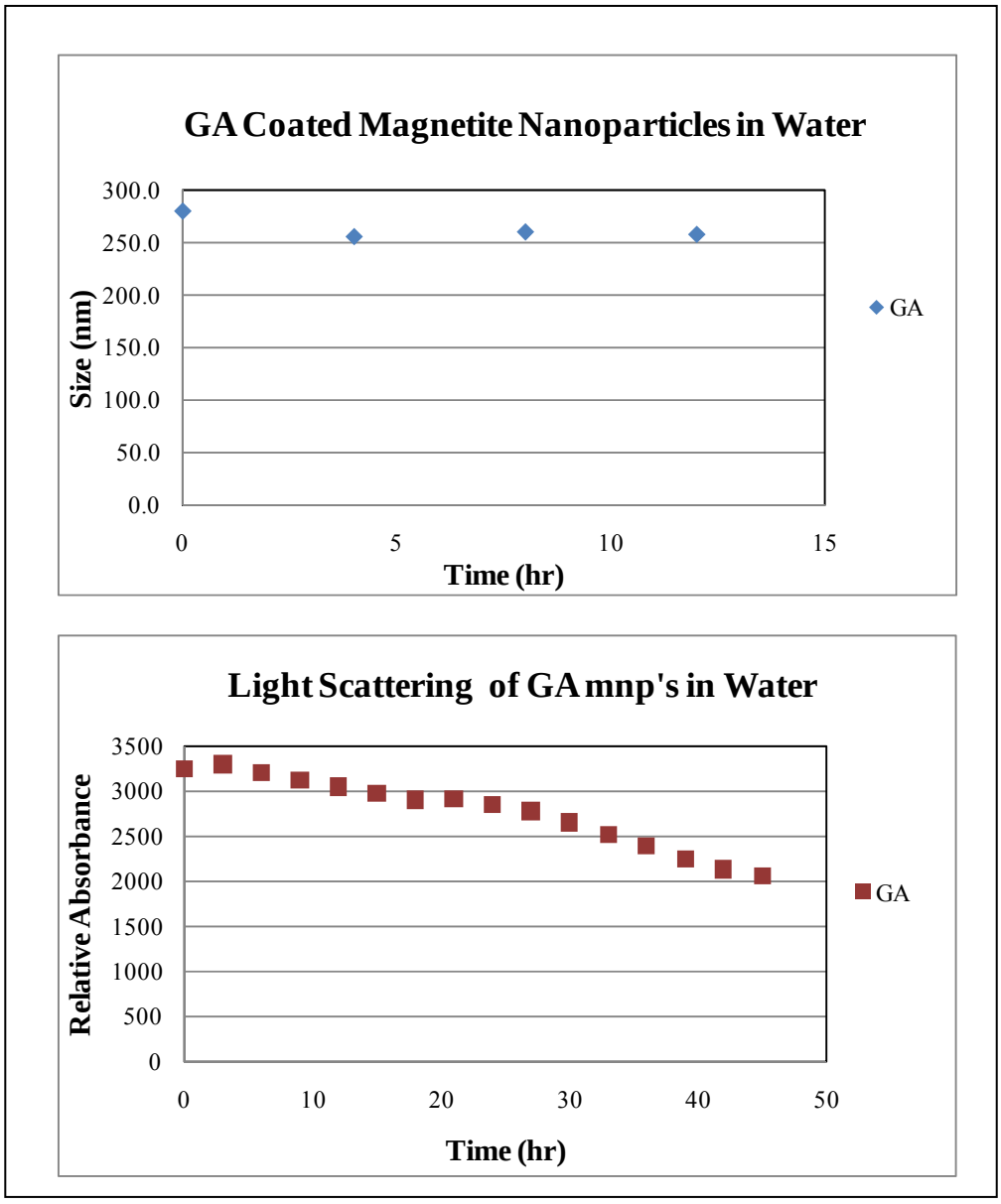

Figure 2.34: Stability analysis, temporal size measurements (top), and light scattering (bottom) of gum arabic coated magnetite nanoparticles in water.

Particle Size Distribution (PSD)			
	GA, water		
	diameter	vol%	time
peak1	309.1	82.9	0
peak2	121	17.1	
peak3	0	0	
peak1	265.9	82.9	4
peak2	4825	17.1	
peak3	0	0	
peak1	254	68.9	8
peak2	680.7	31.1	
peak3	0	0	
peak1	364.7	78	12
peak2	148.6	22	
peak3	0	0	

Table 2.3: Particle size distribution by volume of gum arabic coated magnetic nanoparticles in water.

2.4.4.1.3 Sodium Citrate Coated MNP's in Water

The sodium citrate MNPs consistently provided hydrodynamic diameters within 160 – 167 nm. The light scattering data complimented the trend of consistency, without much deviation. The particle size distribution also supports a fairly uniform system.

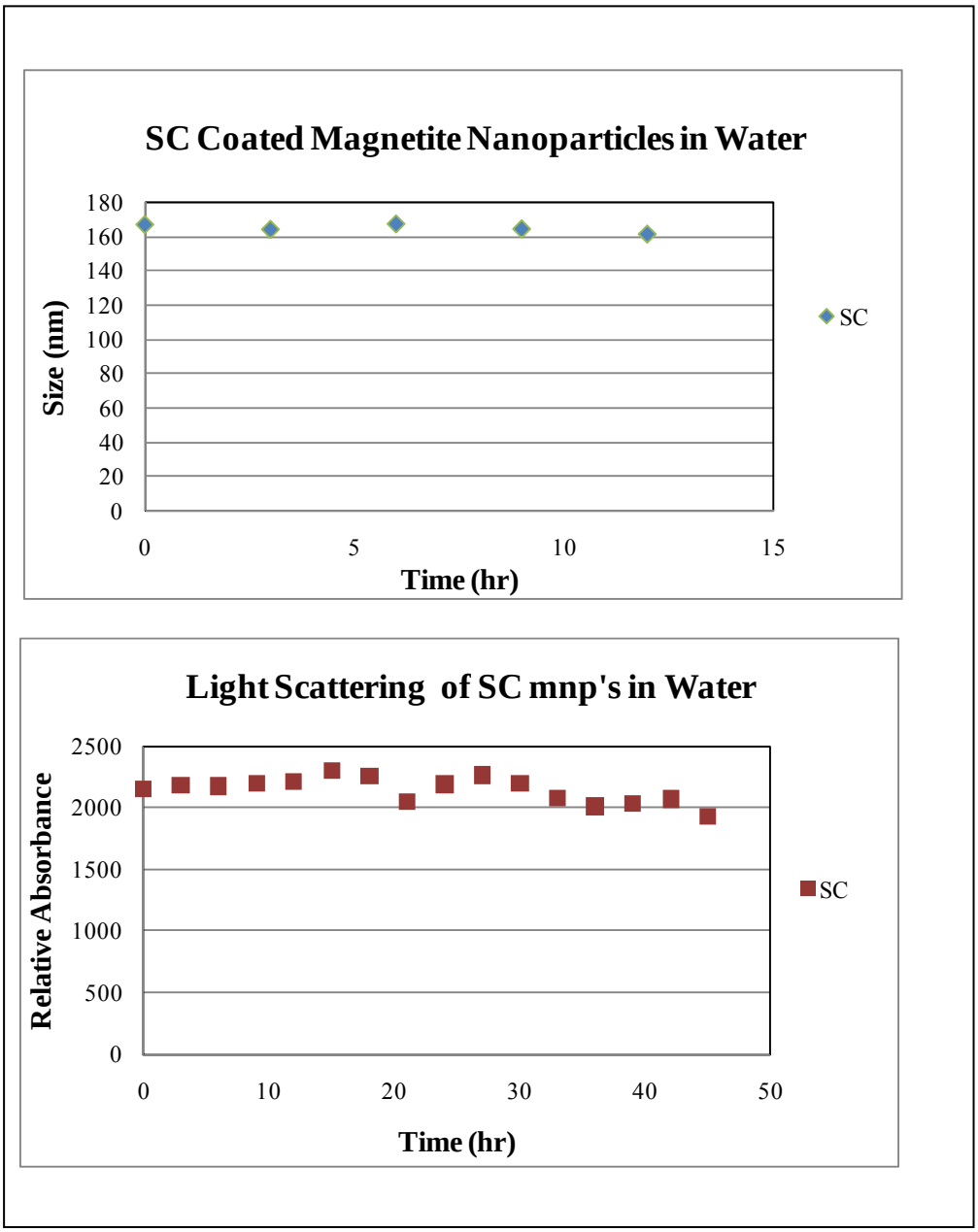

Figure 2.35: Stability analysis, temporal size measurements (top), and light scattering (bottom) of sodium citrate coated magnetite nanoparticles in water.

Particle Size Distribution (PSD)			
	SC, water		
	diameter	vol%	time
peak	184.5	95	0
peak	4771	5	
peak	0	0	
peak	192.5	100	3
peak	0	0	
peak	0	0	
peak	212.6	70.1	6
peak	52.56	29.9	
peak	0	0	
peak	191.2	100	9
peak	0	0	
peak	0	0	
peak	182.1	100	12
peak	0	0	
peak	0	0	

Table 2.4: Particle size distribution by volume of sodium citrate coated magnetic nanoparticles in water.

2.4.4.2 In RPMI

The six well plates displayed in Figure 2.36 contained prostate cancer cells (du-145) which were exposed to various concentrations (50, 10, 7.5, 5, 2.5) $x10^{16}$ of MNP's for 48 hours. The degree of opaqueness or color variability corresponding to the concentration of MNP's in RPMI media, and the colloidal stability can be observed in Figure 2.36. Normal prostate cells were treated in the same fashion.

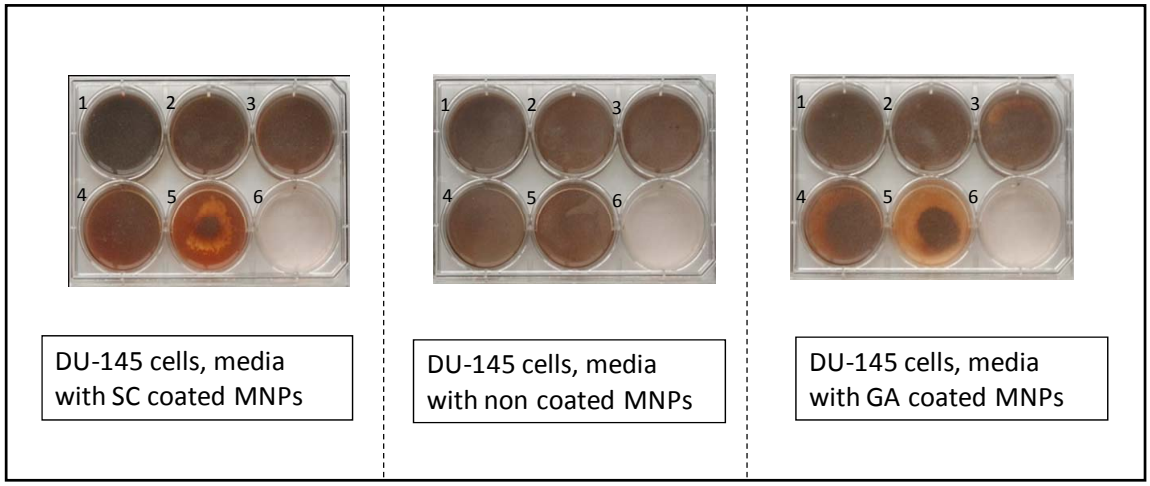

Figure 2.36: Nutrient media (RPMI 1640) which contains different concentrations of MNP's in prostate cell culture

2.4.4.2.1 Non coated MNP's in RPMI Media

There were larger particles in the first 10 hours of size and light scattering analysis of non-coated nanoparticles. Larger particles scatter more light, as compared to smaller particles. The size and light scattering curves show .a decrease in size after the first 10 hours, Figure 2.37. As the particle size began to decrease, the scatter intensity also decreased. The initial large scale particle measurements may be demonstrative of nanoparticle complexation with particular ingredients of the RPMI media. Upon appropriate time for chemical degradation of the media components, the particle size

decreased. Explanation of this decrease in particle size may be representative of delayed release of various initially formed complexes. The observed phenomenon was not indicative of particle agglomeration, but supports the activity of formation, then settlementation.

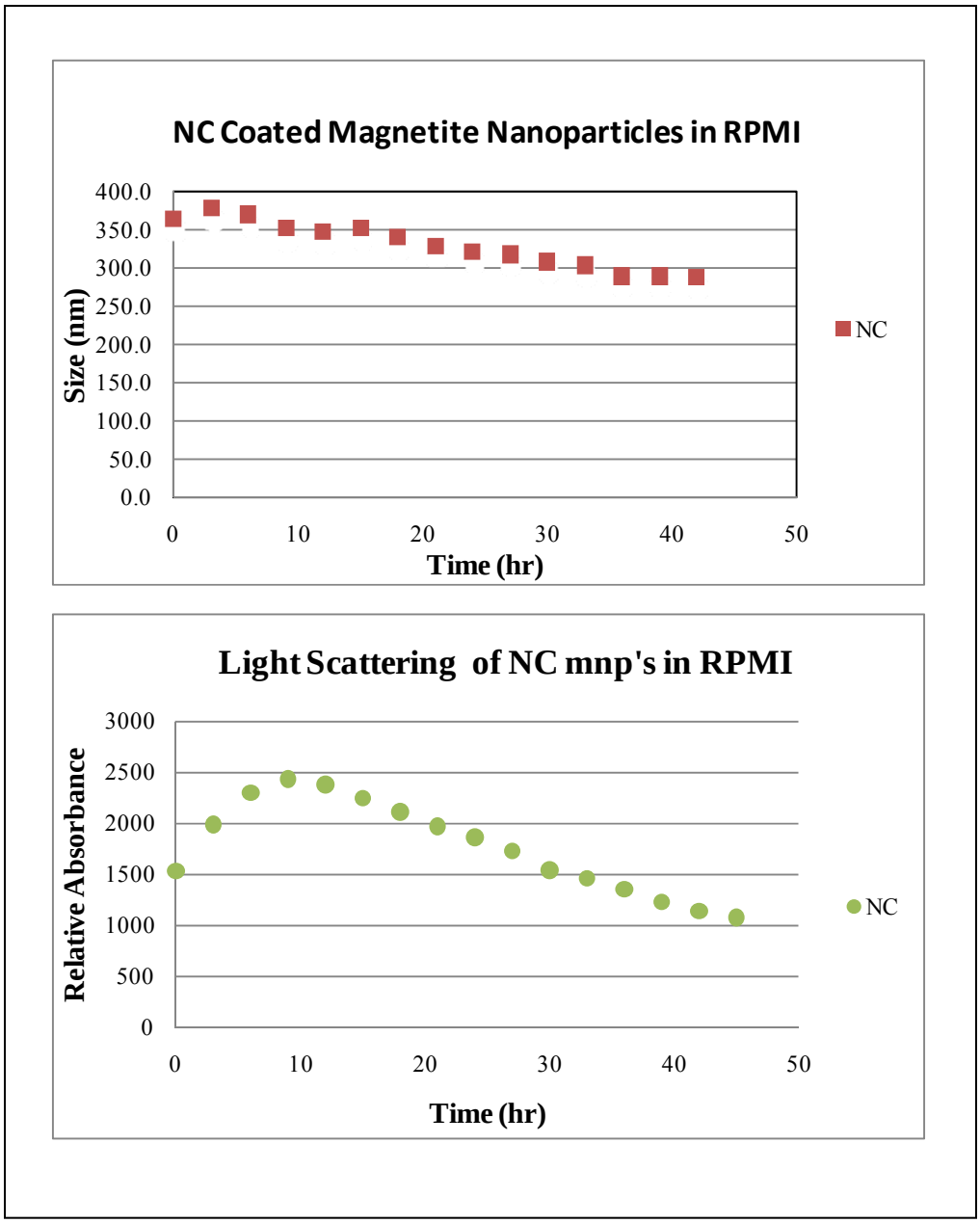

Figure 2.37: Stability analysis, temporal size measurements (top), and light scattering (bottom) of non-coated magnetite nanoparticles in media.

Particle Size Distribution (PSD)			
	NC, media		
	diameter	vol%	time
peak1	360.4	61.9	0
peak2	709	38.1	
peak3	0	0	
peak1	454	90.9	3
peak2	4770	9.1	
peak3	0	0	
peak1	456.4	93.3	6
peak2	5025	6.7	
peak3	0	0	
peak1	462.5	94.5	9
peak2	4493	5.5	
peak3	0	0	
peak1	471.2	98.5	12
peak2	4789	1.5	
peak3	0	0	
peak1	493	100	15
peak2	0	0	
peak3	0	0	
peak1	448.2	100	18
peak2	0	0	
peak3	0	0	
peak1	425.8	97.6	21
peak2	5211	2.4	
peak3	0	0	
peak1	433.2	100	24
peak2	0	0	
peak3	0	0	
peak1	440.8	100	27
peak2	0	0	
peak3	0	0	
peak1	425.5	100	30
peak2	0	0	
peak3	0	0	
peak1	408.5	100	33
peak2	0	0	
peak3	0	0	
peak1	409	95.6	36
peak2	59.23	4.4	
peak3	0	0	
peak1	363.6	100	39
peak2	0	0	
peak3	0	0	
peak1	365.1	100	42
peak2	0	0	
peak3	0	0	

Table 2.5: Particle size distribution of non-coated mnp in RPMI media obtained with Malvern Zetasizer.

2.4.4.2.2 Gum Arabic Coated MNP's in RPMI Media

Gum arabic coated nanoparticles demonstrated excellent particle stability in RPMI media. The size revealed a slow decrease in size (260 – 235 nm) over the 48 hour analysis period. Gum arabic is a long chain polynomial. The interaction between this molecular structure of gum arabic and the ingredients of the RPMI media were favorable.

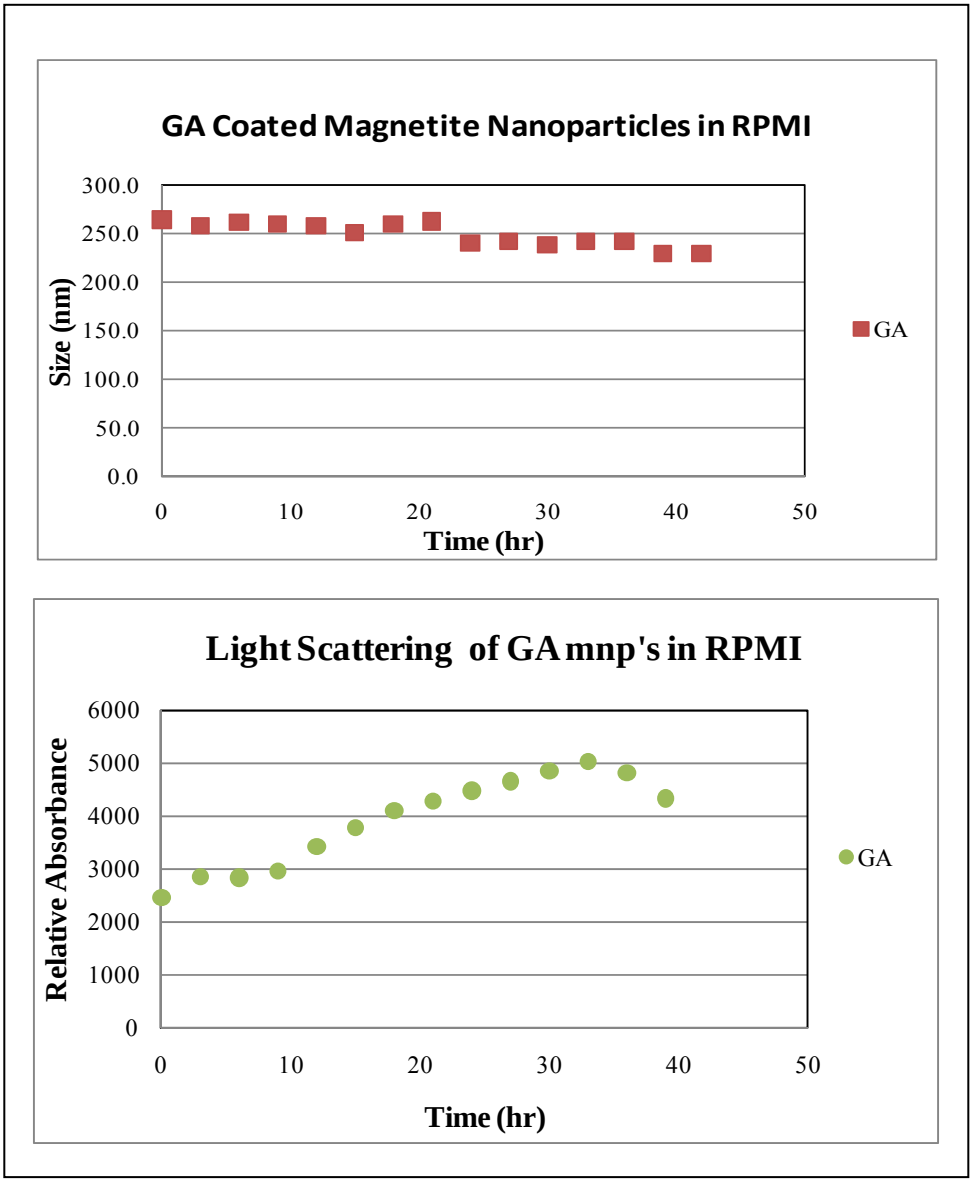

Figure 2.38: Stability analysis, temporal size measurements (top), and light scattering (bottom) of gum arabic coated magnetite nanoparticles in media.

Particle Size Distribution (PSD)			
	GA, media		
	diameter	vol%	time
peak1	363.8	94.1	0
peak2	4732	5.9	
peak3	0	0	
peak1	307.8	95.2	3
peak2	5307	4.8	
peak3	0	0	
peak1	327.1	92.1	6
peak2	5065	7.9	
peak3	0	0	
peak1	330.9	94.6	9
peak2	5060	5.4	
peak3	0	0	
peak1	356.7	100	12
peak2	0	0	
peak3	0	0	
peak1	330	100	15
peak2	0	0	
peak3	0	0	
peak1	385	87.2	18
peak2	34.32	12.8	
peak3	0	0	
peak1	352.8	100	21
peak2	0	0	
peak3	0	0	
peak1	318.8	100	24
peak2	0	0	
peak3	0	0	
peak1	322.2	100	27
peak2	0	0	
peak3	0	0	
peak1	327.5	100	30
peak2	0	0	
peak3	0	0	
peak1	327.5	100	33
peak2	0	0	
peak3	0	0	
peak1	335.3	100	36
peak2	0	0	
peak3	0	0	
peak1	330.6	100	39
peak2	0	0	
peak3	0	0	
peak1	308.1	100	42
peak2	0	0	
peak3	0	0	

Table 2.6: Particle size distribution of gum arabic coated mnp in RPMI media obtained with Malvern Zetasizer

2.4.4.2.3 Sodium Citrate Coated MNP's in RPMI Media

Sodium citrate coated nanoparticles revealed a totally different interaction in RPMI media as compared to its highly stable state in water. The size distribution over the 48 hour period dramatically dropped. The particles initially formed large complexes with the components of the media (see Appendix B), then decreased in size. The 720 nm particles settled out of solution or dissociated from the formed complexes over time to become 375 nm in size.

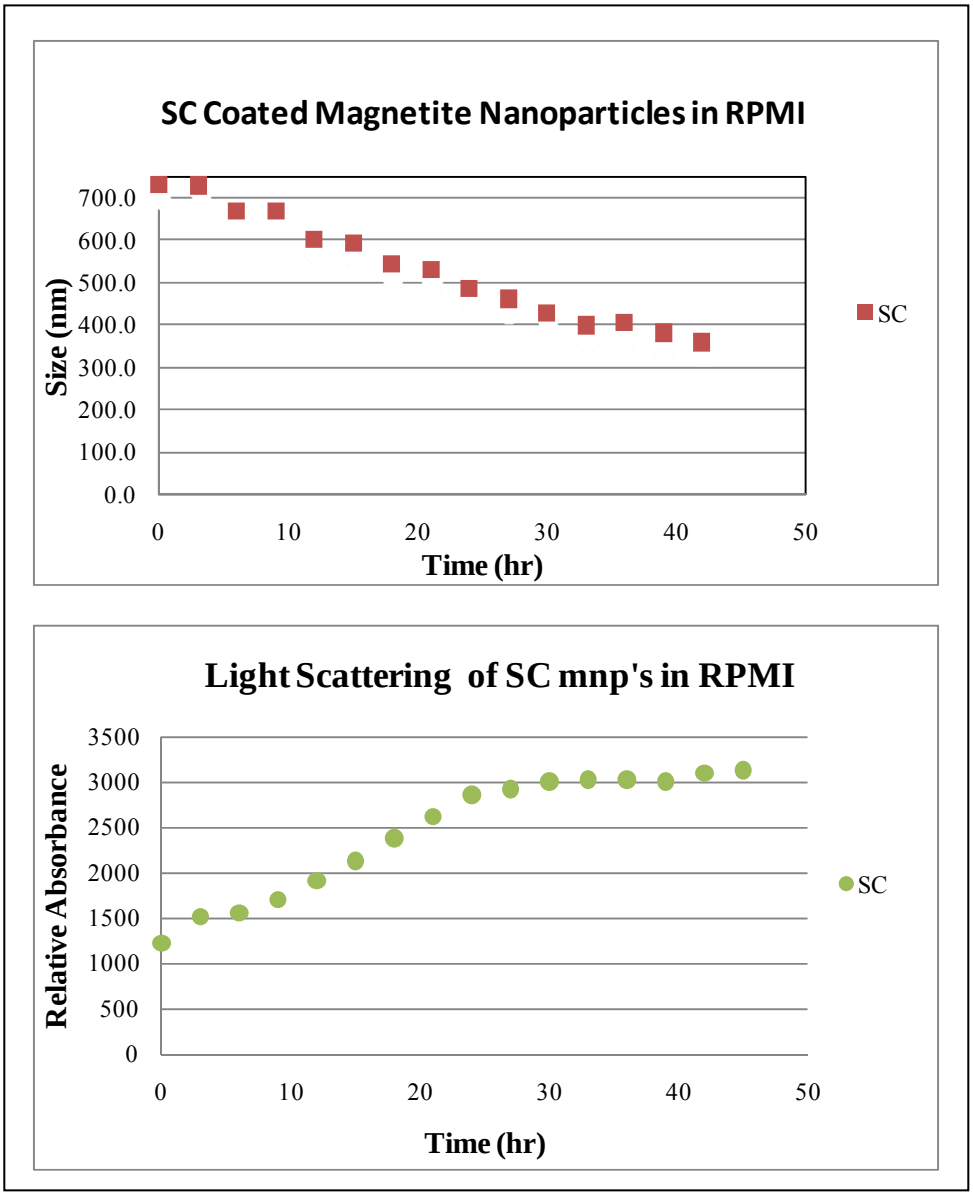

Figure 2.39: Stability analysis, temporal size measurements (top), and light scattering (bottom) of sodium citrate coated magnetite nanoparticles in media.

Particle Size Distribution (PSD)			
	SC, media		
	diameter	vol%	time
peak1	682.6	87.4	0
peak2	4960	12.6	
peak3	0	0	
peak1	929.5	88	3
peak2	248	12	
peak3	0	0	
peak1	742.1	100	6
peak2	0	0	
peak3	0	0	
peak1	778.3	94.4	9
peak2	178.5	5.6	
peak3	0	0	
peak1	714.9	100	12
peak2	0	0	
peak3	0	0	
peak1	686	100	15
peak2	0	0	
peak3	0	0	
peak1	634.5	100	18
peak2	0	0	
peak3	0	0	
peak1	571.9	93.3	21
peak2	5039	6.7	
peak3	0	0	
peak1	577.4	100	24
peak2	0	0	
peak3	0	0	
peak1	555.9	100	27
peak2	0	0	
peak3	0	0	
peak1	535.3	100	30
peak2	0	0	
peak3	0	0	
peak1	522.6	100	33
peak2	0	0	
peak3	0	0	
peak1	495.3	96.6	36
peak2	5333	3.4	
peak3	0	0	
peak1	500.4	100	39
peak2	0	0	
peak3	0	0	
peak1	487.6	100	42
peak2	0	0	
peak3	0	0	

Table 2.7: Particle size distribution of sodium citrate coated mnp in RPMI media obtained by Malvern Zetasizer

Summary of size and stability results

Measurement of particle size by the Malvern Zetasizer is computed based on the resulting defracted pattern as particles scatter light. The scatter pattern is dependent on the size and speed at which it travels. Therefore, the average hydrodynamic diameter is a computed summary. Particle size obtained by the Malvern Zetasizer are measurements made in aqueous medium. The hydrodynamic diameter may demonstrate larger diameter readings in comparison to measurements made by other techniques in which the sample is dry (without liquid).

The combination of size and dynamic light scattering data reveals the phenomena of particle interaction and degree of colloid stability in two separate aqueous mediums. Recognizable differences between water and cell nutrient media as solventss for the mnp's was observed. Magnetic nanoparticles dispersed in water showed an increase in the hydrodynamic diameter from approximately 160 nm to 700 nm. Self assembly of non-coated mnp's produced agglomerates that reached 700 nm over a two day period. The hydrodynamic diameter decreased greatly with the addition of capping agents. Gum arabic helped to reduce the diameter to approximately 300 nm while sodium citrate further reduced it to about 160 nm. The dynamic light scattering curves provided additional information and enhanced the evaluation of the mnp colloid interaction. The absorbance values of the dynamic light scattering curves corresponds to the amount of scattered light received by the detector which correlates with the size and density of particles in the detection region. As the size increases, the amount of light scatter increases The individual particle size of magnetite particles formed during the synthesis

process was obtained and verified for the true particle size with Vibrating Sample Magnetometry, TEM, and AFM.

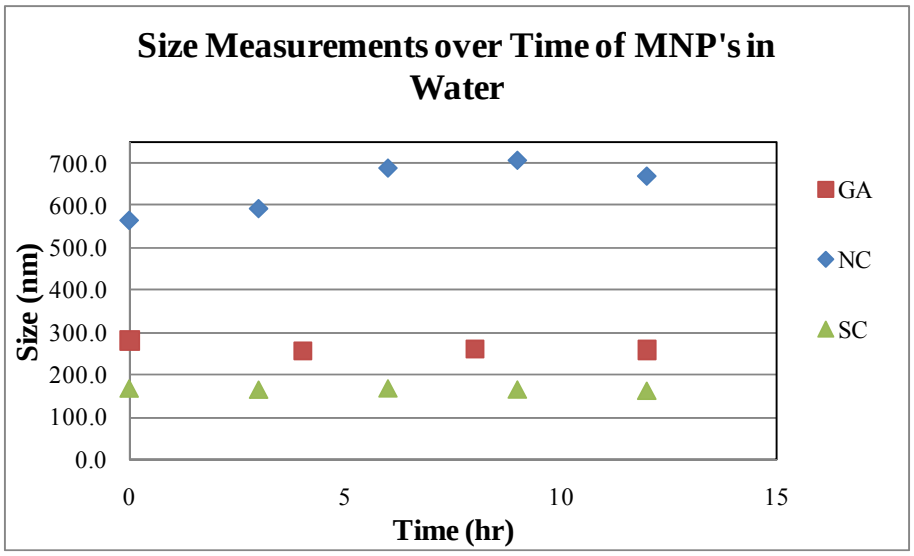

Figure 2.40: Temporal size measurements of modified mnps in water; Gum Arabic (GA), Sodium Citrate (SC) and Non-Coated (NC) obtained with Malvern Zetasizer

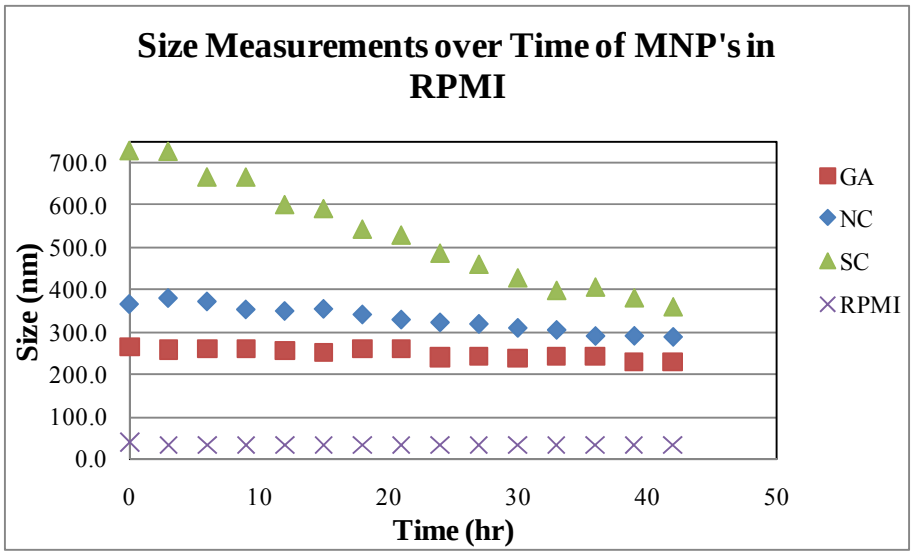

Figure 2.41: Temporal size measurements of modified mnps in RPMI; Gum Arabic (GA), Sodium Citrate (SC) and Non-Coated (NC) obtained with Malvern Zetasizer

In order to further corroborate the stability of the mnps over time, light scattering investigations were conducted. Size measurements of mnp's in water were collected over a period of 12 hours. These initial readings were assessed every 30 minutes in order to capture any small interval changes. The size and consistency over this time period provided information on how to proceed. The NC mnp's were the largest particles, 600-700 nm and fluctuated in size over time. The SC mnp's were the smallest particles, 160 nm and most consistent while the GA mnp's were a little larger, 250-280 nm and fairly consistent in that size range over time. The SC mnp's seemed to be the more attractive coating since it provided the smallest particles and remained consistent over time. The same particles in cell nutrient media however, did not perform as desired. Since the particles would be presented to prostate cells in growth media, the nanoparticle interactions with the ingredients of the growth media was a more pertinent analysis. The size and stability of mnp's changed with media as the solvent. The size of the NC MNP's in media were more stable than in water, and demonstrated a small decrease, 300-400 nm over 48 hours.

The hydrodynamic diameters of the NC, GA, and SC coated mnps were affected by the mediums which provided an aqueous environment during analysis. Comparison of water to cell nutrient media as the dispersant for the mnps of this work, revealed the differences among the properties of the prepared nanoparticles. Two of the three nanoparticle systems demonstrated dramatic change in the measured particle sizes. SC mnps increased in size from 164 nm to 532 nm (70%) while, the largest sized particles (NC) in water decreased by nearly 50% when incorporated in cell nutrient media. The GA coated mnps did not demonstrate a change in hydrodynamic diameter irrespective of

the dispersant. The various components of RPMI 1640 (amino acids, vitamins, inorganic salts, and a few other ingredients) are necessary for biological cell maintenance in culture, however these compounds introduce a potential for increase or decrease physical and/or chemical stability. For example, glutamine is the limiting nutrient in media when utilized under standard conditions for cell culture. It has been reported that glutamine is not chemically stable in cell culture media, which could complicate the analysis of experimental data. The chemical decomposition of glutamine produces ammonia and pyrrolidonecarboxylic acid.

Magnetite nanoparticles dispersed in water display a different size distribution as compared to the same particles solvated in nutrient media. Naked, uncoated nanoparticles produced the largest size particles, 645 nm, while the surface modified, gum arabic and sodium citrate particles, exhibited smaller hydrodynamic diameters. Gum arabic reduced the degree of agglomeration and hence decreased the average particle size by 60% to 264 nm. The SC mnp system was even more stabilized as the average hydrodynamic diameter of the particles was reduced by 75% to 164 nm. The observed decrease in size of the coated magnetite nanoparticles was expected since surfactants and capping agents are known to increase the steric hindrance between particles due to the repulsive nature of the surface ligands thereby reducing the degree of particle agglomeration and overall particle size.

2.4.5 Magnetic Properties of Magnetite Nanoparticles

The formation of magnetic magnetite nanoparticles by co-precipitation of Fe2+ and Fe3+ ions generated a distribution of nano-sized particles. Small and large particles

comprised the particle size distribution. The VSM technique has the means to determine both small and large particle distribution. The average small size particle was 5 nm and the average larger sized particles were 35nm.

The saturation magnetization for the synthesized non-coated MNP's of this work was between 60 - 70 emu/g. The saturation magnetization for pure magnetite nanoparticles is about 70 emu/g and increases with the size of nanoparticles present. In bulk, it is about 90 emu/g **(21)**.

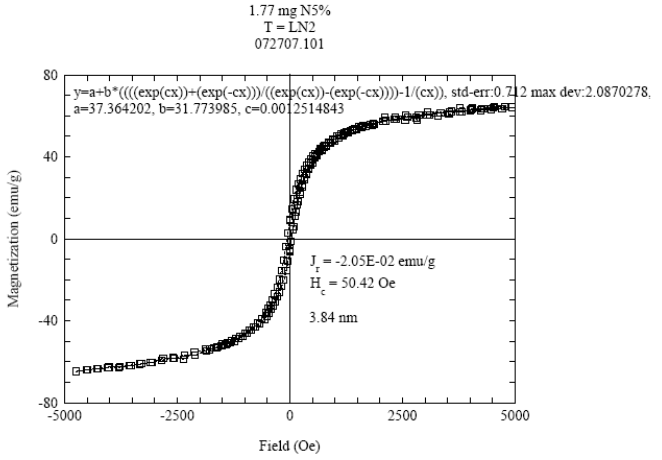

Figure 2.42: Hysteresis Curve for non-coated magnetite nanoparticles

The saturation magnetization for the surface modified nanoparticles was slightly less than that for the non-coated magnetite nanoparticles. The hysteresis curve in Figure 2.43 for sodium citrate coated nanoparticles was approximately 50 emu/g, while it was about 55 emu/g for the gum arabic coated nanoparticles, as seen in Figure 2.44. The magnetic property measurements for each of the three nanoparticle systems were taken at

liquid nitrogen temperature. The magnetic property information obtained for the synthesized nanoparticle systems were in agreement with known published values of magnetite nanoparticles.

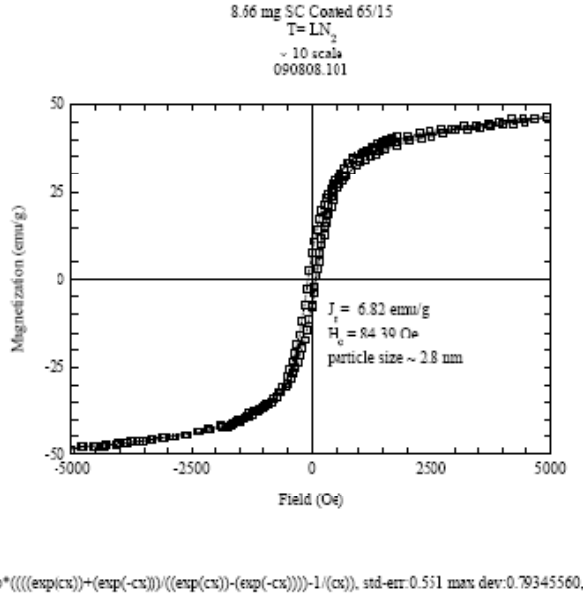

Figure 2.43: Hysteresis curve for sodium citrate coated magnetite nanoparticles

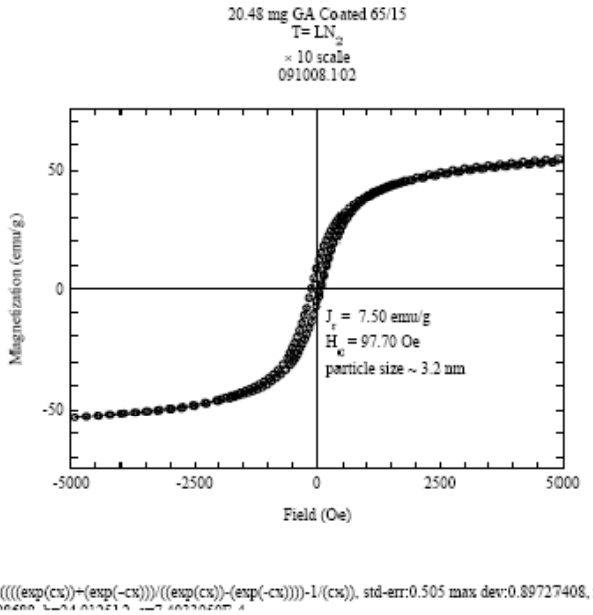

Figure 2.44: Hysteresis curve for gum arabic coated magnetite nanoparticles

CHAPTER 3

EVALUATION OF CELLULAR INCORPORATION OF SUPERPARAMAGNETIC IRON OXIDE NANOPARTICLES

3.1 Abstract

Nanobiotechnology encompasses a wide range of interest involving nano-scaled materials for future biological therapeutics. One aspect of this field involves nanoparticles formed from biocompatible materials which are currently being studied as functionalized carries for delivery, activation, tracking, and/or reporting of biological products or signals. Our particular focus seeks to target and destroy prostate cancer cells. Iron oxide nanoparticles produced by a co-precipitation method yield dry particles with an average size of 35nm in solid form and colloid stable sodium citrate coated iron oxide nanoparticles approximately 150nm in aqueous medium. Nanoparticles were allowed to co-exist with prostate cells for 48 hours under sterile conditions. Normal prostate cells were utilized as controls. Four distinct forms of analysis provided evidence of prostate cell uptake of iron oxide nanoparticles. Transmission Electron Microscopy, videography with a charge-coupled device (CCD) camera, and cellular re-alignment due to iron filing confirmed the presence of iron oxide nanoparticles within the intracellular space of prostate cells, while quantification via VSM determined the average amount of

nanoparticles per cell. Upon the 48 hour exposure period, properly washed prostate cells were resuspended in fresh culture medium. At 400X magnification, the cells demonstrated magnetic interaction and dynamic movement in response to a neodymium (1.5 dia. x .25 inch) magnet which was placed 1.25 inches from the center of view in four distinct locations (N, S, E, W). These data reveal proof of concept and will lead to hyperthermia experiments for evidence of subsequent cell death.

3.2 Introduction

The idea of magnetic induction heating of superparamagnetic nanoparticles to achieve localized hyperthermia in tissue is very interesting and has great therapeutic potential, but is no longer novel **(21) (22)**. The combination of biology with physics and engineering presents many challenges since non-biological materials require high levels of energy to destroy harmful cells which are tightly intertwined with normal cells. Scientific research has made strides in the area of nanotechnology for therapy but has not reached the level of fine tuning that is required for treatment of cancer in human beings. Recent reports reveal the current status of thermotherapy with nanoparticles on prostate cancer and express the need to further develop the techniques required for safe and precise thermal ablation of carcinoma cells **(23) (24) (26)**. The specific areas include (1) the number of nanoparticles required for cell death without overdose and discomfort to the patient (also referred to as the effective dosage of nanoparticles), (2) the correlated field strength, and (3) the ability to direct nanoparticles to the carcimona cells of interest with effective targeting techniques. A few laboratories outside of the United States including Germany, Slovakia, Japan, and Korea have contributed to the body of work concerning carcinoma cell death by hyperthermia, while the U.S. appears to progress at a

rate slower than most. A German group has created a whole body magnetic field applicator called the MFH 300F and magnetofluid MFL 082AS **(26) (27)**. They have conducted clinical trials and developed a non-invasive method for calculation of the 3-dimensional temperature distribution via computed tomography. Although great advances have been made by this research group, several concerns remain unanswered. Utilizing the method of direct injection has led to suboptimal distribution of nanoparticles; and the required high levels of magnetic field strength brought discomfort to the patients.

3.3 Materials and Methods

3.3.1 Prostate Cells

3.3.1.1 Normal Human Prostate Cells

Normal human prostate cells, WPMY-1 (ATCC number CRL-2852) were purchased from American Type Culture Collection (ATCC) Manassas, VA. The conditions for propagation included regular growth media changes (every 2-3 days) and cell passage at approximately 70% confluence. The cells were maintained in complete RPMI with 10% fetal bovine serum (FBS), 100,000 U/L of penicillin and 100 mg/L of streptomycin. The humidified incubator was regulated at 37˚C and 5% CO_2. Cells were obtained from a 54 year old Caucasian male.

3.3.1.2 Cancer Human Prostate Cells

Human prostate cancer cells, DU 145 (ATCC number HTB-81) were purchased from ATCC (Manassas, VA). The conditions for propagation included regular growth media changes (every 2-3 days) and cell passage at approximately 70% confluence. The

cells were maintained in complete RPMI with 10% fetal bovine serum (FBS), 100,000 U/L of penicillin and 100 mg/L of streptomycin. The humidified incubator was regulated at 37˚C and 5% CO_2. Cells were obtained from a 69 year old Caucasian male.

3.3.2 Experimental Design for Cell Interaction with Nanoparticles

3.3.2.1 Directional Growth during Proliferation

Prostate carcinoma cells (approx. 30,000) were seeded in separate single wells (35 mm round). Within two to three days, the cells in culture reached approximately 60% confluence. The normal RPMI 1640 growth media was replaced with media which contained sodium citrate coated magnetite nanoparticles. One hundred microliters of the nanoparticle stock solution was added to 9.9 mL of RPMI media, and 3 mL of this reconstituted nanoparticle/media combination was introduced to the prostate cancer cells in culture. A neodymium magnet was placed beneath the culture dish containing the cells and this media cocktail for 48 hours, as illustrated in Figure 3.1. The cells were viewed under a microscope and video was recorded.

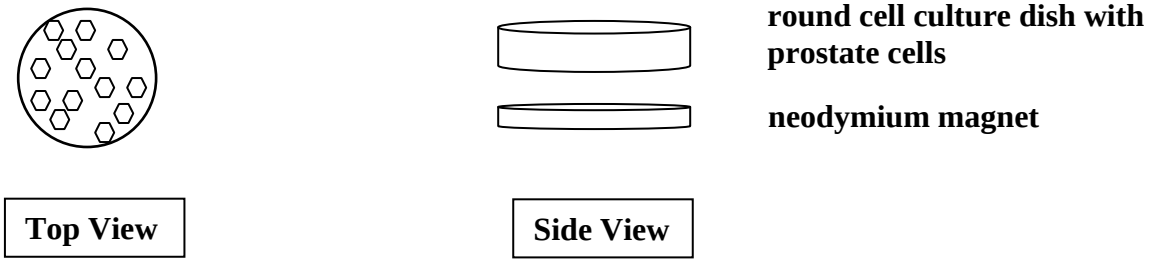

Figure 3.1: Schematic representation of set up for magnetic influence on cell proliferation

3.3.2.2 Cell Motility in Response to Neodymium Magnet Captured by Video

The prostate cells, normal and carcinoma were propagated separately in T-75 flasks. At the time of treatment, the cells were approximately 60% confluent. Twelve milliliters of RPMI growth media with varying concentrations of sodium citrate coated magnetite nanoparticles in the range of 10^4-10^{17} nanoparticles/mL was added to each T-75 flask for comparison of cellular uptake. After 48 hours of cell propagation with magnetic nanoparticles, the process of cell removal involved decanting the media and a wash with 5mL of 1X PBS. To dissociate the adherent cells, 1mL of trypsin/EDTA was added and the flask was incubated for 5 minutes or less at 37˚C. Fresh media (5 mL) was added to the flask to counteract any further degradation of the cells. The cellular suspension was removed from the T-75 flask and added to a clean 15 mL centrifuge tube. It was then centrifuged at 1000rpm for 10 minutes to separate and remove the supernatant along with any extraneous nanoparticles. Fresh media (5mL) was added in order to re-suspend the cells. Two hundred microliters of the well mixed cell suspension was placed on a standard sized glass microscope slide. A neodymium magnetic was strategically placed (north, south, east, west), 7mm from the center field of view, which created a magnetic field of magnitude 0.45 kG. A Nikon microscope (806651, Japan) with a 40X objective was used in concert with a black and white Sony video monitor (model # PVM-122), a charge-coupled device camera CCD100 (DAGE-MTI) and a standard Panasonic DVD recorder (model # DMR-ES20) which captured the dynamic response of the cells containing nanoparticles after experiencing the magnetic field applied due to the presence of the strong magnet.

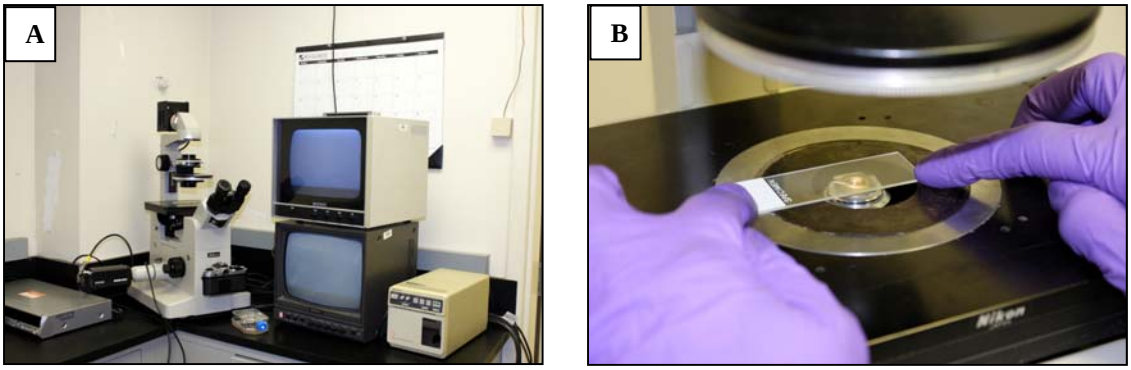

Figure 3.2: Experimental set up for demonstration of cell mobility, (A) microscope and video recording equipment and (B) placement of cells suspension on glass slide

3.3.2.3 Transmission Electron Microscopy (TEM)

Cells within a T-75 flask were treated with media which contained surface modified nanoparticles of a specific concentration; therefore each flask represented an experimental condition. The range of observed nanoparticle concentrations was between $1 \text{ X } 10^4$ and $1 \text{ X } 10^{17}$ nanoparticles per mL. Confirmation by visual observation of magnetite nanoparticles within human prostate cells was performed with transmission electron microscopy (TEM) and required sample preparation before imaging. After the 48 hour treatment/exposure period to magnetite nanoparticles, the treatment media was discarded and 10 mL of FG fixative in 0.2M sodium cacodylate buffer pH 7.4 was added to each T75-flask. The cells remained in fixative overnight. The fixed cells were then scrapped from the surface with a rubber policeman, and collected into 15mL centrifuge tubes. The samples were subsequently washed with 0.2M sodium cacodylate buffer, followed by serial alcohol dehydration (35%, 50%, 75%, 95% and finally in 100% ethanol 3 times @ 10 min each). The specimen were infiltrated using 1:1 spurs with ethanol for 1hr at room temperature, followed by 100 % spurs for 1 hour before they were transferred to capsules and incubated for polymerization. Thick sections (490nm)

of the polymerized pellet were obtained with the Leica microtome until there was indication that the experimental sample was present and available for thin sections. Thin sections (90 microns) were collected on copper grids and stained with uranyl acetate (stain 1) and lead citrate (stain 2) before observation with the Zeiss (Model 10CA) transmission electron microscope.

3.3.3 Cell Viability after 48 Hour Exposure to Magnetite Nanoparticles by MTT and Trypan Blue Exclusion

3.3.3.1 MTT

The cytotoxic effect of magnetite nanoparticles on prostate cancer (DU- 145) and normal prostate (WPMY-1) cells was assessed using MTT assay (ATCC#30-1010K). MTT is a chemical known as 3-(4,5-Dimethylthiazol-2-Yl)-2,5-Diphenyltetrazolium Bromide. It is taken up by cells through the plasma membrane potential and then reduced to formazan by intracellular NAD(P)H-oxidoreductases. The absorbance was determined by a microplate reader. The cells of interest were counted. A 100 µl cell suspension provided 20,000 cells per well in a 96-well plate. The cells were incubated for 24 hours at 37˚C and 5% CO_2 before they were treated with different concentrations of magnetite nanoparticles (0.5×10^{16} - 50×10^{16} particles /ml). There were two controls, cells with normal culture media and culture media only, without cells. The 96 well plate were incubated for 48 hours at 37˚C in the presence of 5% CO_2 followed by washing with 1X PBS before adding medium containing 10% (v/v) of 3mg/ml MTT (Darmani *et al*., 2006). The plates were returned to the incubator for 3-4 hours before aspirating the media and allowing the plates to dry overnight at room temperature. One hundred microliters of a 0.04 N HCl in Isopropanol solution (Storch *et al*., 2004) was added to

each well and incubated at room temperature in the dark for 30 minutes to dissolve the formazan crystals. The absorbance was read at 570 nm wavelength using a microplate reader.

3.3.3.2 Trypan Blue Exclusion

Trypan Blue Exclusion is a method for determination of cell viability in a cell suspension that utilizes blue dye. It is based on the principle that live cells possess intact cell membranes, and have the ability to exclude certain dyes, such as trypan blue, eosin or propidium, while dead cells do not. The experiment involves the mixture of the cell suspension in question with the trypan blue dye. Visual examination with an optical microscope will reveal live cells with clear cytoplasms or dead cells with blue cyctoplasms.

The protocol was conducted as follows, the cell suspension was centrifuged for 5 minutes at 100 x g and the supernantent was discarded. The cell pellet was resuspended in 1 mL of PBS. A mixture of the cells (20 μL) and the dye (2 μL) was created and allow to incubate at room temperature for 3 minutes Ten microliters of the mixture was placed on a hemocytometer and cell counts were recorded. To obtain the total number of viable cells per mL of aliquot, multiply the total number of viable cells by 2 (dilution factor for trypan blue). To obtain the total number of cellsper mL of aliquot, add up the total number of viable and nonviable cells and multiply by 2. Calculate the percentage of viable cells as follows:

Viable cells (%) = (total number of viable cells per mL of aliquot/total number of cells per mL of aliquot) x 100

3.4 Results and Discussion

3.4.1 Dimensional Measurements of Prostate Cells

Prostate cells, normal (WPMY-1) and cancer (DU-145) were cultured separately in standard T-75 cell culture flasks and allowed to propagate for several days. The lengths of the cells were measured with an Olympus light microscope and Sony CCD-iris video camera. The 10X objective was utilized with screen calipers that were calibrated with a sample of known size. The normal prostate cells were 2-3 times larger than the cancer prostate cells. The average prostate cancer cell length was 267.33 nm while the average normal prostate cell length was 83.16 nm.

Length of Measured Cells (μm) x 1.001μm	
WPMY-1	DU-145
262	111
257	56
237	88
278	70
285	72
285	102

Table 3.1: Sizes of prostate cells measured from optical microscope

3.4.2 Cellular Re-alignment in Response to Neodymium Magnet during Proliferation

Prostate carcinoma cells (DU-145) were allowed to divide and expand in the presence of magnetite MNPs. Literature on cellular incorporation of nanoparticles has not shown experimentation such as this. The idea was that successful incorporation of nanoparticles into the cytoplasmic matter of prostate cells would create an effect when a strong neodymium magnet was placed underneath the culture dish of cells. The magnetic interaction between the nanoparticles and the magnet would guide the entire cell and cause it to grow in the direction of the two opposing poles. The thought and driving motivation behind this experimental set up was the expectation of elongated cells in culture. It was designed after a typical general physics experiment which demonstrates iron filing. It was interesting to observe the change in cell morphology in response to the magnetic nanoparticles and the guiding forces of the applied magnet. Uni-directional growth of prostate cancer cells can be seen in Figure3.3B, and compared to the morphology of the controls, one without nanoparticles, and without magnetic field (Figure 3.3A), while the negative control was without nanoparticles, but with the magnetic field (Figure3.3C).The cells responded in the expected manner; however, the question of whether the cells were influenced from the exterior or interior of the cell membrane became the burden of proof.

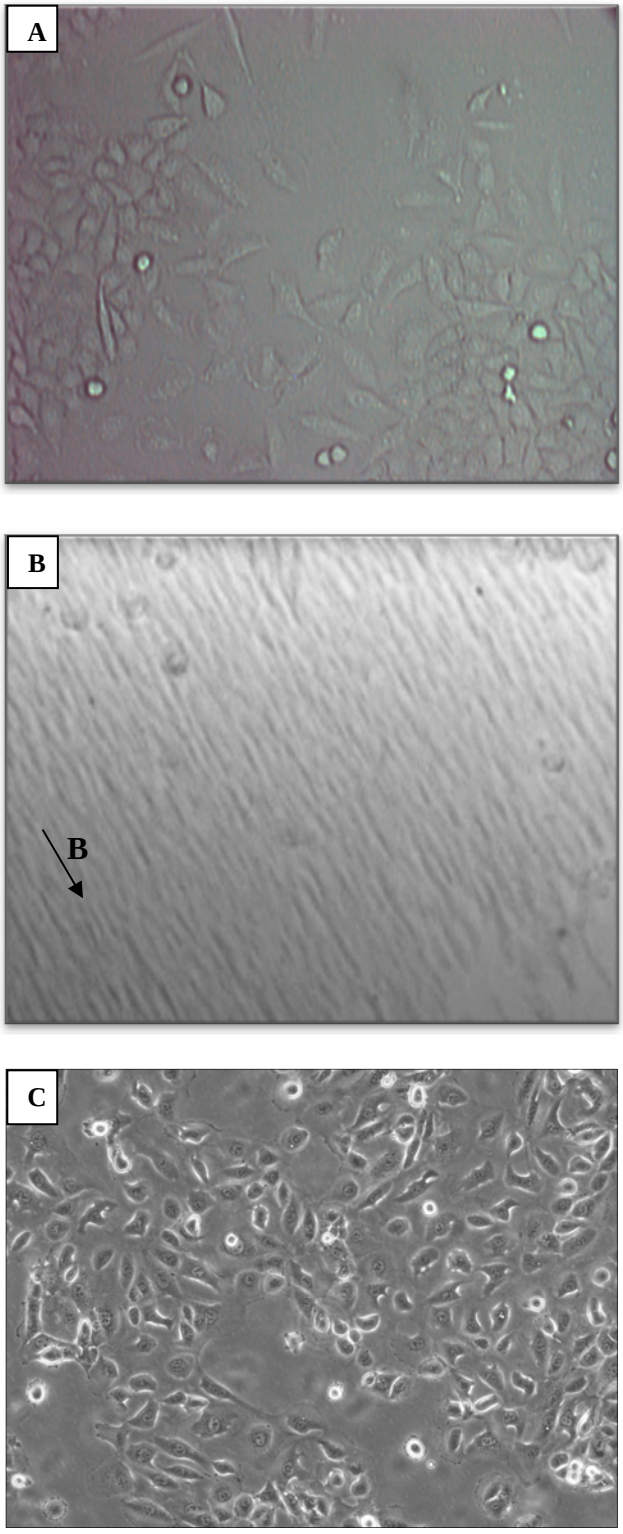

Figure 3.3: Cellular re-alignment in response to a magnetic field. The micrographs demonstrate re-directed growth due to MNP uptake among propagating prostate cancer cells, (A) normal growth, (B) directional growth, (C) unaffected growth

3.4.3 Magnetic Responsiveness of Prostate Cells Containing Magnetite Nanoparticles

Prostate cells (normal and cancer) which were cultured in media with magnetite nanoparticles for approximately 48 hours, demonstrated the ability to receive and take up nanoparticles. Cell displacement was recorded and evidence of magnetic responsiveness was noted. Still images from video has been captured and displayed in Figure 3.3. Upon placement of a neodymium magnet on the west side of the glass slide, a single prostate cancer cell entered the field of view from the top. It rotated and temporarily stopped when the greatest mass of nanoparticles interacted with the magnetic field and resultantly led it to the left, out of the field of view.

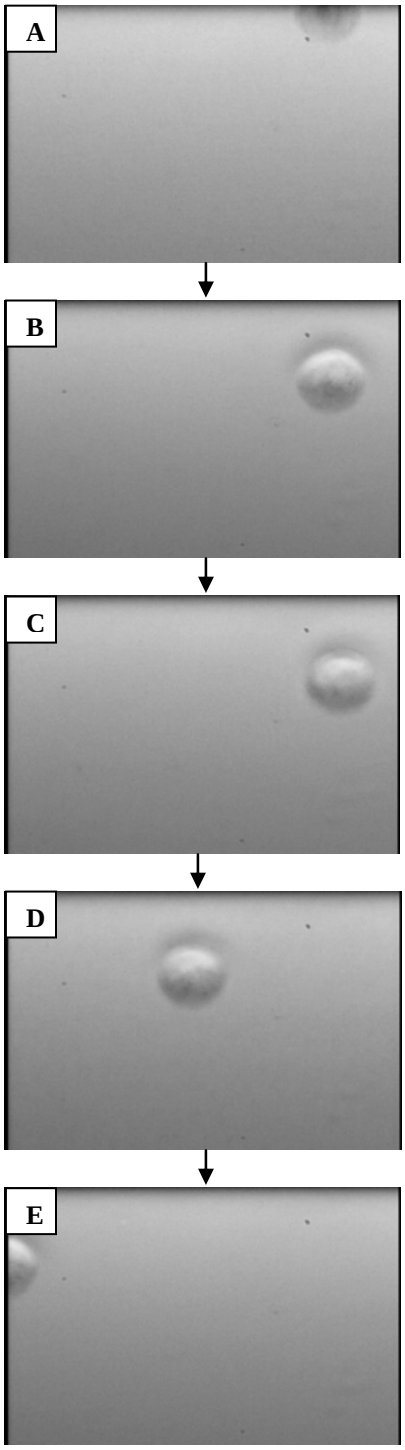

A cell containing sc coated magnetite nanoparticles entering the field of view from the top

The same cell containing sc coated magnetite nanoparticles at starting position (x_0) and time (t_0)

The same cell containing sc coated magnetite nanoparticles rotating in response to placed magnet

The same cell containing sc coated magnetite nanoparticles moving left toward the applied field

The same cell containing sc coated magnetite nanoparticles at ending position, leaving the field of view

Figure 3.4: Prostate cell movement in response to applied magnetic field

3.4.4 Visual Verification of Nanoparticles within Prostate Cells by Transmission Electron Microscopy

The transport of magnetic iron nanoparticles (MNPs) from the external to the internal portion of prostate cells was captured by transmission electron microscopy (TEM). The initiation of the journey begins when nanoparticles which are present in the nutrient media interact with microvilli on the surface of the prostate cell. Nanoparticles are engulfed and allowed into the cell by endocytosis. Upon entry into the cell, nanoparticles are collected and compartmentalized in small vacuoles. These vacuoles which contain magnetic iron nanoparticles are clearly visible in Figures 3.5 – 3.8. Smaller vacuoles may join to form larger vacuoles which increases the number of compartmentalized nanoparticles and creates a greater concentration of MNPs within this assembly of the cell cytoplasm. After fusion of smaller vacuoles into larger vacuoles, the transport of nanoparticles seems to be toward the nucleus, where possible chromosomal interaction may be the next order of interaction. The larger vacuole with a collection of sodium citrate coated iron nanoparticles is displayed in Figure 3.8 and is adjacent to the nuclear membrane.

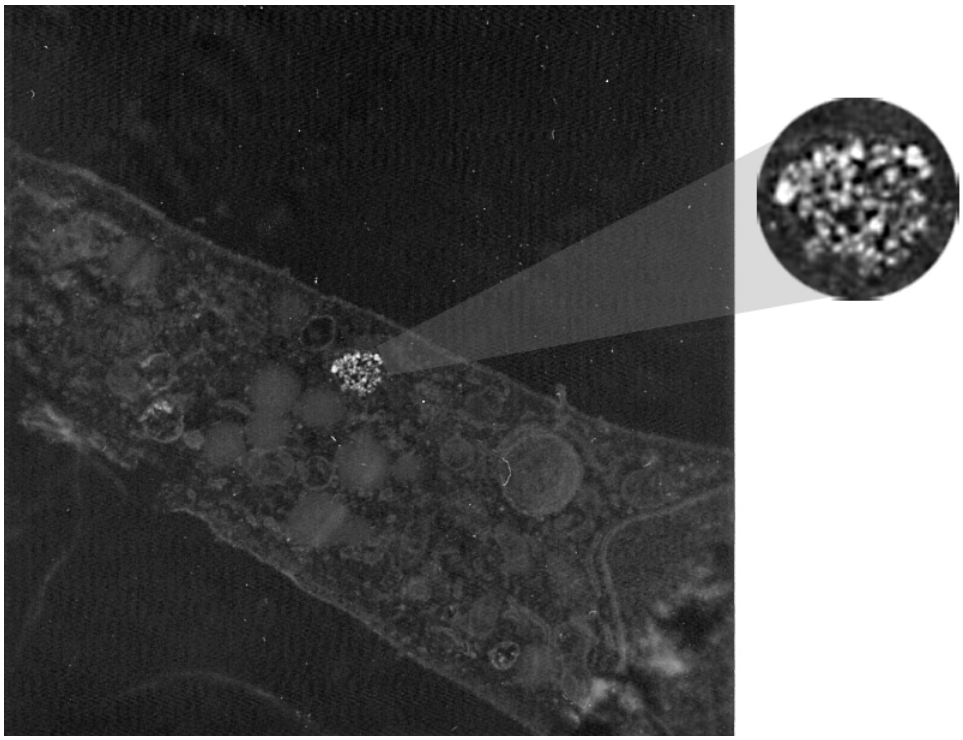

Figure 3.5: Sodium citrate coated magnetite nanoparticles within a vaculoe of a prostate cancer cell at 15,000X

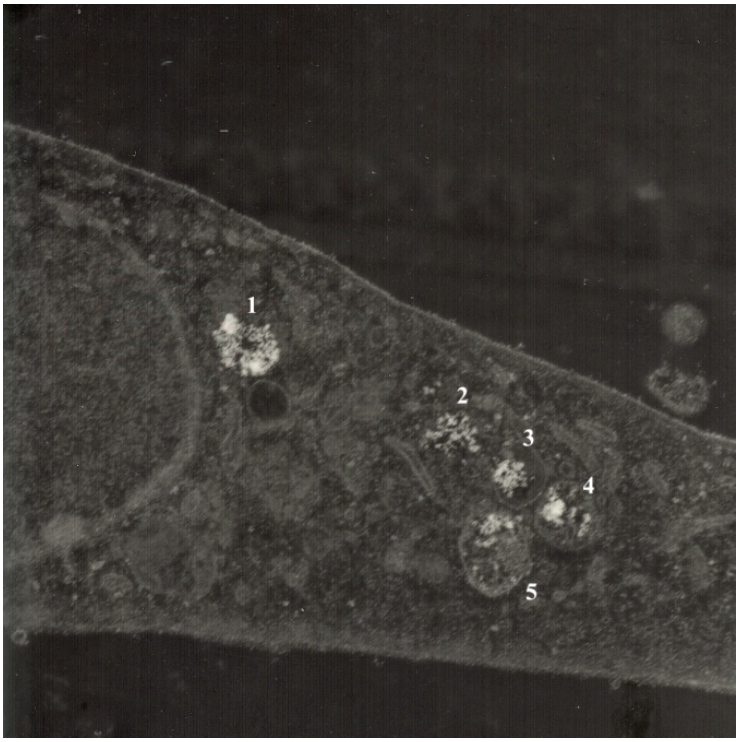

Figure 3.6: Sodium citrate coated magnetite nanoparticles within various vacuoles of a prostate cancer cell at 15,000X

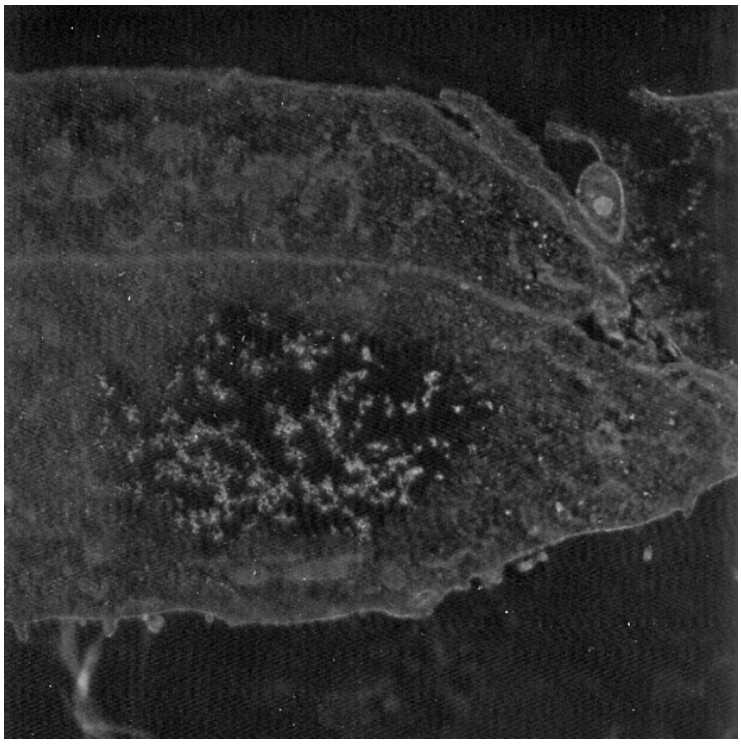

Figure 3.7: Sodium citrate coated magnetite nanoparticles within a larger sized vacuole of a prostate cancer cell at 20,000X

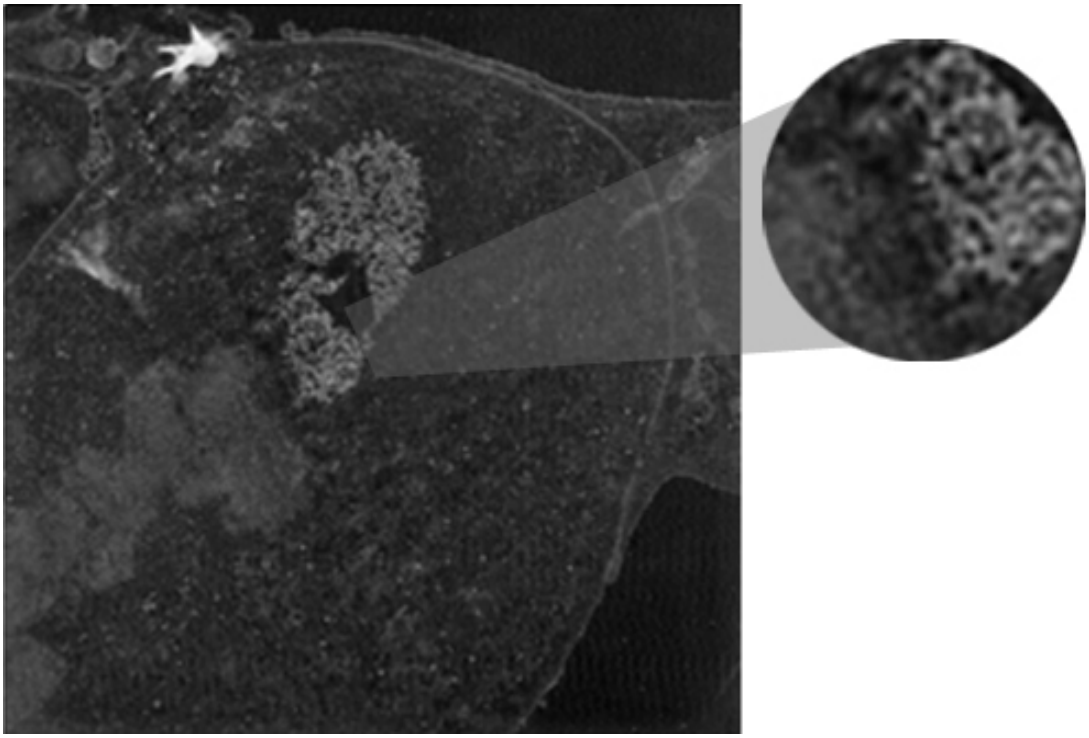

Figure 3.8: Sodium citrate coated magnetite nanoparticles densely populated within a larger vacuole of a prostate cancer cell at 20,000X

Prostate cancer cells were treated and observed for intracellular uptake of iron nanoparticles. Treatment of the prostate cells involved an incubation period with growth media which contained iron nanoparticles functionalized with sodium citrate. Physical interaction with colloid stable nanoparticles allowed transport of magnetite nanoparticles from the external side of the prostate cell, across the cell membrane and into the cytosol. The cellular encapsulation process described above is termed endocytosis and the resulting effect was experimentally demonstrated with TEM images. During the incubation period, phagocytosis occured. One of three phenomena which describes endocytosis, phagocytosis, allows cells to ingest large objects on a relative basis. The cell membrane invaginates to collect the particulate matter in a pocket then pinches it off to engulf it. The material of interest is sealed into vacuoles within the cytoplasm. This result is clearly visible in Figure 3.6.The larger vacuoles may be a result of smaller vacuoles which fused together, increasing the quantity of iron nanoparticles per unit area. Before uptake was confirmed on the nanoscale with TEM, cell motility in response to a strong magnet on a micro-and macro-level was accepted as valuable information. In an effort to further confirm cellular uptake of nanoparticles, two additional experimental approaches were implemented. A “call and response” relationship was observed when biological cells became magnetically loaded vessels that were controlled by magnets. Evidence of uptake was distinctly demonstrated with uni-directional cell alignment when nanoparticles were placed with propagating prostate cells for 48 hours. The experimental set-up displays the neodymium magnet that was placed beneath the round petri dish during cell propagation which guided the patterned growth of prostate cells impregnated with magnetic nanoparticles. After a 42 hour exposure period, prostate cancer cells were

rinsed free of treatment media and external nanoparticles. The cells were re-dispersed in fresh culture media, placed on a microscope slide, exposed to a neodymium magnet at a known distance in four distinct positions (n, s, e, w) and observed with video. If a connection or affiliation was made between propagating prostate cells and iron nanoparticles during the incubation period, the applied magnet would generate a translational response in the form of motion. Indeed motion was observed and recorded. Cells containing iron nanoparticles "spun"/ rotated and travelled toward the neodymium magnet. Video was analyzed and the velocity of cells in motion which contained nanoparticles was determined. The speed of the cells was calculated. The velocity which defines the direction of the speed was determined by the distance traveled over time. This calculated value which describes the motility of cells in an aqueous environment is affected by a phenomenon known as drag which varies based on surface texture, size and shape. Drag must be considered during the quantitative analysis of cellular uptake of nanoparticles. The appropriate equation for the force exerted due to drag considers low Reynolds number, Re < 1. Since the particles move through the fluid at relatively slow speeds and no turbulence is present, the Stoke's Law was utilized,

$F_d = -bv$ where, b is the drag constant and v is the velocity of the object

For small spherical objects moving slowly through a viscous fluid, Stokes derived an expression for the drag constant, $b = 6\pi\eta r$ where η is the fluid viscosity, and r is the Stokes radius of the particle.

Therefore, drag force $F_d = (-6\pi\eta r)(v)$ [eqn 3.1]

There are several differences between normal and carcinoma prostate cells. The higher metabolic demand of prostate carcinoma cells is a well known characteristic of cancer

cells. A surprising observation was the size disparity among the normal and carcinoma prostate cells. Prostate cancer cells are much smaller than normal prostate cells. In relation to mobility, larger sized prostate cells in the same aqueous environment will experience a greater drag force. This relationship was observed in the resulting calculations of the velocities measured in real time video, (still images in Figure 3.4). Visual analysis via light microscope revealed a qualitative differentiation between cells containing varying amounts of nanoparticles. A reddish color was observed from cell to cell. This differentiation in color is thought to be related to the amount of nanoparticles taken in per cell. Although each cell should theoretically have equal access to nanoparticles in a colloid stable solution, it was not assumed that each prostate cell would engulf the same amount of material throughout the exposure period. Therefore, the number of nanoparticles per sample would have to be determined by experimentation and analytical calculation.

The uptake of nanoparticles by prostate cells was compared quantitatively by VSM. Prostate cells exposed to varying concentrations of nanoparticles ranging from 10^4 to 10^{17} nanoparticles per milliliter were analyzed for uptake. The range included concentrations of nanoparticles at 10^4, 10^7, 10^9, 10^{11}, 10^{13}, 10^{15}, and 10^{17}. Cells which were exposed to concentrations of 10^{15} and below did not give reliable readings for determination of uptake. The highest concentration of 10^{17} was lethal, and did not contribute to healthy cell proliferation.

3.4.5 Prostate Cell Viability after Exposure to Various Nanoparticle Concentrations

Preliminary experiments were conducted with lower concentrations of synthesized magnetite nanoparticles. It was determined that concentrations between 10^4 - 10^{15} were not dense nor concentrated enough to obtain magnetic property information via VSM. At these concentrations, however, the prostate cells were not killed, and in fact maintained a population above the positive controls. The working concentration range for the nanoparticle solutions was determined based upon prostate cell samples that were exposed to nanoparticles and provided a detectable and reasonable hysteresis curve.

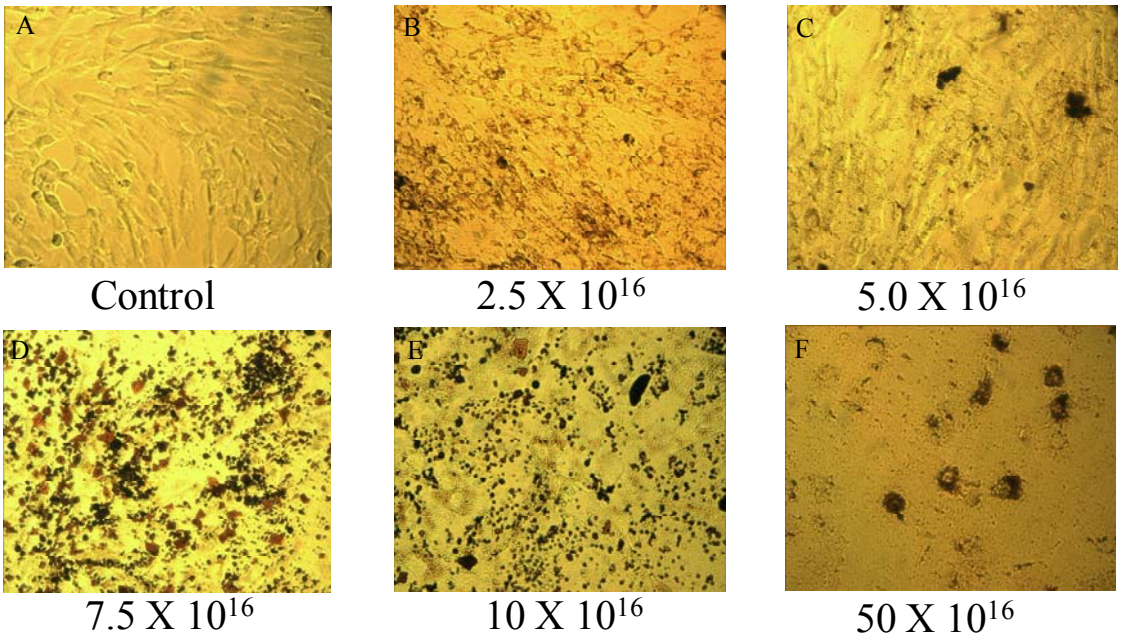

Figure 3.9: Normal prostate cells in culture which have been exposed to non coated magnetic nanoparticles at various concentrations, A) control, B) 2.5 x 10^{16}, C) 5.0 x 10^{16}, D) 7.5 x 10^{16}, E) 10 x 10^{16}, F) 2.5 x 10^{16} nanoparticles/mL

Cell viability was verified by visual examination through an optical microscope, Figure 3.9. Cell counts with a hemocytometer upon removal of cells from culture after the 48 hour treatment period revealed the effect of the concentration on cell health and survival. The highest nanoparticle concentration of 50 x 10^{16} nanoparticles/mL was lethal to prostate cells. As the nanoparticle concentration per mL decreased, the cell

survival increased. These findings were not recognized by MTT or Trypan blue exclusion; however, they were found by visual inspection while cells were adherent and in culture flasks. Cell aliquots (10 μL) for cell counts with a hemocytometer further confirmed cell survival and viability. This quantitative information demonstrated greater cell survival with decreasing concentrations of nanoparticle solutions in RPMI media. MTT results were not reliable since the nanoparticles stained the walls of the wells and interfered with the spectrophotometric reading of the plate reader. A particular research group that was interested in determining the effects of iron oxide nanoparticles on a particular cell type created a control for MTT analysis in an attempt to counteract the deviation experienced with the light sensitive MTT reading. The use of Trypan blue for exclusion of blue stained dead cells was not appropriate since the reddish stained living prostate cells interfered with clear visualization and distinction between the living and dead prostate cells.

CHAPTER 4

QUANTIFICATION OF NANOPARTICLE UPTAKE BY PROSTATE CELLS

4.1 Abstract

Quantification of nanoparticles received by cellular uptake is an important addition to cancer research which utilizes the properties of magnetic heating for cell death. The amount of magnetic material encapsulated in a cancer cell as compared to a normal cell defines the parameters required for cell death of the cancer cell and preservation of the normal cell. Prostate cancer and normal cells were grown separately in vitro and exposed to various concentrations of nanoparticles (0.5 – 50) x 10^{16} nanoparticles per milliliter for a period of 48 hours. The cells were rinsed well, centrifuged, resuspended in fresh media, counted, placed on glass slides to dry, then prepared for vibrating sample magnetometer analysis. The magnetic information per sample was obtained and the number of nanoparticles per cell was calculated. It was found that prostate cells intracellularly received nanoparticles among the three nanoparticle systems, but was greater for the surface modified nanoparticle systems. Differential uptake for prostate cancer cells increased with decreasing nanoparticle concentration for the non-coated nanoparticle system. At the lowest nanoparticle concentration (0.5 x 10^{16}) nanoparticles per milliliter, the differential uptake almost doubled the amount received by normal

prostate cells. The sodium citrate coated nanoparticle system did not seem to be concentration dependent, and remained around 2 times greater for prostate cancer cells. The greatest uptake was achieved with the gum arabic coated nanoparticle system and increased as the nanoparticle concentration per milliliter decreased. The most impressive differential uptake by prostate cancer cells was demonstrated at 2.5×10^{16} gum arabic coated nanoparticles per milliliter and occurred at a rate 6.8 times greater than the uptake for normal prostate cells.

4.2 Introduction

The concept of quantifying magnetic material within biological cells that have been exposed to iron oxide nanoparticles over a period of time is one which has been considered in research but has not been extensively demonstrated, or well documented. It is however a very important analysis which would greatly contribute to research for cancer therapy. A known amount of magnetic material would determine the parameters necessary for fine tuning the killing rate of carcinoma cells. Nanoparticles with surface modifiers and specific biological tags for specific targeting of cancer cells will exist in a concentrated fashion within these cells. The application of an alternating current magnetic field, external to the body would magnetically interact with the encapsulated nanoparticles, cause them to heat up to a temperature above 42˚C and result in cell death by hyperthermia **(29) (30) (31) (32)**.

The goal of determining the uptake of nanoparticles within human cells has not been extensively studied, but has been attempted by a research group with a method known as magnetophoresis **(28) (29) (30) (31) (37) (34)**. Our approach for quantification

of nanoparticles within human prostate cells utilizing the method of vibrating sample magnetometry has not been often attempted **(35) (36)**. The results of this research will greatly contribute to the nanobiotechnical, medical and health science fields.

4.3 Materials and Methods

4.3.1 Quantification of MNP's within Prostate Cells by VSM

Prostate cells, normal and carcinoma, were seeded in separate 6-well plates at a density of 30,000 cells per well. At approximately 60% confluent, the normal RPMI 1640 growth media was replaced by RPMI 1640 containing sodium citrate coated iron oxide nanoparticles at various concentrations (10^4-10^{17} particles/mL). After 48 hours, the media was discarded; the cells were washed with 1X PBS, and then dissociated with 200 μL 0.25 Trypsin/EDTA. Fresh media was added to the cell suspension upon a 5 minute incubation period in 37°C, and centrifuged at 1000 rpm for 10 minutes to separate the cells which contain iron oxide nanoparticles from free floating nanoparticles, waste and cellular debris. Two milliliters of fresh media was added to resuspend the cells. The cells in each well were counted to determine the number of cells per milliliter. The entire cell suspension from each well (2 mL) was deposited on pre-cleaned and UV sterilized 75 x 38 cm microscope slides. The liquid deposits of cells were allowed to air dry in an enclosed hood. The completely dried samples were then prepared for VSM analysis. Collection of the sample for VSM was obtained by scraping the glass sample slide with the edge of a clean glass microscope slide of the same dimensions and collected into the sample holder of the vibrating sample magnetometer. The magnetic susceptibility curve for each sample was generated and the magnetic properties were compared to the control sample to determine the average amount of iron oxide nanoparticles per cell.

4.3.2 Magnetic Measurements with Vibrating Sample Magnetometer

The stationary magnets produce a constant magnetic field which magnetize the sample and cause the internal magnetic domains of the sample to align with the field. In response, the magnetic dipole moment will create a magnetic field around the sample. As the value of the magnetic field varies, the sample vibrates up and down. The change in the sample magnetic field (alternating magnetic field) is a function of time, and will cause an electric field in the pick-up coils (according to Faraday's Law of Induction) which will be amplified and relayed to the computer interface of the system. The flux change caused by the moving magnetic sample causes an induction voltage across the terminals of the pick-up coils which is proportional to the magnetization of the sample. The greater the magnetization, the greater the induced current:

$$V(t) = C\, d(fi)/dt$$

where fi(t) represents the (changing) flux in the pick-up coils caused by the moving magnetic sample. Software manipulation will provide the degree of magnetization of the sample and the relationship between its magnetization and the strength of the constant magnetic field. The output data is presented as a hysteresis curve of magnetization by field strength.

4.4 Results and Discussion

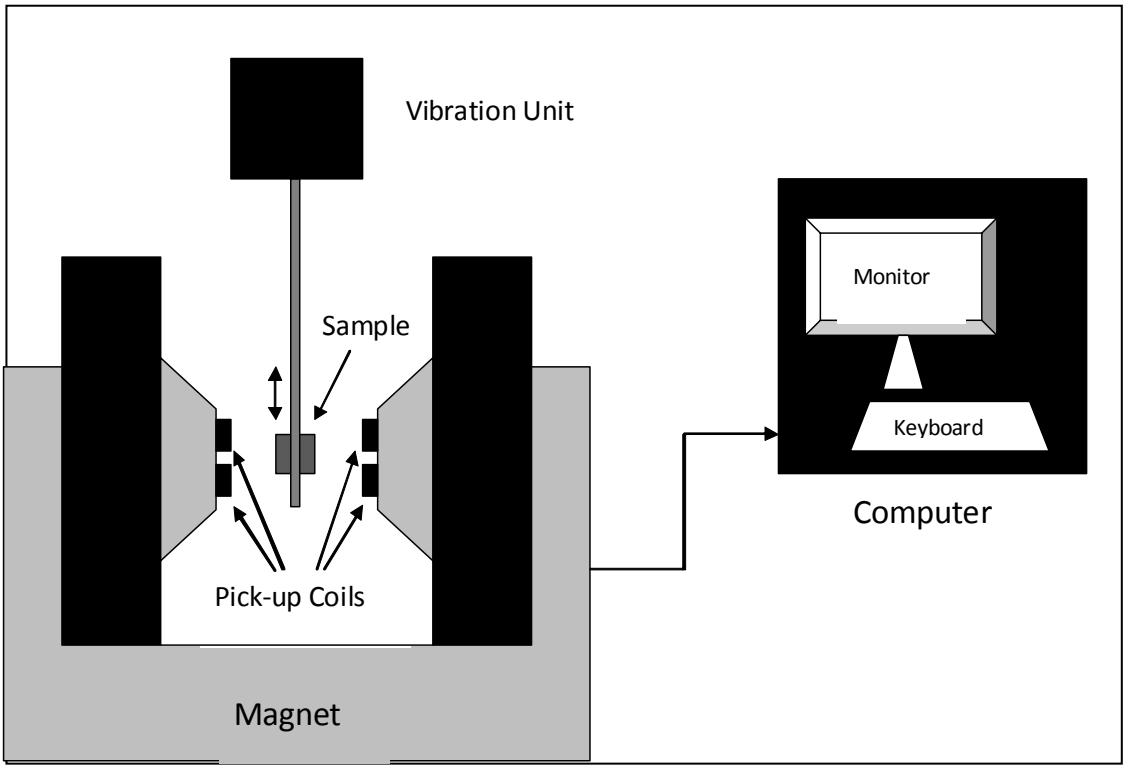

Figure 4.1: Schematic representation of a vibrating sample magnetometer

4.4.1 Physical Verification of Nanoparticles within Prostate Cells by Vibrating Sample Magnetometry

The burden of proof for demonstrating cellular uptake of nanoparticles was achieved with a variety of methods. Nanoparticles were intracellularly received by prostate cells and clearly observed with TEM (see Chapter 3). The goal of this chapter was to quantify the uptake of magnetic nanoparticles among a known number of prostate cells in vitro. The vibrating sample magnetometer is an instrument that utilizes a magnet to interact with the magnetic sample and provide the magnetic properties, such as,

saturation magnetization, magnetic susceptibility, coercivity, and with some manipulation and calculation, the size of particles.

The hysteresis curve in Figure 4.2 provides magnetic property information for prostate cancer cells that were exposed to MNP at a concentration of 10 x 10^{16} nanoparticles per milliliter. The magnetization for this sample was approximately 3 emu/g.

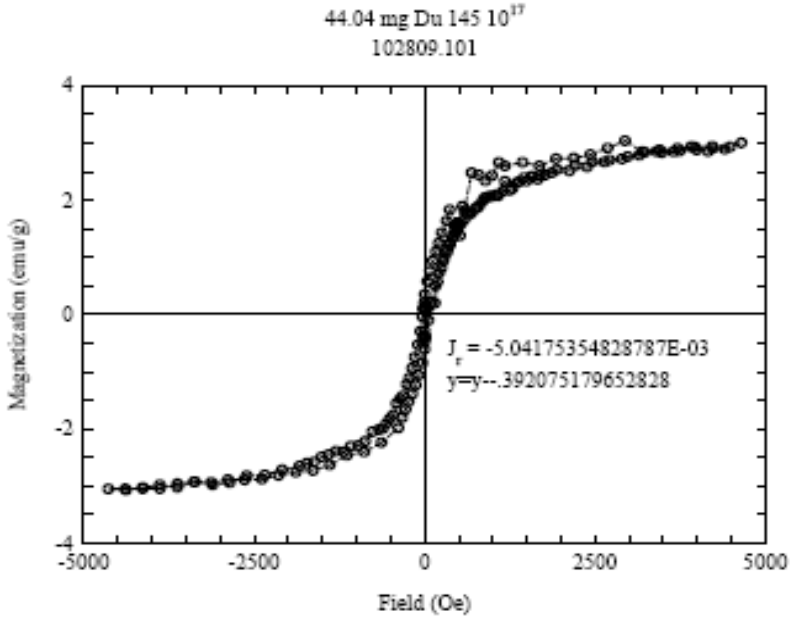

Figure 4.2: Magnetization of prostate cancer cells exposed to magnetite nanoparticles at 10 x 10^{16} MNP/mL for 48 Hours

The hysteresis curve in Figure 4.3 represents magnetic property information for normal prostate cells which were exposed to MNPs at 10 x 10^{16} nanoparticles/mL for 48 hours. The saturation magnetization was approximately 1.5 emu/g for this sample.

Comparison of the magnetizations between prostate carcinoma and prostate normal cells exposed to the same concentration of nanoparticles demonstrate a 2-fold increase in nanoparticle uptake for carcinoma cells (Figure 4.2 and Figure 4.3) respectively. Although prostate carcinoma cells are 2 - 3 times smaller than normal cells, they take up twice as much magnetic material.

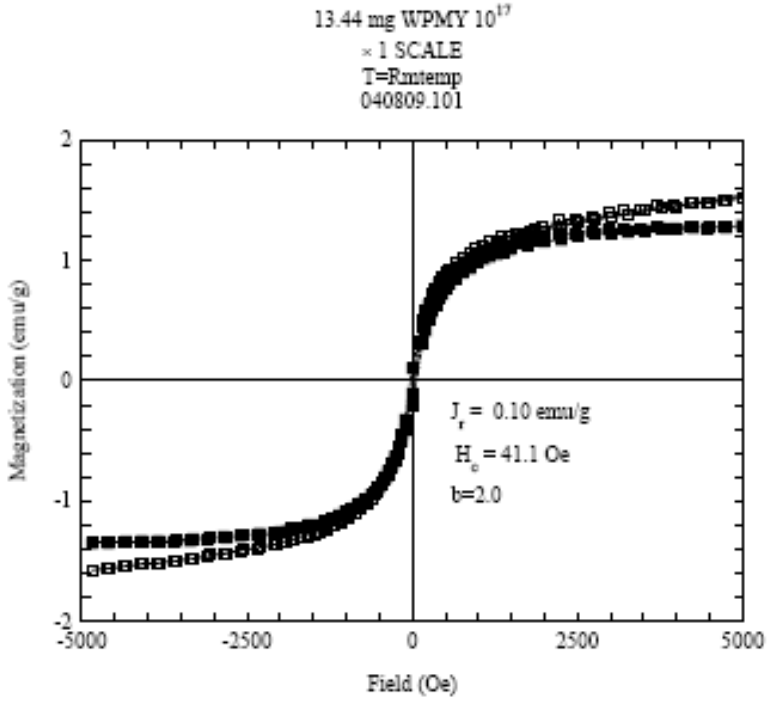

Figure 4.3: Magnetization of prostate normal cells exposed to magnetite nanoparticles at 10 x 10^{16} MNP/mL for 48 hours

Each of the three MNP systems contained 14 sample types (2 cell types @ 7 mnp concentrations for each). A table was generated to present the magnetic susceptibility data, specifically the number of nanoparticles per prostate cell, as shown in (Table 4.1).

The mathematical calculations below describe the method by which the number of nanoparticles per cell was obtained.

Number of MNP/cell = [magnetization/cell]/[magnetization/particle] [Eqn 4.1]

The magnetization per cell was calculated by dividing the magnetization per sample by the number of cells for the particular sample. The magnetization per particle was determined by dividing the magnetization of a pure MNP sample by the number of particles per gram for that sample (stock solution). Upon calculation, the value of the magnetization per particle was fixed, and did not require alteration because the magnetite nanoparticle stock solution remained the same.

Concentration X 10^{16} MNP/mL	Non-coated MNP		Gum Arabic coated MNP		Sodium Citrate coated MNP	
	Normal	Cancer	Normal	Cancer	Normal	Cancer
50	N/A	N/A	N/A	N/A	N/A	N/A
10	9.40E+08	3.79E+08	2.76E+09	8.49E+07	2.17E+09	5.87E+07
7.5	8.33E+08	3.11E+08	2.89E+09	1.05E+08	1.33E+09	8.25E+07
5	4.82E+09	8.25E+07	1.65E+09	2.62E+08	2.77E+09	5.31E+08
2.5	4.66E+09	1.05E+08	7.27E+08	4.45E+08	1.46E+09	bad fit
1	4.87E+07	1.44E+08	N/A	N/A	N/A	N/A
0.5	6.93E+06	5.31E+08	2.77E+08	1.00E+09	N/A	N/A

Table 4.1: Number of nanoparticles per prostate cell obtained with VSM

The prostate cells that were exposed to non-coated MNPs for 48 hours were prepared for VSM analysis and the results showed a trend toward greater MNP uptake with decreasing MNP concentration in media (Table 4.2).

MNP Concentration in RPMI Media $x10^{16}$/mL	Normal (N)	Cancerous (C)	C/N
50	N/A	N/A	
10	9.40E+08	3.79E+08	0.257
7.5	8.33E+08	3.11E+08	0.545
5	4.82E+09	8.25E+07	1.054
2.5	4.66E+09	1.05E+08	0.696
1	4.87E+07	1.44E+08	1.011
0.5	6.93E+06	5.31E+08	1.971

Table 4.2: Non-coated magnetic nanoparticle uptake relationship between prostate cancer and prostate normal cells as a calculated ratio

Since sodium citrate coated nanoparticles demonstrated excellent stability in water over time, it was expected that the same effect would be displayed in cell nutrient media (RPMI); however, the opposite effect was observed. In media very large particles initially formed and over time fell out of solution. The resulting differential uptake of SC coated MNPs may be related to the size and dynamics of nanoparticles in the media. Despite the

range of MNP concentrations, differential uptake was independent of MNP concentration in RPMI (Table 4.3). It should be noted however, that nanoparticles were received by prostate cells.

MNP Concentration in RPMI Media x10^{16}/mL	Normal (N)	Cancerous (C)	C/N
50	N/A	N/A	
10	2.17E+09	5.87E+07	1.613
7.5	1.33E+09	8.25E+07	2.051
5	2.77E+09	5.31E+08	2.037
2.5	1.46E+09	N/A	
1	N/A	N/A	
0.5	N/A	N/A	

Table 4.3: Sodium citrate coated magnetic nanoparticle uptake relationship between prostate cancer and prostate normal cells as a calculated ratio

The greatest uptake and demonstration of cell selectivity was observed with the gum arabic coated MNP system (Table 4.4). The disparity in the values noted for quantitative uptake between prostate normal and prostate carcinoma cells is evident with the ratios which are much larger than one. The greatest difference in uptake among the cell types occurred when the MNP concentration was 2.5 x 10^{16} particles per mL. The greatest number of nanoparticles that were intracellularly received (2.5102 x 10^{16}) was

accomplished by prostate cancer cells exposed to gum arabic coated nanoparticles at the lowest MNP concentration (0.5 x 10^{16}) particles per mL.

MNP Concentration in RPMI Media x10^{16}/mL	Normal (N)	Cancerous (C)	C/N
50	N/A	N/A	
10	2.76E+09	8.49E+07	5.738
7.5	2.89E+09	1.05E+08	5.804
5	1.65E+09	2.62E+08	3.623
2.5	7.27E+08	4.45E+08	6.801
1	N/A	N/A	
0.5	2.77E+08	1.00E+09	2.352

Table 4.4: Gum arabic coated magnetic nanoparticle uptake relationship between prostate cancer and prostate normal cells as a calculated ratio

A global look of the uptake ratios among the three nanoparticle systems clearly highlighted the effects of the coating material on intracellular uptake for prostate cells. The greatest ratio for each system is presented in Table 4.5. It is important to mention the concentrations for which the greatest uptake of nanoparticles was achieved. The lower concentrations (1.5 – 2.5 x 10^{16}) nanoparticles per mL provided the cells in culture an adequate pool of nanoparticles for uptake and an environment conducive for nutrient exchange and cell proliferation.

MNP Coating	MNP Concentration in RPMI Media $x10^{16}$/mL	Normal (N)	Cancerous (C)	C/N
Non-Coated	0.5	6.93E+06	5.31E08	1.971
Sodium Citrate	5	2.77E+09	5.31E+08	2.037
Gum Arabic	2.5	7.27E+08	4.45E+08	6.801

Table 4.5: Comparison of prostate cell uptake ratios for the three nanoparticle systems

The images in Figure 4.4 demonstrate the difference in dimensions between prostate cancer and prostate normal cells. Prostate normal cells are 2 – 3 times larger than prostate carcinoma cells, which is clearly recognizable. The comparisons stated earlier for intracellular uptake by prostate cells were purely quantitative values from VSM analysis; however, if we consider the sizes of the prostate cells, the differential uptake would be much greater. The basic principle of density states,

$$D = m/v \qquad \text{[Eqn 4.1]}$$

where, D is density, m = mass, and v = volume

Density is inversely proportional to volume for a given mass, so if the volume of the prostate cell is 2 – 3 times smaller than the volume a normal prostate cell, then the density for a given mass is 2 – 3 times greater. This information greatly increases the effectiveness of the nanoparticle coatings, the resultant properties of their system and provides a mechanism for fine tuning the specifications required for precise targeting of prostate cancer cells.

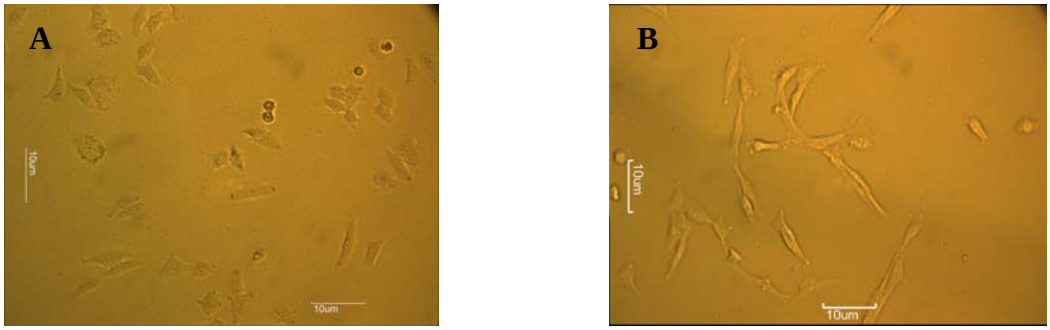

Figure 4.4: Adherent prostate cells (A) cancer and (B) normal in cell culture

CHAPTER 5

CONCLUSION

The co-precipitation method was a reliable technique for generating magnetite nanoparticles. Uncoated nanoparticles demonstrated larger particle sizes; between 585 – 700 nm in water and between 280 – 390 nm in RPMI 1640 media. These measurements were hydrodynamic diameters which were obtained by Malvern zetasizer. The reported sizes were nanoparticle clusters which had agglomerated; since magnetic nanoparticles have a tendency to self assemble due to their magnetic properties. This agglomeration phenomena was confirmed by Vibrating Sample Magnetometry. Individual particle size measurements between 5-35 nm were revealed. The addition of surface materials improved the degree of agglomeration and increased the particle stability in aqueous mediums. Steric stabilization was achieved in water with sodium citrate as the capping agent for the magnetic nanoparticles, and showed a consistent particle size measurement of approximately 160 nm by the Malvern zetasizer. Sodium citrate was not very effective as a homogenizing agent in cell nutrient media. Particle size measurements obtained with the Malvern zetasizer and particle stability via light scattering with a spectrophotometer revealed the incompatibility among the SC coated nanoprticles and the required ingredients of the cell culture media. Upon the addition of SC coated MNP's into RPMI 1640 growth media; particles slightly larger than 700 nm were reported. Over the 48 hour period, the initially formed large sized complexes fell out of solution and the

particle size gradually decreased to about 350 nm. Gum arabic, in turn was excellent as a stabilizing agent in cell nutrient media, but not in water. The reported nanoparticle size with gum arabic in media was consistently 250 nm over a 48 hour period. Although each of the three nanoparticle systems offered different characteristics, it was found that gum arabic provided the most stable nanoparticle solution over the 48 hour period with consistent size measurements in the required cell nutrient media.

Intracellular uptake was achieved and confirmed with a variety of techniques. Cells which were allowed to interact with nanoparticles in culture for 48 hours, were washed free of the nanoparticle solution, and then exposed to a magnetic field for 24 hours, which resulted in elongated, directional growth of cells. A second technique involved mobility of unrestrained cells that were exposed to nanoparticles for 48 hours, washed, then resuspended in fresh media. Prostate cells exposed to higher concentrations of nanoparticles displayed distinctive movement in response to the externally applied magnetic field. The third technique visually exposed the cross section of prostate cells which undeniably showed nanoparticles within vacuoles of the cells. The results of these three methods established the fact that magnetite nanoparticles are able to penetrate the cell membrane of prostate cells and gain entry into the cytoplasm, particularly the vacuoles. Cell viability after the 48 hour exposure to magnetite nanoparticles and encapsulation of the material is a required necessity. It was found that the highest observed concentration of 50×10^{16} nanoparticles per mL did not support cell survival.

Nanoparticle concentrations between 10 x 10^{16} and 0.5 x 10^{16} revealed increased viability as the nanoparticle concentration decreased.

The uptake was further confirmed with the quantitative assessment of the three nanoparticle systems. Magnetization outputs were recorded for each nanoparticle concentration with each of the three nanoparticle systems. The degree of magnetization varied per sample due to the concentration of nanoparticles that the cells were exposed to and subsequently received internally. Prostate cancer cells received more nanoparticles than normal prostate cells, especially within the coated nanoparticle systems. A ratio was calculated to determine the uptake relationship between prostate normal and carcinoma cells. The C/N value divided the number of nanoparticles received by prostate carcinoma cells by the number of nanoparticles received by prostate normal cells. A value above one demonstrated greater uptake for prostate carcinoma cells. The non-coated nanoparticle system demonstrated C/N ratio's between .257 – 1.971, and this trend of greater uptake occurred as the MNP concentration decreased. The sodium citrate nanoparticle system demonstrated differential uptake by the prostate carcinoma cells, with C/N values between 1.613 - 2.051, but did not appear to be concentration dependent. The nanoparticle system that revealed the greatest differential uptake was the gum arabic coated nanoparticle system; and the most impressive differences occurred at the lower nanoparticle concentrations. The highest C/N value among the three nanoparticle systems occurred with the GA coated MNP system, C/N = 6.8 at 2.5 x 10^{16} nanoparticles per milliliter. The greatest uptake of nanoparticles by prostate cells was achieved by prostate

carcinoma cells which were exposed to the lowest concentration of MNP's $0.5x10^{16}$ nanoparticles per milliliter.

The VSM quantification method required the number of viable cells for the calculation of the number of nanoparticles per cell, but is not an instrument for measurement or determination of cell viability. The traditional methods for verifying cell viability are MTT assay and trypan blue exclusion; however the nanoparticle treated media could not be completely removed from the wells of the 96-well plates. If was found that an additional control was required in order to compensate for the nanoparticle residues that are easily detected by sensitive spectrophotometric measurements. The color of iron inside prostate cells in combination with the blue dye of the trypan blue stain provided a degree of difficulty since visual cell counts determine viability. The cell counts utilized for VSM analysis demonstrated healthy adherent cells, and the counts were utilized as indicators of cell viability. The highest nanoparticle concentration ($50x10^{16}$) was not suitable for cell viability, while cell viability increased as the nanoparticle concentrations decreased. The increased cell viability at lower nanoparticle concentrations correlated well with the greater uptake values which also occurred at lower concentrations. The magnetization values from the VSM did not consider the difference in size of the prostate normal and prostate cancer cells. Utilization of optical tweezers with an optical microscope provided a two-dimensional measurement of the prostate cells. Prostate carcinoma cells were found to be 2 – 3 times smaller than prostate normal cells.

Differential uptake was observed for prostate carcinoma cells from VSM analysis, however, increased potential for greater disparity between prostate carcinoma and prostate normal cell uptake quantities was calculated when the size difference was re-evaluated, thus increasing the density of nanoparticles within the prostate carcinoma cells. This density difference should greatly aid in selectively heating prostate cancer cells to mortality without killing normal prostate cells. Further fine tuning the specifications required for precise targeting of prostate cancer cells may include the use of prostate cancer specific antibody, determination of the time for magnetic field exposure, frequency and field strength. The results of this research provided excellent contributions to the various fields of research which define it as interdisciplinary, such as nanotechnology, biology, physics and engineering.

APPENDIX

Calculation of mass, volume, and magnetization of magnetite nanoparticles

---

Molecular Weight (MW) of Fe_3O_4:

MW = 3 (55.85) + 4 (16)

MW = 167.55 + 64

MW = 231.55

Determine the amount of Fe in magnetite:

167.55/231.55 = 0.763 = 76.3%

1gram of mnp contains .763g of Fe, and 160 mg Fe exist in 1L (Microbac Lab) which is equal to the weight of iron/mL of the stock solution so, determine the amount of magnetite in 160 mg Fe:

solve for x in the ratio:

1 g Fe_3O_4 = 76.3 mg Fe

x_g Fe_3O_4 = 160 mg

x = 160/76.3

x = 209.69 mg magnetite in 1L (dilution = 1mL in 100mL)

so, the amount of magnetite in 1 mL of the mnp stock solution is 209.69 mg

---

Volume of one magnetic nanoparticle (mnp):

$V = 4/3\ \pi\ r^3$

d = 10nm so use, r = 5 nm

$1nm = 10^{-7}$ cm

$V = (4/3)\ (3.14)\ (5 \times 10^{-7}cm)^3$

$V = 5.23 \times 10^{-19}\ cm^3$

Mass of one mnp:

$M = \rho V$

Use, $\rho_{magnetite} = 5.18\ g/cm^3$

$V_{magnetite} = 5.23 \times 10^{-19}\ cm^3$

$M = (5.18\ gm)\ (5.23 \times 10^{-19} cm^3)$

$M = 2.7 \times 10^{-18}\ g$

$M = 2.7 \times 10^{-15}\ mg$

Determine the number of mnp in 1mL (stock) soln:

No. mnp/mL = amount of magnetite in 1mL (stock) / mass of one mnp

No. mnp/mL = (209.69 mg) / $(2.7 \times 10^{-15}$ mg)

No. mnp/mL = 7.77×10^{16} particles/mL = The number of mnp in 1mL (stock)

Determine the total mass of sample (# of mnp) in a 2 mL volume:

Consider the amount of magnetite in 1mL mnp (stock):

209.69 mg/mL= 0.21 g/mL

For 2 mL of sample, (0.21 g/mL) x (2mL) = 0.42 g

The amount of magnetite in 2 mL = 0.42 g

The following relationship in grams relates the amount of magnetite in 2mL of media (dried) to the mass of dried media (only), 0.42 g magnetite (in 2 mL) ≈ 0.0578 g (mass of the media)

For example, in the case of WPMY-1, there were 880,000 cells/mL

So, in 2 mL, there are 1,760,000 = 1.76×10^6 cells

From the relationship above, relate the number of cells in 2 mL media to the mass in 2 mL of media (only) to determine the number of cells/g

1.76×10^6 cells/ 0.0578 g = x/ 1

Therefore, x = 3.04×10^7 cells/g

Determine the number of particles per gram:

No. mnp/gram = 1/ (mass of one mnp)

No. mnp/gram = 1/ (2.7×10^{-18}g)

No. mnp/gram = 3.69×10^{17}

Determine the magnetization (mag) per particle; and per cell:

Use, magnetization = 60 emu/g for d = 10nm magnetite nanoparticles

and magnetization/gram = 2 emu (obtained from VSM for actual mnp only samples)

Mag/particle = (magnetization/gram for 10nm mnp) / (number of mnp/gram)

Mag/particle = 60 emu/ 3.69×10^{17} = 1.66×10^{-16} emu

Note: The value for mag/particle will not change per sample, but will remain the same for each sample

Mag/cell = (magnetization/gram) / (number of cells/gram)

Mag/cell = 2 emu/ 3.04×10^{7} cells/g = 6.578×10^{-8} emu

Note: The values for the mag/cell will change for each sample being observed

---

Determine the number of particles per cell:

(mag/cell)/ (mag/particle) = $(6.578 \times 10^{-8}) / (1.66 \times 10^{-16}) = 3.96 \times 10^{8}$ particles/cell

---

MP Biomedicals, LLC
29525 Fountain Parkway
Solon, Ohio 44139
Telephone: 440/337-1200
Toll Free: 800/854-0530
Fax: 440/337-1180
mailto:biotech@mpbio.com
web: www.mpbio.com

TECHNICAL INFORMATION

Catalog Number: 1060120, 1060121, 1060124, 1060122

RPMI 1640 Medium, powder, with L-glutamine, without sodium bicarbonate

Description: This medium was originally developed by Moore and his colleagues at Roswell Park Memorial Institute (RPMI). It was based on the RPMI 1630 line of media which utilized a bicarbonate buffering system and alterations in the amounts of amino acids and vitamins. RPMI has successfully been used for the cultivation of normal human and neoplastic leukocytes. It is now a popular general purpose medium when properly supplemented.

A Dutch Modification of RPMI 1640 is also available through MP. The Dutch Modification contains 6400 mg/l sodium chloride instead of 6000 mg/l; contains 1000 mg/l sodium bicarbonate instead of 2000 mg/l; and contains 20 mM HEPES.

Formulation:

Components	*mg/L*	*Mol. Wt.*	*Mol. (mM)*
Amino Acids			
L-Arginine HCl	200.000	210.7	1.15
L-Asparagine H_2O	56.820	150.1	0.38
L-Aspartic Acid	20.000	133.1	0.15
L-Cystine 2HCl	65.200	313.2	0.21
L-Glutamic Acid	20.000	147.1	0.14
L-Glutamine	300.000	146.1	2.05
Glycine	10.000	75.07	0.13
L-Histidine	15.000	155.2	0.10
L-Hydroxyproline	20.000	131.1	0.15
L-Isoleucine	50.000	131.2	0.38
L-Leucine	50.000	131.2	0.38
L-Lysine HCl	40.000	182.6	0.22
L-Methionine	15.000	149.2	0.10
L-Phenylalanine	15.000	165.2	0.09
L-Proline	20.000	115.1	0.17
L-Serine	30.000	105.1	0.29
L-Threonine	20.000	119.1	0.17
L-Tryptophan	5.000	204.2	0.02

L-Tyrosine 2Na $2H_2O$	28.830	261.2	0.11
L-Valine	20.000	117.1	0.17
Vitamins			
Biotin	0.200	244.3	0.0008
Choline Chloride	3.000	139.6	0.0215
D-Calcium Pantothenate	0.250	238.3	0.0010
Folic Acid	1.000	441.4	0.0023
myo-Inositol	35.000	180.2	0.1942
Nicotinamide	1.000	122.13	0.0082
para-Aminobenzoic Acid	1.000	137.1	0.0073
Pyridoxine HCl	1.000	205.6	0.0049
Riboflavin	0.200	376.4	0.0005
Thiamine HCl	1.000	337.3	0.0030
Vitamin B12	0.005	1355.4	0.000004
Inorganic Salts			
Calcium Nitrate [$Ca(NO_3)_2$ $4H_2O$] Tetrahydrate	100.000	236.2	0.42
Magnesium Sulfate [$MgSO_4$]	48.800	120.4	0.41
Potassium Chloride [KCl]	400.000	74.55	5.37
Sodium Bicarbonate [$NaHCO_3$]	0.000	84.01	0.00
Sodium Chloride [NaCl]	6000.000	58.44	102.67
Sodium Phosphate Dibasic [Na_2HPO_4]	800.700	141.96	5.64
Other			
Dextrose	2000.000	180.2	11.10
Glutathione (reduced)	1.000	307.33	0.0033
Phenol Red Sodium Salt	5.000	376.4	0.01
Add			
$NaHCO_3$ Powder (g/L)	2.00		
$NaHCO_3$ 7.5% Solution (mL/L)	26.72		

Availability :

1X Liquid :

Catalog Number	Description	Size
1260249 1260254	1X RPMI 1640 without L-glutamine, pH 6.9-7.2	100 ml 500 ml
1260354	1X RPMI 1640 with L-glutamine	500 ml
1260554	1X RPMI 1640 with 25 mM HEPES, 4750 mg/l sodium bicarbonate, without L-glutamine	500 ml
1260654	1X RPMI 1640 with 25 mM HEPES, 4750 mg/l sodium chloride, L-glutamine	500 ml
1260449 1260454	1X RPMI 1640 with 25 mM HEPES, without sodium bicarbonate, L-glutamine	100 ml 500 ml

1265254	1X RPMI 1640 without L-glutamine, pH 7.2-7.4	500 ml
1260954	1X RPMI 1640 Dutch Modification without L-glutamine	500 ml
1265349 1265354	1X RPMI 1640 without L-glutamine, myo-inositol	100 ml 500 ml
1629149	1X RPMI 1640 without L-glutamine, L-leucine	100 ml
1629249 1629254	1X RPMI 1640 without L-glutamine, L-methionine	100 ml 500 ml
1646449 1646454	1X RPMI 1640 without L-glutamine, cystine, methionine, cysteine	100 ml 500 ml
1646754	1X RPMI 1640 without L-glutamine, phenol red	500 ml
1646854	1X RPMI 1640 without L-glutamine, dextrose	500 ml
1629749 1629754	1X RPMI 1640 with 850 mg/l sodium bicarbonate, without L-glutamine, phosphate	100 ml 500 ml

10X Liquid:

Catalog Number	Description	Size
1460054	10X RPMI 1640 without L-glutamine, sodium bicarbonate	500 ml

Powders:

Catalog Number	Description	Size
1060120 1060122 1060124	RPMI 1640 with L-glutamine without sodium bicarbonate	10 x 1 liter 1 x 10 liter 1 x 50 liter
1060222 1060224	RPMI 1640 with L-glutamine without sodium bicarbonate, phenol red	1 x 10 liter 1 x 50 liter
1060520 1060522	RPMI 1640 with L-glutamine, 25 mM HEPES, without sodium bicarbonate	10 x 1 liter 1 x 10 liter

References:

1. Moore, G.E., et. al., "Culture of Normal Human Leukoctyes." *JAMA*, **v. 199**, 519-524 (1967).
2. Moore, G.E. and Woods, L.K., "Culture media for human cells RPMI 1603, RPMI 1634, RPMI 1640 and GEM 1717." *Tissue Culture Association Manual*, **v. 3**, 503-508 (1976).
3. Moore, G.E., Gerner, R.E. and Minowada, J., "Studies of normal and neoplastic cells. Studies of normal and neoplastic human hematopoietic cells in vitro." *Twenty-first Annual Symposium on Fundamental Cancer Research*, February 1967, p. 41-43.
4. Moore, G.E. and Kitamura, H., "Cell line derived from patient with myeloma." *NY State Journal of Medicine*, **v. 68**, 2054-2060 (1968).

REFERENCES

1. Company, Anatomical Chart. ***The Prostate Anatomical Chart.*** **Lippincott Williams and Wilkins; Wal Chrt edition, 2000.**

2. ***Cancer Statistics.*** Jemal A, Siegel R, Ward E, Murray T, Xu J, Thun M J. **2007, Vol. 57, pp. 43-66.**

3. ***Cancer Statistics.*** Jemal A, Siegel R, Ward E, Murray T, Xu J, Thun M J. **CA Cancer Clin, 2010, Vol. 60, pp. 277-300.**

4. American Cancer Society. ***www.americancanersociety.org.*** **[Online] 2010.**

5. Prostate Cancer Foundation. ***www.prostatecancerfoundation.org.*** **[Online] 2010.**

6. Prostae Cancer Institute. ***www.prostatecancerinstitute.com.*** **[Online] 2010.**

7. ***Metabolic alterations and targeted therapies in prostate cancer.*** Flavin R., Zadra G., Loda M. **2, 2011, The Journal of pathology, Vol. 223, pp. 283 -294.**

8. ***Men of Higher Socioeconomic Status Have Improved Outcomes After Radical Prostatectomy for Localized Prostate Cancer.*** Hellenthal N. J., Parikh-Patel A., Bauer K., Ralph W., deVere W., Koppie T. M. **6, 2010, Urology, Vol. 76, pp. 1409-1413.**

9. Clinic, Cancer. **www.itlcancerclinic.org. [Online] 2010.**

10. ***Use of PEI-coated magnetic iron oxide nanoparticles as gne vectors.*** W, Wei. **6, s.l. : Huazhong Univ Sci Technolog Med Sci, 2004, Vol. 24, pp. 618-620.**

11. ***Magnetically based enhancement of nanoparticle uptake in tumor cells: Combination of magnetically induced cell labeling and magnetic heating.*** Kettering, M. **Fortscher Rontgenstr, 2006, Vol. 178, pp. 1255-1260.**

12. Guimarães, Alberto P. ***Principles of Nanomagnetism.*** **Springer, 2009.**

13. ***Novel environmentally friendly synthesis of superparamagnetic magnetite nanoparticles using mechanochemical effect.*** Iwasaki T., Kosaka K., Watano S., et al. **4, 2010, Materials Research Bulletin, Vol. 45, pp. 481-485.**

14. ***Surface modification of superparamagnetic iron nanoparticles with calcium salt of poly(gamma-glutamic acid) as coating material.*** Kumar R., Inbaraj B. S., Chen B. H. **11, 2010, Materials Research Bulletin, Vol. 45, pp. 1603-1607.**

15. Kim K. H., Kim M. .J, Choa Y. H., et al. **Synthesis and Magnetic Properties of Surface Coated Magnetite Superparamagentic Nanoparticles.** ***International***

Magnetics Conference, IEEE Transactions on Magnetics. **May 04-08, 2008, Vol. 44, 11, pp. 2940-2943 .**

16. ***Synthesis and characterization of surfactant-coated superparamagnetic monodispersed iron oxide nanoparticles.*** Kim D. K., Zhang Y., Voit W., et al. **1-2, 2001, Journal of Magnetism and Magnetic Materials, Vol. 225, pp. 30-36.**

17. ***Synthesis and characterization of magnetic nanoparticles.*** Qiu, X.P. **6, NOV-DEC 2000, Chinese Journal of Chemistry, Vol. 18, pp. 834-837.**

18. Cornell, Rochelle M. ***The Iron Oxides: Structure, Properties, Reactions, Occurrences and Uses.*** **2. Wiley-VCH, 2003.**

19. Petri-Fink A, Hofmann H ***Superparamagnetic iron oxide nanoparticles (SPIONs): from synthesis to in vivo studies-a summary of the synthesis, characterization, in vitro and in vivo investigations of SPIONs with particular focus on surface colloidal properties.*** **4, IEEE Trans Nanobioscience, 2007, Vol. 6, pp. 289-297.**

20. ***Synthesis and surface engineering of iron oxide nanoparticles for biomedical applications.*** Gupta ak, Gupta M. **18, Biomaterials, 2005, Vol. 26, pp. 3995-4021.**

21. ***Magnetization, micro-x-ray fluorescence, and transmission electron microscopy studies of low concentrations of nanoscale Fe3O4 in epoxy resin.*** Thorpe, A. N., Holt, S. M. and Grant, J. **2000, J Mater Res, pp. 15, (11), 2488-2493.**

22. ***Current Role and Future Perspectives of Hyperthermia for Prostate Cancer Treatment.*** Baronzio G., Gramaglia A., Fiorentini. G. **1, 2009, In Vivo , Vol. 23.**

23. ***Inductive heat property of Fe3O4/polymer composite nanoparticles in an ac magnetic field for localized hyperthermia.*** Zhao D L, Zhang H L, Zeng X W. **Biomedical Materials, 2006, Vol. 1, pp. 198-201.**

24. ***Thermotherapy of Prostate Cancer Using Magnetic Nanoparticles: Feasibility, Imaging, and Three-Dimensional Temperature Distribution.*** Johannsen, M., et al., et al. **2006., Eur Urol .**

25. ***Magnetic nanoparticle hyperthermia for prostate cancer.*** Johannsen M., Thiesen B., Wust P., et al. **8, 2010, International Journal of Hyperthermia, Vol. 26, pp. 790-795.**

26. ***Magnetic nanoparticles: biomedical applications and challenges.*** Tran N., Webster T. J. **40, 2010, Journal of Materials Chemistry, Vol. 20, pp. 8760-8767 .**

27. ***Current devices for high-performance whole-body hyperthermia therapy.*** Jia D. W., Liu J. **3, MAY 2010, Expert Review of Medical Devices, Vol. 7, pp. 407-423.**

28. ***Description and Characterizatoin of the novel hyperthermia- and thermoablation-system MFH (R) 300F for clinical magnetic fluid hyperthermia.*** Gneveckow U, Jordan A, Scholz R. **6, s.l. : Medical Physics, 2004, Vol. 31.**

29. ***Magnetic Field Synthesis in the Design of Inductors for Magnetic Fluid Hyperthermia.*** Di Barba, P, Dughiero, F and Sieni, E. **Santa Catarina : IEEE Transactions on Magnetics, 2010. 17th International Conference on the Computation of Electromagnetic Fields (COMPUMAG 09). Vol. 46, pp. 2931-2934.**

30. ***Nanoparticle mediated Thermal therapy;Evolving strategies for prostate cancer therapy.*** Krishnan, S., Diagaradjane, P and Cho. **8, 2010, International Journal of Hyperthermia, Vol. 26, pp. 775-789.**

31. ***Hyperthermia and Cancer Treatment.*** Saniei, N. **2009, Heat Transfer Engineering, pp. 915-917.**

32. ***Clinical applications of magnetic nanoparticles for hyperthermia.*** Thiesen, B. and Jordan, A. **6, 2008, International Journal of Hyperthermia, Vol. 24, pp. 467-474.**

33. ***The effect of magnetic targeting on the uptake of magnetic-fluid-loaded liposomes by human prostatic adenocarcinoma cells.*** Martina M S, Wilhelm C, Lesieur S,. **30, Biomaterials, 2008, Vol. 29, pp. 4137-4145.**

34. ***Fluorescence-modified superparmagnetic nanoparticles: Intercellular uptake and use in cellular imaging.*** Bertorelle F, Wilhelm C, Roger J. **12, Langmuir, 2006, Vol. 22, pp. 5385-5391.**

35. ***Magnetophoresis and ferromagnetic resonance of magnetically labeled cells.*** Wilhelm C, Gazeau f, Bacri J C,.**European Biophysics Journal with Biophysics Letters, 2002, Vol. 31, pp. 118-125.**

36. ***Functional extrapolation of the mass-operational characteristic of magnetophoresis as a basis for a precision method of monitoringferroparticles.*** Sandulyak A A, Polismakova M N, Ershov D V. **8,: Measurement Techniques, 2010, Vol. 53, pp. 814-918.**

37. ***Cellular uptake of magnetic fluid particles and their particles and their effects on human adenocarcinoma cells exposed to AC magnetic fields in vitro.*** Jordan, A., et al., **Nov-Dec 1996, International Journal of Hyperthermia, Vol. 12, pp. 705-722.**

38. ***Increased cellular uptake of biocompatible superparamagnetic iron oxide nanoparticles into malignant cells by an external magnetic field.*** Prijic S, Scancar J, Romih R, Cemazar M, Bregar V B, Znidarsic A, Sersa G. **1, J Membr Biol, 2010, Vol. 236, pp. 167-179.**

39. ***Magnetic/luminescent core/ shell particles synthesized by spray pyrolyisis and their application in immunoassays with internal standard.*** Dosev, D, et al. **5, 2007, Nanotechnology, Vol. 18. Article number :055102.**

40. ***Synthesis and characterization of noscapine loaded magnetic plymeric nanoparticles.*** Abdalla, MO, Aneja, R. and Dean, D,et al. **2, 2010, Journal of magnetism, Vol. 322, pp. 190-196.**

41. ***Progress in applications of magnetic nanoparticles in biomedicine.*** Q A Pankhurst, N K T Thanh, S K Jones and J Dobson. **s.l.: J. Phys. D: Appl. Phys. , 2009, Vol. 42, p. 1-15.**

42. ***Gum arabic surface-modified magnetic nanoparticles for cancer therapy Gum arabic-coated magnetic nanoparticles for potential application in simultaneous magnetic targeting and tumor imaging.*** Zhang L., Yu F., Cole A. J., et al. **4, 2009, AAPS J, Vol. 11, pp. 693-699.**

43. ***Therapeutic Effect of Fe2O3 Nanoparticles Combined with Magnetic Fluid Hyperthermia on Cultured Liver Cancer Cells and Xenograft Liver Cancers.*** Yan, S., et al. **2005, J Nanosci Nanotechno, pp. (5), 1185-1192.**

44. ***Magnetic and Optical Properties of Fe3O4 Nanoparticle Ferrofluids Prepared by Coprecipitation Technique.*** Wu, K. T., et al. **2001, IEEE T Magn, pp. 37, (4), 2651-2653.**

45. ***Surface modification of magnetic nanoparticles with oleylamine and gum Arabic.*** Wilson, O. C. Jr., et al. **2008, Mat Sci Eng C, pp. 28, (3), 438-442.**

46. ***Room temperature synthesis of single-crystal Fe3O4 nanoparticles with superparamagnetic property.*** Wan, J, Tang, G and Qian, Y. **86, s.l.: J. Appl. Phys., 2007, Vol. A. 261-264.**

47. ***Properties of magnetite nanoparticles synthesized through a novel chemical route.*** Thapa, Deepa, et al. **2004, Mater Lett, pp. 58, (21), 2692-2694.**

48. ***Heat Immunity Using Magnetic Nanoparticles and Dendritic Cells for T-Lymphoma.*** Tanaka, K., et al. **2005, J Biosci Bioeng, pp. 100, (1), 112-115.**

49. ***Synthesis and characterization of biocompatible Fe3O4 nanoparticles.*** Sun, J., et al. **2006, J Biomed Mater Res A , pp. 80, (2), 333-341.**

50. ***Folate-Conjugated Iron Oxide Nanoparticles for Solid Tumor Targeting as Potential Specific Magnetic Hyperthermia Mediators: Synthesis, Physiochemical Characterization, and in Vitro Experiments.*** Sonvico, F., et al. **2005, Bioconjugate Chem, pp. 16, 1181-1188.**

51. ***Monoclonal Antibody Therapy for Prostate Cancer: Finally a Reality?*** Small, E. J. **2004, J Clin Oncol, pp. 22, (13), 2515-2516.**

52. ***Heating Effect in Biocompatible Magnetic Fluid.*** Skumiel, A., et al. **2007, Int J Thermophys, pp. 28, (5), 1461-1469.**

53. ***Dendrimer-Entrapped Gold Nanoparticles as a Platform for Cancer-Cell Targeting and Imaging. .*** Shi, X., et al., **2007, Small, pp. 7, (3), 1245-1252.**

54. ***Superparamagnetic nanoparticles in tap water.*** Senftle, F. E., et al. **2007, Water Res, pp. 41, 3005-3011.**

55. ***Adsorption of gum Arabic on bioceramic nanoparticles.*** Roque, A. C. A. and Wilson, O. C. Jr. **2007, Mater Sci Eng.**

56. ***MR of Carinoma-Specific Monoclonal Antibody Conjugated to Monocrystalline Iron Oxide Nanoparticles: The Potential for Noninvasive Diagnosis.*** Remsen, L. G., et al. **1996, ANJR Am J Neuroradiol, pp. 17, 411-418.**

57. ***Citric-acid-coated magnetite nanoparticles for biological applications.*** Racuciu, M., Creanga, D. E. and Airinei, A. **2006, Eur Phys J E, pp. 21, 117-121.**

58. ***Biological and thermic effects of magnetic fluids for photodynamic therapy and hyperthermia.*** Park, S. I., et al. **2006, J Magn Magn Mater, pp. 304, e403-e405.**

59. ***Size dependent heat generation of magnetite nanoparticles under AC magnetic field for cancer therapy.*** Motoyama, J., et al. **2008, Biomagn Res Technol, pp. 6, (4).**

60. ***Tumor Therapy with Targeted Atomic Nanogenerators.*** McDevitt, M. R., et al. **2001, Science, p. 294.**

61. ***An α-Particle Emitting Antibody ([213Bi]J591) for Radioimmunotherapy of Prostate Cancer. .*** McDevitt, M. R., et al. **2000, Cancer Res, pp. 60, 6095-6100.**

62. ***Bifunctional Magnetic Silica Nanoparticles for Highly Efficient Human Stem Cell Labeling.*** Lu, C-W., et al. **2006, Nano Lett, pp. 7, (1), 149-154.**

63. ***Magnetic Nanoparticles: Synthesis, Protection, Functionalization, and Application.*** Lu, A-H, Salabas, E. L. and Schüth, F. **2007, Angew Chem-Ger Edit, pp. 46, (8), 1222-1244.**

64. Lu, A. H., Salabas, E. L. and Schüth, F. ***Magnetic Nanoparticles: Synthesis, Protection, Functionalization, and Application.*** **s.l.: Angew. Chem. Int. Ed., 2007. Vol. 46. 1222-1244.**

65. ***Nanoparticle Interaction with Biological Membranes: Does Nanotechnology Present a Janus Face? .*** Leroueil, P. E., et al. **2007, Acc Chem Res, pp. 40, 335-342.**

66. ***Inductive heat property of Fe3O4/polymer composite nanoparticles in an ac magnetic field for localized hyperthermia.*** L., Zhao D., L., Zhang H. and Zeng X.W., et al. **2006, Biomedical Materials, Vol. 1, pp. 198-201.**

67. ***Preparation of sub-100-nm -lactoglobulin (BLG) nanoparticles. .*** Ko, S. and Gunasekaran, S. **2006, J Microencapsul, pp. 23, (8), 887-898.**

68. ***Surface modification of magnetite nanoparticles using lactobionic acid and their interaction with hepatocytes.*** Kamruzzaman Selim, K. M., et al. **2007, Biomaterials, pp. 28, 710-716.**

69. ***Clinical hyperthermia of prostate cancer using magnetic nanoparticles: Presentation of a new interstitial technique.*** Johannsen, M., et al. **2005, Int J Hyperther, pp. 21, (7), 637-647.**

70. ***Thermotherapy of prostate cancer using magnetic nanoparticles: Feasibility, imaging, and three-dimensional temperature distribution.*** Johannsen, M, Gneueckow, U and Thiesen, B, et al. **6, 2007, European Urology, Vol. 52, pp. 1653-1662.**

71. ***Au nanoparticles target cancer.*** Jain, P. K., El-Sayed, I. H. and El-Sayed, M. A. **2007, Nanotoday, pp. 2, (1), 18-29.**

72. ***Application of High Amplitude Alternating Magnetic Fields for Heat Induction of Nanoparticles Localized in Cancer.*** Ivkov, R., et al. **2005, Clin Cancer Res, pp. 11, (19), 7093s-7103s.**

73. ***Medical Application of Functionalized Magnetic Nanoparticles.*** Ito, A.,et al. **2005, J Biosci Bioeng, pp. 100, (1), 1-11.**

74. ***Synthesis, Properties, and Applications of Iron Nanoparticles. .*** Huber, D. L. **2005, Small, pp. 1, (5), 482-501.**

75. ***Size-Controlled Synthesis and Characterization of Fe3O4 Nanoparticles by Chemical Coprecipitation Method.*** Hua, C. C., et al. **2008, Sains Malays, pp. 37, (4), 389-394.**

76. ***Preparation and properties of magnetic nano- and microsized particles for biological and environmental separations.*** Horak, D., et al. **2007, J Sep Sci, pp. 30, 1751-1772.**

77. ***The Binding Avidity of a Nanoparticle-Based Multivalent Targeted Drug Delivery Platform.*** Hong, S., et al. **2007, Chem Biol, pp. 14, 107-115.**

78. ***Synthesis and antibody conjugation of magnetic nanoparticles with improved specific power absorption rates for alternating magnetic field cancer therapy.*** Gruttner C., Muller K., Teller J., Wastphal F., Foreman A., Ivkov R. **2007, J Magn Magn Mater, pp. 311, 181-186.**

79. ***The cancer stem cell: Evidence for its origin as an injured autoreactive T Cell.*** Grandics, P. **2006, Mol Cancer, pp. 5, (6).**

80. ***Effect of Initial pH and Temperature of Iron Salt Solutions on Formation of Magnetite Nanoparticles.*** Gnanaprakash, G., et al.**, s.l.: Mater. Chem. Phys., 2007, Vol. 103. 168-175.**

81. ***Nanoparticle- Aptamer Bioconjugates: A New Approach for Targeting Prostate Cancer Cells.*** Farokhzad, O. C., et al. **2004, Cancer Res, pp. 64, 7668-7672.**

82. ***Calculation of heating power generated from ferromagnetic thermal seed (PdCo-PdNi-CuNi) alloys used as interstitial hyperthermia implants.*** El-Sayed A. H., Aly A. A., El-Sayed N. I., Mekawy M. M., El-Gendy A. A. **2007, J Mater Sci: Mater Med, pp. 18, 523-52.**

83. ***Interaction of silver nanoparticles with HIV-1.*** Elechiguerra, J. L., et al. **2005, J Nanobiotechnology, pp. 3, (6).**

84. ***Gum arabic surface-modified magnetic nanoparticles for cancer therapy.*** Effiong U., Williams D., Otto W., Anderson W. **[ed.] Cezeaux J. L., Muratore D. M. Schreiner S. 2004. Proceedings of the IEEE 30th Annual Northeat Bioengineering Conference. 243-244.**

85. ***Development of Tumor Targeting Bioprobes(111In-Chimeric L6 Monoclonal Antibody Nanoparticles) for Alternating Magnetic Field Cancer Therapy. Clin Cancer Res , 19,.*** DeNardo, S. J., et al. **2005, Clin Cancer Res , 19, pp. (11), 7087s-7092s.**

86. ***Emerging Implications of Nanotechnology on Cancer Diagnostics and Therapeutics. .*** Cuenca, A. G., et al. **2006, Cancer, pp. 107, (3), 459-466.**

87. Company, Anatomical Chart. ***The Prostate Anatomical Chart.*** **Wal Chrt edition . s.l. : Lippincott Williams & Wilkins, 2008.**

88. ***Magnetic properties of monodispersed iron oxide nanoparticles.*** Chun-Rong Lin, Ray-Kuang Chiang, Jiun-Shen Wang, and Ti-Wen Sung. **8, J. Appl. Phys., 2006, Vol. 99. 08N710.**

89. ***Size-controlled synthesis and characterization of Fe3O4 nanoparticles by chemical coprecipitation method.*** Chin, H. C., et al. **2008, Sains Malays , pp. S37, (4), 389-394.**

90. ***Characterization of aqueous dispersions of Fe3O4 nanoparticles and their biomedical applications.*** Cheng F-Y., Su C-H., Yang Y-S., Yeh C-S., Tsai C-Y., Wu C-L., Wu M-T., Shieh D-B. **2005, Biomaterials, pp. 26, 729-738.**

91. Cao, G. ***Nanostructure and Nanomaterials.*** **London: Imperial College Press, 2004. 1-86094-415-9.**

92. ***Nanoparticle and targeted systems for cancer therapy.*** Brannon-Peppas L., Blanchette J. O. **2004, Adv Drug Deliver Rev, pp. 56, 1646-1659.**

93. ***Functionalisation of magnetic nanoparticles for applications in biomedicine.*** Berry C. C., Curtis A. S. G. **2003, J Phys D: Appl Phys, pp. 36, R198-R206.**

94. ***Phase I Trial of 177Lutetium-Labled J591, a Monoclonal Antibody to Prostate-Specific Membrane Antigen, in Patients With Adrogen-Independent Prostate Cancer.***

Bander N. H., Milowsky M. I., Nanus D. M., Kostakoglu L., Vallabhajosula S ., Goldsmith S. J. **2005, J Clin Oncol, pp. (21), 4591-4600.**

95. ***In vivo heating magnetic nanoparticles in alternating magnetic field.*** Babincova M., Altanerova V., Altaner C., Cicmanec P., Babinec P. **8, 2004, Med Phys, pp. 2219-2221.**